OPTICALLY STIMULATED LUMINESCENCE DATING OF GRAVELLY ALLUVIAL FAN DEPOSITS: LINKS BETWEEN CLIMATE AND GEOMORPHIC RESPONSE IN THE LOST RIVER RANGE, IDAHO

By

Megan Kearney Kenworthy

A thesis

submitted in partial fulfillment

of the requirements for the degree of

Master of Science in Hydrologic Sciences

Boise State University

December 2011

BOISE STATE UNIVERSITY GRADUATE COLLEGE

DEFENSE COMMITTEE AND FINAL READING APPROVALS

of the thesis submitted by

Megan Kearney Kenworthy

Thesis Title: Optically Stimulated Luminescence Dating of Gravelly Alluvial Fan Deposits: Links Between Climate and Geomorphic Response in the Lost River Range, Idaho

Date of Final Oral Examination: 30 April 2010

The following individuals read and discussed the thesis submitted by student Megan Kearney Kenworthy, and they evaluated her presentation and response to questions during the final oral examination. They found that the student passed the final oral examination.

Jennifer L. Pierce, Ph.D.	Chair, Supervisory Committee
Tammy M. Rittenour, Ph.D.	Member, Supervisory Committee
Matthew J. Kohn, Ph.D.	Member, Supervisory Committee

The final reading approval of the thesis was granted by Jennifer L. Pierce, Ph.D., Chair of the Supervisory Committee. The thesis was approved for the Graduate College by John R. Pelton, Ph.D., Dean of the Graduate College.

ACKNOWLEDGEMENTS

Funding for this research was generously provided by the National Science Foundation (awarded to Dr. Jennifer Pierce and Dr. Tammy Rittenour, grant number NSF-EAR-0720391). I would like to thank my thesis Supervisory Committee: Dr. Jennifer Pierce, Dr. Tammy Rittenour, and Dr. Matthew Kohn for their guidance and insight. Thank you as well to Dr. Kenneth Pierce for sharing your tremendous knowledge of the Lost River Range and guidance in the field, and Dr. Warren Sharp for thoughtful insights in the field as well. Thank you to the Nicholas Sutfin, Benjamin McVeigh, and Mike Poulos for your extensive assistance in the field and meaningful contributions to this research. I'm very grateful to the many other people who braved the wind and dusty trenches to assist me in the field, including Kara Ferguson, Denis Baldwin, my parents, Bob and Kathy Kenworthy, and my husband, Mark Robertson. Thank you to Shannon Mahan at the USGS Luminescence Laboratory in Denver, CO for your help with OSL samples as well as Washington State University's GeoAnalytical Lab, and Dr. Shawn Benner and Dr. Paul Olin for their help identifying the tephra sample. Dr. I.J. Winograd kindly provided climate data from his own research at Devil's Hole, NV. I appreciate the assistance and cooperation of the Upper Snake and Challis BLM field offices in allowing this research go forward on lands under their care. I am grateful to the folks at the Lost River Field Station who gave us a friendly place to warm up, get some shade, or hide from the always present wind. Dr. Pierce, you have been an

inspiring, patient, and wonderful advisor from the classroom to the field to mountain biking and even raising our babies. And most of all, thank you to my family, whom I could never thank enough. This would not have been possible without all of your endless help, support, and love.

ABSTRACT

The Big Lost River Basin in east-central Idaho is characterized by numerous sheetflood- dominated alluvial fans that debouche from catchments along the western front of the Lost River Range (LRR) and extend ~2-6 km from the range front. Curiously, these significant geomorphic features sit largely inactive under modern conditions, prompting the question of when and why these large fans formed. Potential drivers of alluvial fan aggradation include tectonism, autogenic behavior, and climate; however, investigation of these drivers has been impeded by a lack of dating methods that can provide accurate ages for the timing of sediment deposition. The main goals of this study are twofold: first, to determine how to apply optically stimulated luminescence (OSL) dating to the predominately clast-supported, sheetflood gravels that lack sand lenses, and second, to investigate the role of climate as a driver of alluvial fan aggradation in the LRR. In order to assess the role of climate in fan aggradation we (1) determine whether OSL ages for sediment deposition suggest a climatic driver of fan aggradation, (2) examine fan aggradation within the context of regional climate records, (3) compare the roles of glacial activity versus general climate in driving deposition on fans, and (4) infer probable climatically-driven processes that produce alluvial fan aggradation.

We selected five fans representing the variation in late Pleistocene glaciation within contributing basins (0-80% of basin area) for OSL dating and geomorphic mapping, and mapped similar-age fan surfaces using OSL dates, deposit characteristics and soil development. Deposit characteristics examined include the areal extent of surfaces, average slopes, relative surface heights, and grain-size distributions. For soil development, particular attention was paid to the amount of loess accumulation, stage of pedogenic $CaCO_3$ accumulation, and the average thickness of pedogenic $CaCO_3$ coats developed on clasts within soil profiles. Soil characteristics were compared with corresponding OSL ages in order to assess their reliability as indicators of surface age in the absence of absolute dating.

The gravelly sheetflood deposits of LRR fans lacked the well-sorted, thick sand lenses typically targeted for OSL dating. As a result, most samples were collected by excavating sediment from exposures while under light-safe tarps or at night, with samples for equivalent dose estimates sieved to retain the <2mm portion. Sediment chemistry for dose-rate estimation was analyzed for numerous grain sizes. Sand grain-size fractions (<2 mm and 0.15-2.0 mm) produced the highest dose-rate estimates, pebbles (>5 mm) the lowest, with results from bulk samples generally in-between. Bulk sample dose-rate estimates were preferred as they likely provide the best estimate of the average dose contribution of the sediment. Equivalent dose distributions do not suggest significant partial bleaching, but overdispersion values of >20% for some samples may result from the heterogeneity in the sediment dose rate. Despite potential dose rate problems, resulting ages are consistent with fan morphology and multiple ages from single surfaces show good agreement.

Ages from 31 OSL samples ranged from ~4-115 ka and combined with mapped fan surfaces suggest that aggradation occurred during four distinct intervals: 0-10 ka, 10-20 ka, 20-35 ka, and 35-60 ka. Surprisingly, the timing of deposition is similar for all fans, regardless of past glacial extent within contributing basins. Further, major aggradation is not limited to the Pinedale (OIS 2, ~12-24 ka) or Bull Lake (OIS 6, ~130-200 ka) glacial intervals as is often assumed for significant but undated alluvial and fluvial deposits throughout the western U.S. Approximately 80% of the total fan area was deposited during late Pleistocene intervals of aggradation with only ~10% of fan area deposited during the Holocene. In addition, late Pleistocene surfaces had steeper average slopes and a greater predominance of coarse-grained facies than Holocene surfaces, suggesting greater transport capacity of streams and sediment delivery to fans during the late Pleistocene than the Holocene.

Regional climate records indicate generally cold climate in the LRR throughout 10-60 ka, but more variable moisture delivery. Cold conditions may have increased transport capacity with greater effective moisture and larger spring discharges in response to accumulation of bigger winter snowpacks. Concurrently, sediment delivery may have increased by mobilization of stored hillslope sediment, decreased vegetation cover, glacial activity (where present), enhanced weathering rates and more effective frost weathering. Overall, this research shows that cool to cold climate conditions between 10-60 ka increased sediment supply and transport capacity within contributing basins throughout the LRR, regardless of the extent of late Pleistocene glaciation, resulting in significant and largely snychronous alluvial fan aggradation throughout the Big Lost River Basin.

TABLE OF CONTENTS

LIST OF TABLES

LIST OF FIGURES

CHAPTER ONE: LUMINESCENCE DATING WITHOUT SAND LENSES – AN APPLICATION OF OSL TO COARSE-GRAINED ALLUVIAL FAN DEPOSITS OF THE LOST RIVER RANGE, IDAHO, USA

1.1 Abstract

Optically stimulated luminescence (OSL) dating is increasingly used to estimate the age of fluvial deposits. One challenge to obtaining accurate age estimates for fluvial deposits is partial bleaching, but a variety of methods can now detect and correct for this problem, including single-grain dating and the use of a minimum age model. A challenge that remains in OSL dating is its application to geomorphically and climatically significant deposits that lack the thick sand lenses typically targeted for sample collection. The alluvial fans along the western front of the Lost River Range in east-central Idaho, USA are one example; deposits are typically pebble to cobble sheetflood gravels with a sandy matrix but small to absent sand lenses. As a result, the majority of samples were collected by excavating gravelly deposits under light-safe tarps or at night with the aid of red lights. Multiple grain-size fractions from the coarse-grained sheetflood deposits were analyzed for dose-rate contribution by ICP-MS, geranium semiconductor gamma spectrometer and XRF. Dose rates from bulk sediment samples were 0.4-40% (average of 18%) less than dose-rate estimates from sand-grain size fractions due to the contribution from low-dose carbonate pebbles and cobbles. Where possible, dose rates were based on bulk sediment samples as they integrate the dose-rate contribution from all grain sizes. Equivalent dose distributions showed little evidence for

partial bleaching. Many samples had significant kurtosis and/or overdispersion, possibly due to microdosimetry effects, accumulation of pedogenic $CaCO_3$, or post-depositional sediment mixing. Resulting age estimates range from approximately 4-120 ka, and ages show good agreement with previous age control, fan morphology, and a Mazama tephra at one site. Further, multiple ages from deposits produced ages in good agreement. This study demonstrates that with modified sampling methods and careful consideration of the dose rate, OSL dating can be applied to many coarse-grained deposits that lack datable material for other methods.

1.2 Introduction

Many deposits used for geomorphic and climatic reconstruction, such as fluvial sequences and alluvial fans, are composed of predominately coarse-grained sediment and commonly lack datable material (e.g., organic material for ^{14}C dating) for age estimation. These types of deposits have proven challenging even for optically stimulated luminescence (OSL) dating as they sometimes lack the thick sand lenses upon which this method generally relies. For fluvial deposits that contain sand lenses, OSL dating has become one of the methods of choice to estimate the timing of sediment deposition. Recent advances in the application of OSL dating to fluvial deposits (e.g., Wallinga, 2002; Jain et al., 2004; Rittenour, 2008) as well as general improvements in OSL dating methods (e.g., Murray and Wintle, 2000; Duller, 2004, 2008; Lian and Roberts, 2006) have improved the accuracy of OSL ages. OSL dating can have advantages over radiocarbon or cosmogenic radionuclide dating (e.g., Granger and Muzikar, 2001; Granger, 2006) because of (1) its reliance on sand and silt-sized quartz and feldspar grains, which are common in fluvial deposits, (2) a dating range up to ~300 kyr (Murray

and Olley, 2002; Rittenour, 2008) that surpasses the ~40 kyr limit of radiocarbon dating, and (3) a direct estimate of the timing of deposition, rather than a minimum age estimate as is commonly the case with cosmogenic dating or U-series dating of pedogenic carbonate (e.g., Gosse and Phillips, 2001; Sharp et al., 2003). OSL techniques have not, however, been widely applied to coarse-grained fluvial and alluvial environments (but see Rizza et al., 2011) due to difficultly both sampling these types of deposits, and correctly calculating dose rates and interpreting ages for coarse-grained deposits.

OSL dating provides an estimate for the last time quartz or feldspar grains were exposed to light (Huntley et al., 1989). Upon deposition and burial, the luminescence signal is generated through exposure to ambient radiation in the surrounding sediment and grows with time. OSL dating requires an estimate of the amount of radiation required to generate the measured luminescence signal of a sample, called the equivalent dose (D_e), and an estimate of the radioactive environment the sample was exposed to, called the dose rate. Dividing the D_e by the dose rate provides an age estimate for the timing of sediment deposition.

One of the main challenges for OSL dating of fluvial deposits is the possibility of incomplete solar resetting of the OSL signal prior to deposition, termed partial bleaching. Factors that influence partial bleaching in fluvial settings include the duration of exposure to direct sunlight as well as the depth and turbidity of the water column through which sediment is being transported. Numerous methods have been developed to detect and correct for partial bleaching, including analysis of coarser grain sizes that are thought to be better bleached during transport (Olley et al., 1998; Colls et al., 2001; Truelson and Wallinga, 2003), single-grain dating (see review by Duller, 2008), and statistical

treatment of D_e distributions to exclude portions representing poorly bleached grains (Galbraith et al., 1999; Olley et al, 1999; Truelson and Wallinga, 2003; Rodnight et al., 2006).

Researchers who wish to apply OSL techniques to coarse-grained fluvial environments are confronted with two primary challenges: 1) sampling deposits that lack thick sand lenses (Kock et al., 2009), and 2) correctly calculating dose rates in samples with mixed grain sizes. Sediment for equivalent dose (D_e) estimate is traditionally collected by pounding a metal tube into a sand lens then removing it, retaining a core of sediment that is protected from exposure to light. If sediment is cohesive enough, it is also possible to remove a block of sediment and use the internal sediment shielded from light exposure for D_e estimation. The sample for dose-rate calculation is traditionally collected from sediment within a ~30 cm radius around the sample tube or block. However, in coarse-grained fluvial environments, sand lenses are often thin or absent and sediment commonly lacks cohesiveness. Often these deposits contain ample quartz or feldspar grains of the right size range for dating which can be collected by modified sampling strategies, such as collecting larger bulk sediment samples at night or under light-proof tarps (e.g. Rizza et al., 2011).

In coarse-grained fluvial settings, large distributions in sediment clast sizes can lead to heterogeneities in the dose rate that need to be accounted for in order to produce accurate dose rate and age estimates. However, correctly accounting for this potential heterogentiety can be difficult, particularly where *in situ* gamma spectrometry may not be feasible as the coarse-grained nature of the sediment precludes placing the gamma spectrometer within the sediment from which the sample was collected. The use of

dosimeters may also not be feasible due to limitations on how long dosimeters can be left in place, and because dosimeters may not provide values that are representative for a sample that was collected over a broader area than a traditional sample collected in a pipe.

The large and geomorphically spectacular alluvial fans of the Lost River Range (LRR) in east-central Idaho, USA provide one example of a fluvial environment that has not favored the preservation of thick sand lenses. The fans are of interest because the timing of major episodes of aggradation may provide insight into hillslope sediment production and geomorphic response to past climate change in this region. In this study, we apply OSL dating to LRR fans in order to investigate how best to sample for and estimate dose rates in fluvial deposits in which the quartz grains are contained within the sandy matrix of largely coarse-grained deposits.

1.2.1 Regional Setting

The Lost River Range (LRR) lies within the northeastern extent of the Basin and Range Province of the western U.S. in east-central Idaho (Fig. 1.1). Bedrock within the LRR is composed of Precambrian and Paleozoic limestones and quartzarenites that were folded and faulted during the Laramide and Sevier orogenies in the Cretaceous and Eocene (Haller and Crone, 2004; Skipp and Hait, 1977). Regional extension leading to the development of the LRR and other parallel ranges began ~4-7 Ma (Haller and Crone, 2004), and may be related to passage of the Yellowstone hot spot (e.g., Pierce and Morgan, 1990). Relief of the LRR has resulted from movement along the Lost River Fault (LRF), a west-dipping normal fault that bounds the western flank of the range. The most recent activity along the Lost River fault occurred during the magnitude 7.3 Borah

Peak Earthquake of October, 1983. This event resulted in 34 km of surface rupture with new scarps averaging 0.8 m and reaching a maximum of 2.7 m in height (Crone and Machette, 1984).

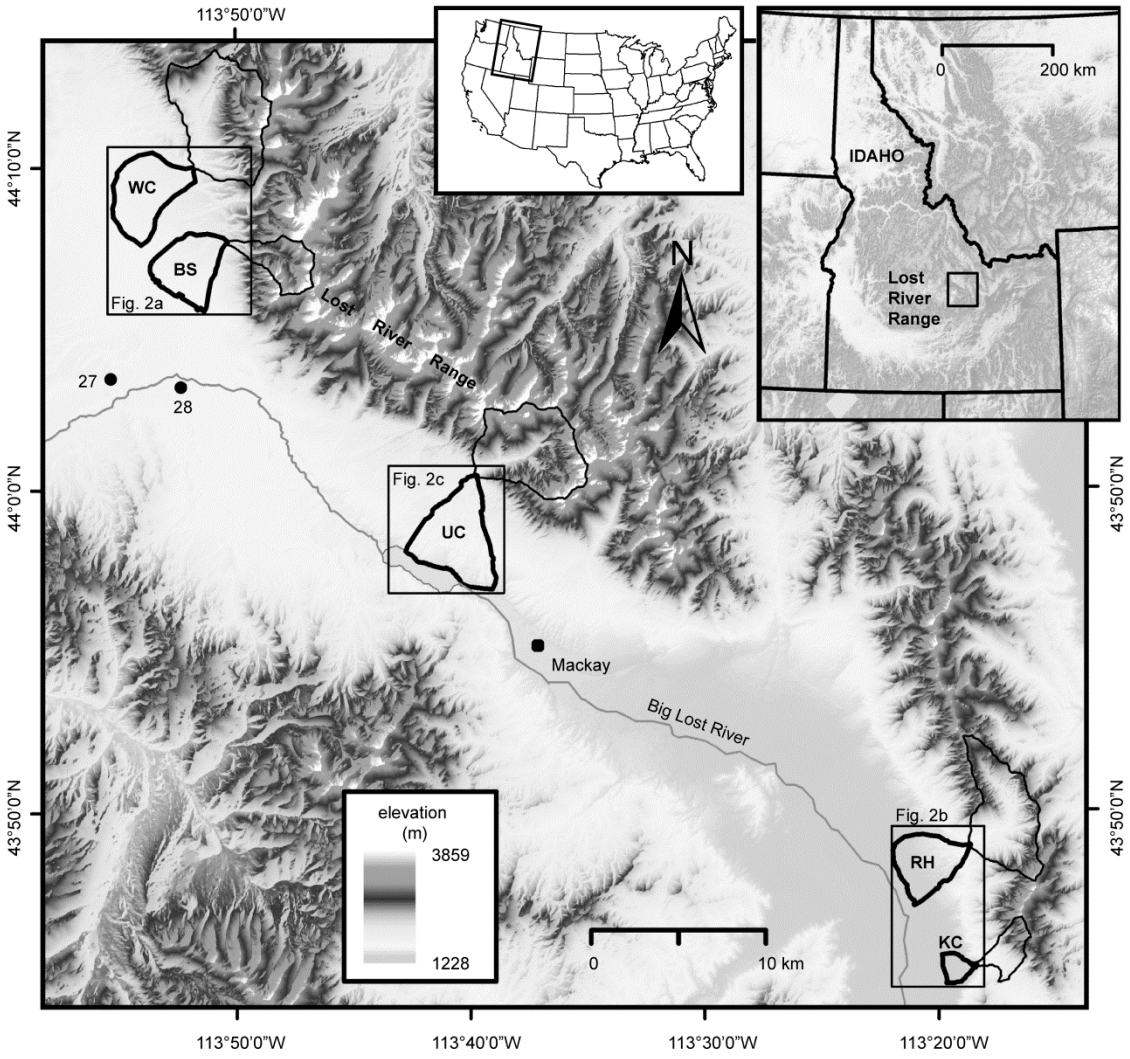

Figure 1.1 Location of the Lost River Range and Big Lost River Basin within the western U.S. and Idaho. Alluvial fans included in this study are highlighted (thick outline) along with their contributing basins (thin outline). The alluvial fans from north to south are Willow Creek (WC), Birch Springs (BS), Upper Cedar Creek (UC), Ramshorn (RH), and King Canyon (KC).

In the LRR, modern climate varies from arid on the valley floor (approximately 1650-1900 masl) to sub-humid at higher elevations on the peaks (up to 3861 masl). In the southern portion of the basin, mean annual temperature and precipitation are 5.87 ± 1.03 °C and 246 ± 67 mm/yr, respectively (1948-2006, Arco 3 SW weather station; Western Regional Climate Center, 2009). In the northern portion of the basin, mean annual temperature and precipitation are 4.08 ± 1.06 °C and 203 ± 61 mm/yr, respectively (1948-2005, Chilly Barton Flat weather station; Western Regional Climate Center, 2009).

The alluvial fans of interest in this study formed on the western side of the LRR and are predominately low-gradient (~2-4°), large-radius fans (~2-6 km). Many LRR fans are composed of two to four large, distinct, and currently inactive geomorphic surfaces (Fig. 1.2). Surface morphology and stratigraphy suggest that the fans have developed in a stacked rather than telescoping nature. Under modern conditions contributing basins produce low-volume, intermittent discharges and fan activity appears to be limited to minor incision where active channels are present and some debris flow deposition at fan heads (Patterson, 2006). Five of these large, low-gradient fans were selected for OSL dating (Figs. 1.1 and 1.2).

Deposit characteristics (Fig. 1.3) suggest fluvial transport and sorting, particularly from sheetflooding, have been the dominant depositional processes on LRR fans (Pierce and Scott, 1982; Patterson, 2006), producing deposits composed of clast supported gravels with planar to sub-horizontal bedding and low percentages of silt and clay (Funk, 1976; Pierce and Scott, 1982; Pierce and Colman; 1986; Patterson, 2006). Alternating

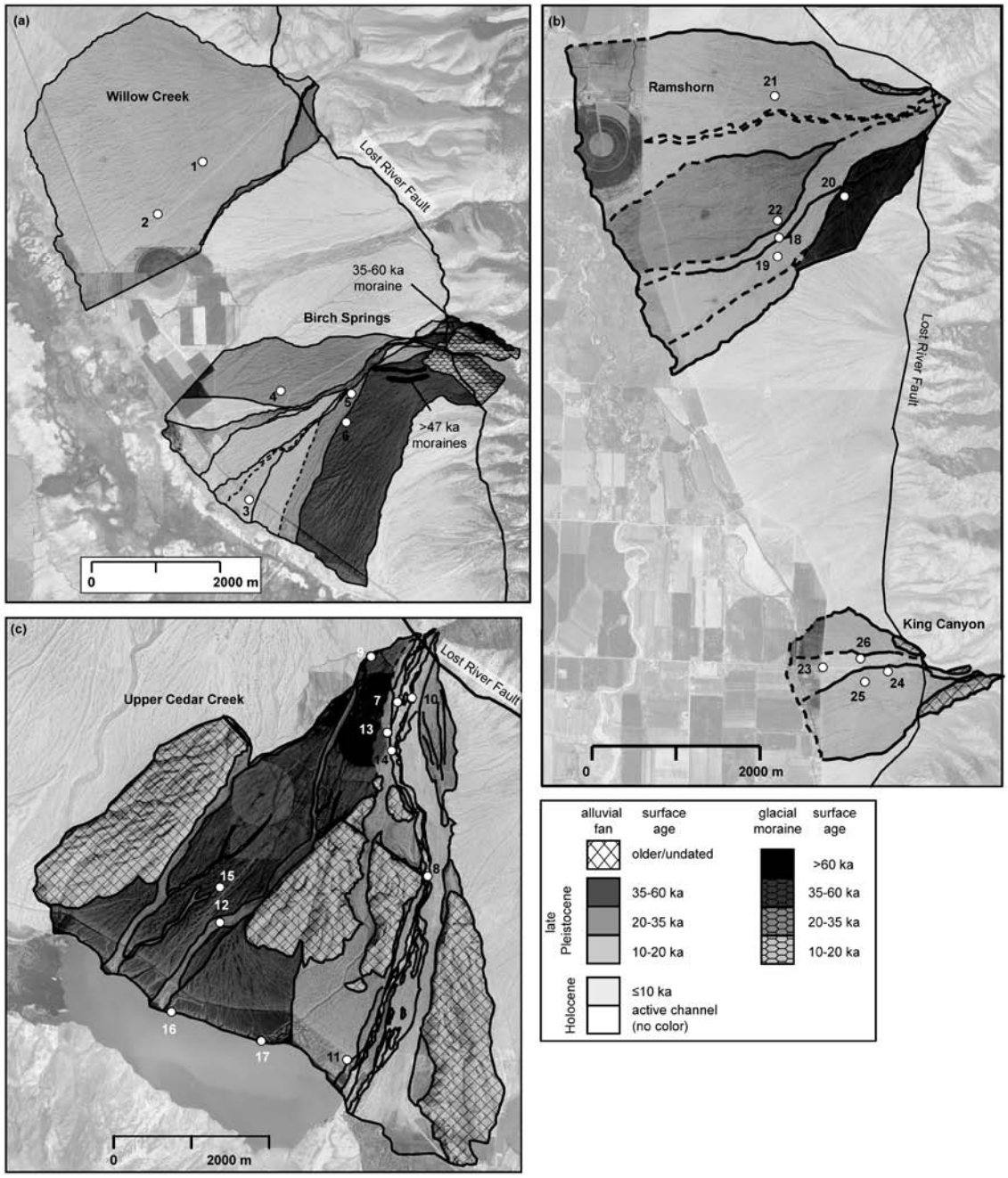

Figure 1.2 Geomorphic maps of similar age alluvial fan surfaces based on OSL results, surface relationships, deposit characteristics, soil development and the average thickness of $CaCO_3$ coats developed on the underside of clasts within soil profiles. Ages of glacial deposits are estimated from relationships with dated alluvial fan surfaces and average $CaCO_3$ coat thickness. Numbers refer to the location of sample sites discussed in text and tables. (a) The alluvial fans of the northern portion of the Big Lost River basin, Willow Creek and Birch Springs. (b) The alluvial fans of the southern portion of the basin, Ramshorn and King Canyon. (c) Upper Cedar Creek Alluvial Fan, situated in the central portion of the basin.

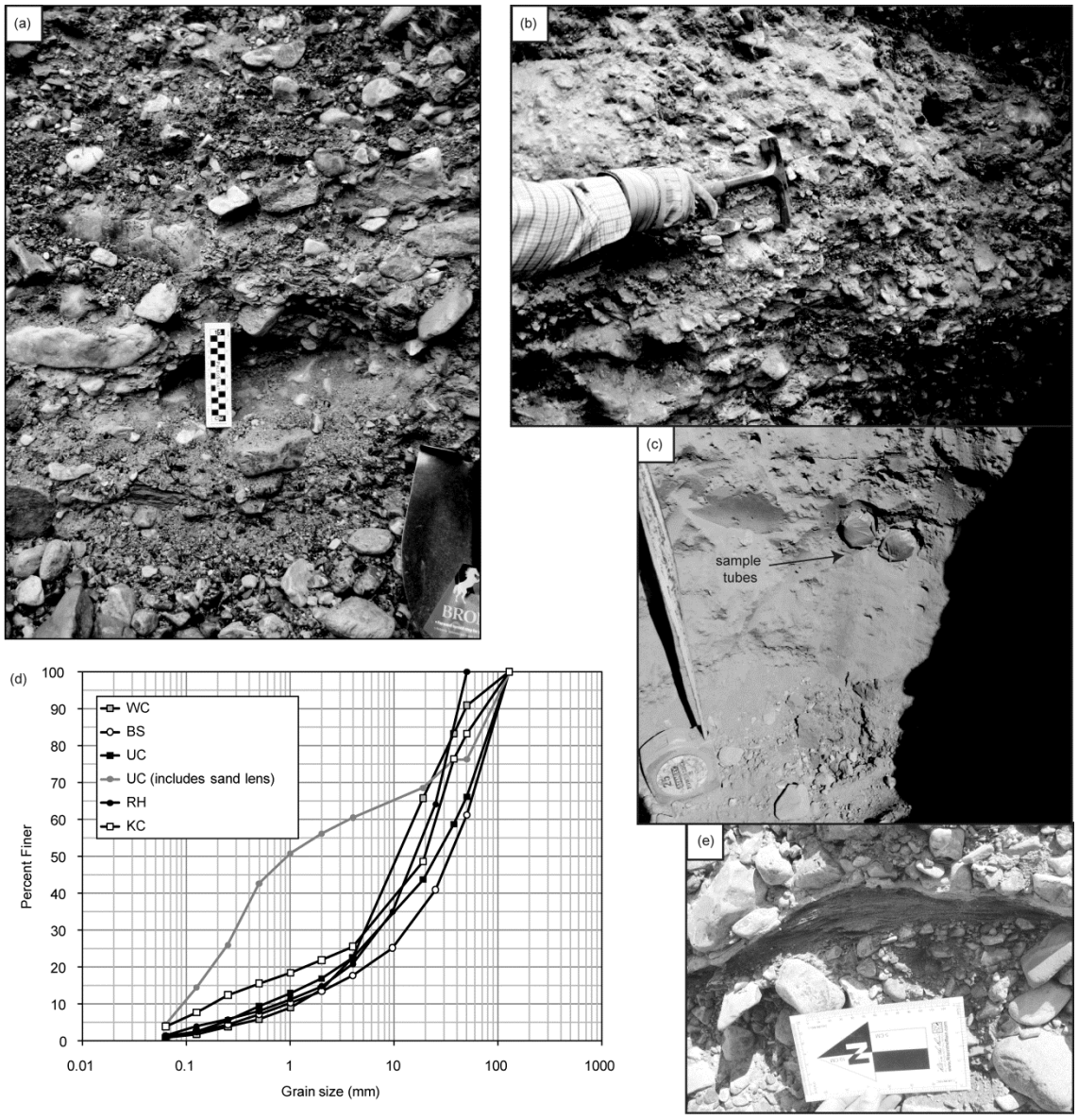

Figure 1.3 Examples of alluvial fan sediments sampled for OSL dating in the Lost River Range. (a) Typical coarse grained sediments sampled when sand lenses were small or absent. Black squares on ruler in center of picture are 1 cm, and ruler sits in front of site excavated for sample USU-646 (26.64 ± 3.29 ka) from site 4. (b) Another example of typical coarse grained sediments. Characteristic coarse to fine sheetflood couplets are visible. (c) Example of traditional OSL sample collected by pounding metal pipes into a sand lens at site 3 (USU-414; 10.78 ± 0.92 ka). (d) Typical grain size distributions for coarse-grained alluvial fan sediments from all five study fans. Also included is one sample containing a sand lens. (e) Example of a small sand lens preserved within coarser gravels sampled by excavation rather than pounding a metal tube into the sediment. This lens is from site 8 (USU-417; 7.26 ± 0.54 ka).

coarse-fine couplets characteristic of sheetflooding (Blair and McPherson, 1994) are visible in many natural exposures and trenches dug for this study (Fig. 1.3b). Thick sand lenses like that in Fig. 1.3c are rarely present and generally found in the younger, less spatially extensive deposits that do not represent the main episodes of aggradation on LRR fans. The older and spatially broader surfaces that represent significant episodes of aggradation largely lack sand lenses, but still contain sufficient sand within the pebble-cobble gravel matrix for OSL dating.

Fan deposits have been capped by loess accumulation and altered by soil development. Loess accumulation can be found on the surface of most fans, with more significant accumulation (>1 m) on the southerly fans and older surfaces. Soil development in the upper fan gravels and loess deposits is generally weak (Bw and Bt horizons), with the exception of significant pedogenic $CaCO_3$ accumulation (stage I-III+; Giles et al., 1966; Machette, 1985; Birkeland et al., 1991) found at approximately 0.15-1.15 m depth on Pleistocene-age surfaces.

Previous assessments of the ages of LRR fans have large uncertainties and only provide estimates for the timing of surface stabilization and abandonment, rather than deposition. Pierce and Scott (1982) hypothesized that many fans in the LRR were latest Pleistocene, or Pinedale (Late Wisconsin, OIS 2), in age based on relationships of fans to moraines and glacial outwash and the thickness of pedogenic $CaCO_3$ coats developed on clasts within soils on fan surfaces. Limited U-series dating of pedogenic $CaCO_3$ coats produced minimum ages of surface abandonment of ~160, ~30, and ~23 ka in the southern portion of the LRR (Scott et al., 1985; Pierce, 1985). Patterson (2006) obtained similar ages (~10-60 ka) for major fan surfaces using a growth rate for pedogenic $CaCO_3$

coats developed by Pierce (1985). Again, these ages apply to the timing of surface abandonment rather than active deposition, and the large uncertainties in the age estimates pose challenges when trying to infer linkages between climate and geomorphic response.

1.3 Methods

1.3.1 Sample Collection and Preparation

Five of the large, low-gradient alluvial fans on the western side of the LRR and two terraces of the East Fork of the Big Lost River (which drains the Pioneer Range to the west) were selected for optical dating (Figs. 1 and 2). On each fan, major geomorphic depositional surfaces were targeted for dating. Where it was possible, samples were collected from natural exposures and abandoned gravel pits (17 samples). Samples were also collected from back-hoe dug trenches in strategically placed locations to ensure sampling of all major fan surface deposits (18 samples). In total, 34 ages were obtained, with 32 samples collected from alluvial fan deposits and two samples from East Fork Big Lost River terraces.

Of these 34 samples, only six were collected from sand lenses large enough for sampling by traditional methods: four from alluvial fan deposits, and two from river terrace deposits. Sand lenses were sampled by pounding an opaque metal tube into the sediment. All other samples required collection by non-traditional methods in which the sediment was excavated from the deposit at night or under light-safe tarps to avoid light exposure. In three locations, sand lenses were located, but too thin or discontinuous for sampling by pounding a tube into the sediment (see example in Fig. 1.3c). Instead, these

small lenses were sampled at night with the aid of red headlamps, by first removing the outer 3-4 cm of light-exposed sediment, then excavating the remaining sand into a light-safe container.

The majority of samples were collected from coarse-grained sheetflood gravels that lacked sand lenses with collection taking place at night or under light-safe tarps with the aid of red headlamps. The sandier sheetflood facies were targeted for sampling and contained ample material within the matrix for OSL dating, with up ~9-20% of the sediment by weight in the less than 2 mm grain-size fraction (Fig. 1.3d). Once under the light-safe tarps or at the sample location at night, this matrix sediment was collected by first clearing away the outer ~3-5 cm of light-exposed sediment from the target sediment layer. In addition, a large area above the target layer was also cleared of loose sediment to avoid contamination by light-exposed grains falling into the sample during collection. Sediment for dating was then excavated from an ~ 20 cm by 20 cm area, sieved with a 2 mm sieve, and the <2 mm portion retained in light-safe containers for further processing and OSL analysis.

All samples were sent to the Utah State University Luminescence Laboratory in Logan, Utah, USA for preparation and analysis under amber safe lights. Sample preparation included wet-sieving to isolate the desired grain-size fraction, which was generally 75-150 μm as the majority of quartz grains fell into this range and larger grain sizes were predominately limestone. The 75-150 μm grain-size fraction was then treated with HCl and floated in 2.7 g/cm^3 sodium polytungstate heavy liquid to separate the quartz from the heavier minerals. Three 30-minute treatments with hydrofluoric acid followed to remove feldspars and to etch quartz grains. Immediately following, samples

were washed in concentrated HCl to remove fluorides and other precipitants. Finally, samples were dry sieved to remove partially dissolved feldspars and any quartz grains less than 63 μm. The purity of all aliquots was checked using infrared stimulation (IR), and aliquots containing feldspar were not included in age calculations.

1.3.2 Dosimetry

To determine the dose rate for samples collected using the traditional method of pounding a metal pipe into a sand lens, representative samples were collected from an approximately 30 cm radius around each sample site. For samples excavated from sheetflood gravels, initial dose rate samples were collected from the same material excavated for OSL dating then sieved to retain the <2 mm portion. Concentrations of U, Th, K, and Rb were measured by ICP-MS and ICP-AES at ALS Chemex Labs, Elko, NV, USA. However, due to concerns about dose-rate heterogeneity introduced by the coarse-grained nature of the sediment, a second dose rate sample was collected for most excavated samples and additional grain sizes analyzed (some sites could not be re-accessed because back-hoe dug trenches were already filled). This second sample was collected from same site as the first but retained all grain sizes present in the deposit, with the exception of a few large clasts that could not be removed.

The chemistry of additional grain-size fractions was measured by ICP-MS and ICP-AES (also at ALS Chemex Labs), as well as by geranium semiconductor gamma spectrometry and XRF at the USGS Luminescence Dating Laboratory in Denver, CO. In situ gamma spectrometry was not considered practical because the coarse-grained nature of the sediment prohibited placement of a gamma probe within a specific sample hole. In situ dosimeters were similarly not practical and also could not be left for adequate time in

most locations due to permit regulations requiring trench closure as quickly as possible. To test for the influence of difference grain sizes on dose rates, a number of grain sizes were analyzed. Grain sizes analyzed by ICP-MS and ICP-AES included the <2 mm fraction, the 0.15-2 mm fraction, >2 mm pebbles, as well as a bulk sample that contained all grain sizes present in their correct proportions. Bulk samples were also analyzed by XRF and gamma spectrometry. Dose rate determined through gamma spectrometry is based on at least eight separate measurements per sample, with the sample shaken between each measurement to obtain results for a variety of geometric arrangements of the sediment. For samples collected from sand lenses by a metal pipe and excavated samples with a bulk sediment sample for dose rate, error calculations for chemistry values are those determined by Goble et al. (2004) with errors assumed to approach 100% as detection limits are approached for each element. For excavated samples lacking a bulk sediment sample for dose rate, the error for chemistry values also represents the standard deviation on repeat measurements.

Moisture content used in calculating dose rate was based on the measured *in situ* water content and assumed values for the Holocene and late Pleistocene conditions (with 10 ka used as the boundary between the two time periods). Moisture content of the deposits was assumed to be 3 ± 3% during the Holocene, and 8 ± 8% during the late Pleistocene. For samples of late Pleistocene age, the dose rate was calculated by multiplying the dose rate calculated for Holocene water content and the dose rate calculate for late Pleistocene water content by the fraction of time the sample is assumed to have experienced each condition. As age is affected by using different moisture contents, the final dose rate was calculated in an iterative fashion.

Final dose rates for samples were calculated based on cosmic contribution, sediment chemistry, and moisture content of the sediment (Adamiec and Aitken, 1998; Aitken, 1998; Brennan, 2003). The contribution to dose rate by cosmic radiation was calculated using sample depth, elevation, and location (latitude and longitude) using the methods of Prescott and Hutton (1994) and a 10% error was assumed. Elemental abundances of U, Th, K, and Rb were converted to a dose rate using the methods of Adamiec and Aitken (1998) and include a 3% error for the conversion of chemical data to dose rate (Murray and Olley, 2002). Finally, errors were calculated in quadrature using the methods of Aitken and Allred (1972) and Aitken (1976, 1985).

1.3.3 Equivalent Dose Measurements

1.3.3.1 Optical Measurements

Optical measurements were performed on Risø OSL/TL DA-20 luminescence readers equipped with Sr^{90} beta radiation sources (0.13-0.16 Gy/sec dose rates). The purified quartz sand was mounted in a 2 mm diameter region (~200 grains per aliquot) on stainless steel disks with a silicone-based spray. Quartz grains were stimulated for 40 s with blue-green LEDs (470 nm) at 90% power ($40 W/m^2$). Photon detection was measured through a 7.5 mm U340 filter. The luminescence signal was calculated as the first 0.64 s of the resulting decay curve minus the background, which was averaged over the last 5s. Examples of decay curves for the natural OSL of five samples are shown in Fig. 1.4a and indicate that the luminescence signal of LRR alluvial fan samples are dominated by the fast component.

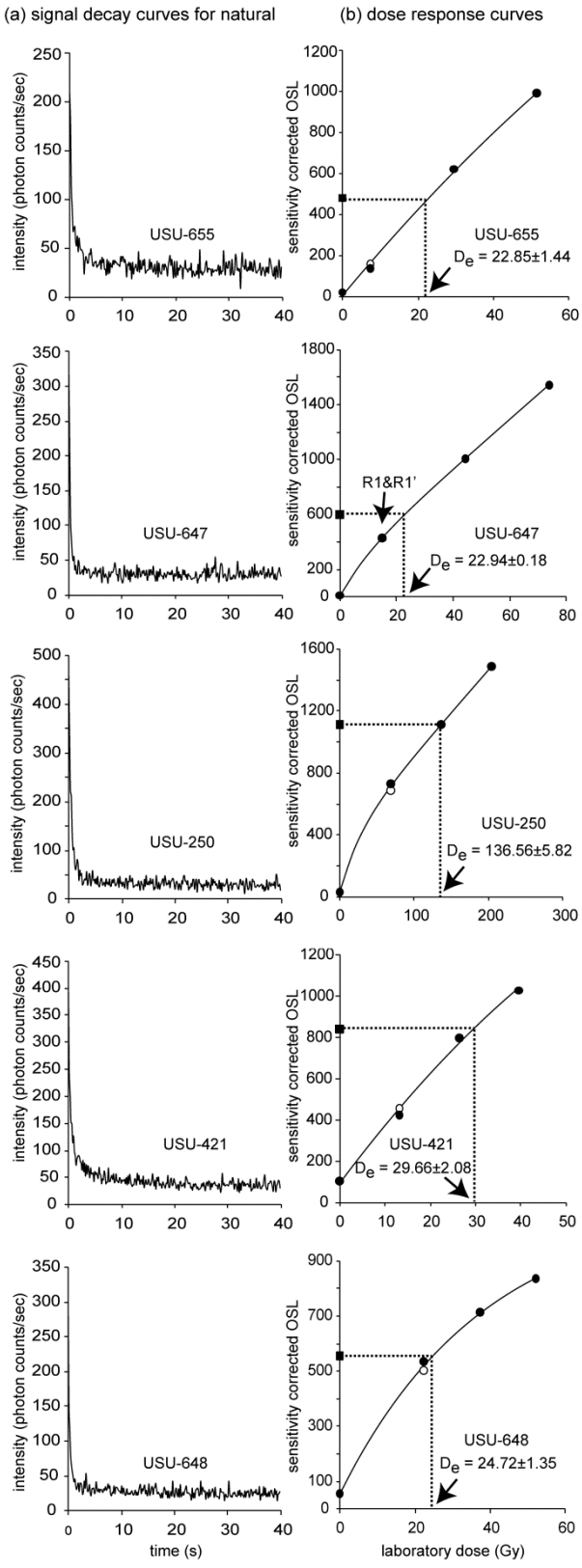
(a) signal decay curves for natural
(b) dose response curves
intensity (photon counts/sec)
sensitivity corrected OSL
USU-655
De = 22.85±1.44
USU-647
R1&R1'
De = 22.94±0.18
USU-250
De = 136.56±5.82
USU-421
De = 29.66±2.08
USU-648
De = 24.72±1.35
time (s)
laboratory dose (Gy)

Figure 1.4. (previous page) (a) Signal-decay curves for the natural signal of five samples. (b) Dose response curves for the same samples. Data was fit with saturating exponential or saturating exponential plus linear curves.

1.3.3.2 SAR Protocol

The single aliquot regenerative dose (SAR) protocol of Murray and Wintle (2000) was used to determine equivalent doses (D_e). In the SAR sequence, the natural luminescence signal was measured as well as the luminescence response to five regenerative doses, which included a repeated dose and a zero dose. Dose response data were fit with saturating exponential or saturating exponential plus linear curves.

As part of the SAR protocol, samples were subject to a 10 s preheat (PH) before measurement of the natural or regenerated luminescence. Dose recovery and PH plateau tests were conducted to select the most appropriate PH temperature that would allow the SAR sequence to accurately recover given doses. Three samples from fans (USU-251 from Upper Cedar Creek, USU-305 from Ramshorn, USU-645 from Birch Springs) and one from a terrace of the E. Fork Big Lost River (USU-651) were selected for PH and dose recovery testing. These samples were selected to represent the possible variability in source area sediment and ages of deposits and are assumed to be representative of the variability in luminescence response to PH temperatures. For the PH plateau test, 30-35 pristine aliquots of each sample were bleached at room temperature for 40 s at 90% LED power, followed by a 1000 s pause. This bleaching and pause was repeated a second time to ensure zeroing of the sample and equilibration of charge transfer prior to the next measurement. Aliquots were then given a beta dose similar to their natural dose and analyzed with PH temperatures ranging from 180-300 °C at 20 °C increments (5 aliquots

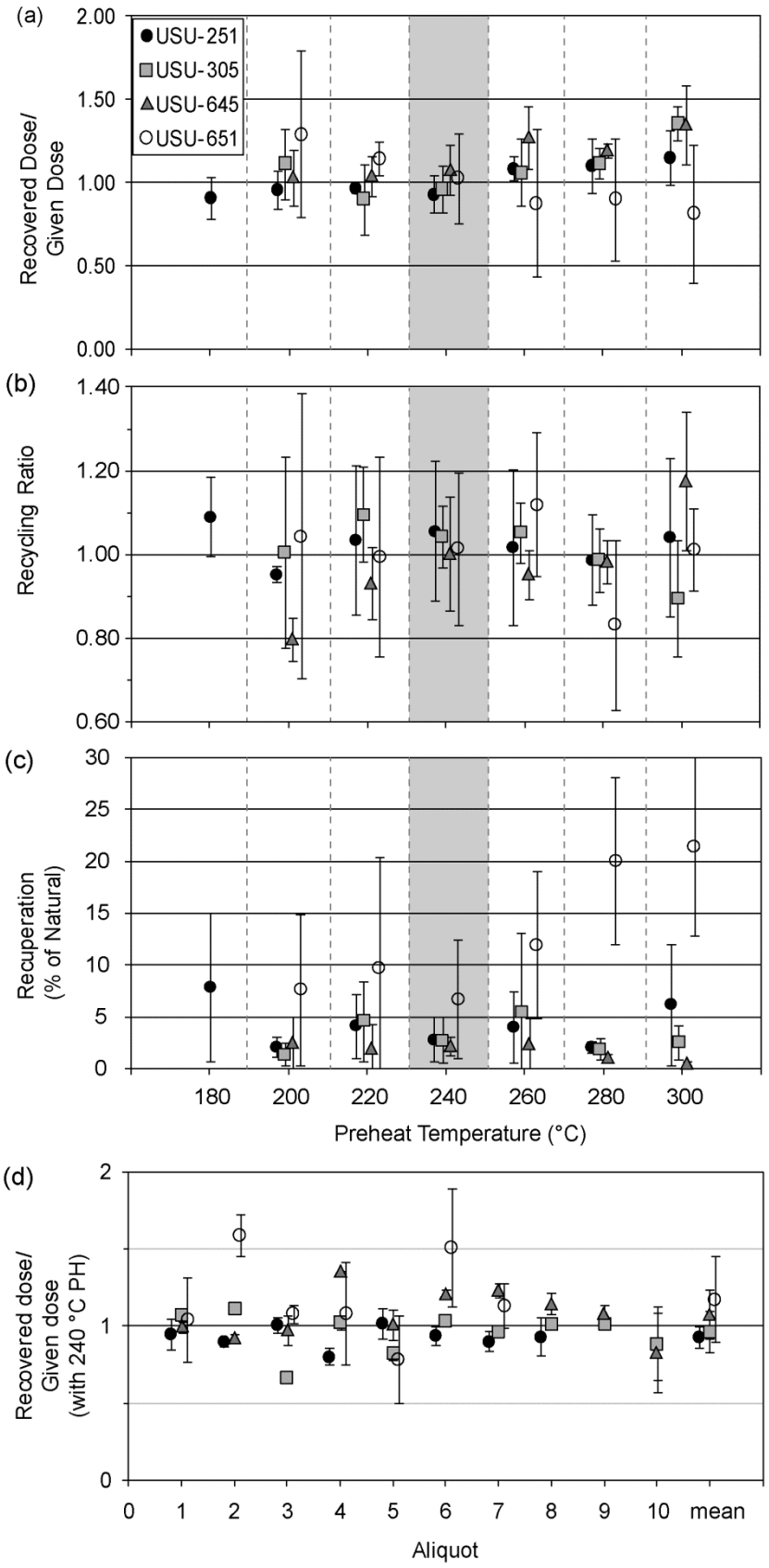
(a)
Recovered Dose/ Given Dose
2.00
1.50
1.00
0.50
0.00
USU-251
USU-305
USU-645
USU-651
(b)
Recycling Ratio
1.40
1.20
1.00
0.80
0.60
(c)
Recuperation (% of Natural)
30
25
20
15
10
5
0
180
200
220
240
260
280
300
Preheat Temperature (°C)
(d)
Recovered dose/ Given dose (with 240 °C PH)
2
1
0
0
1
2
3
4
5
6
7
8
9
10
mean
Aliquot

Figure 1.5 (previous page) Results from preheat plateau and dose recovery tests. (a) Dependence of D_e on preheat temperature for samples USU-251 from site 7 on Upper Cedar Creek Fan (Fig. 1.2c), USU-305 from site 18 on Ramshorn Fan (Fig. 1.1), USU-645 from site 4 on Birch Springs Fan (Fig. 1.1) and USU-651 from site 28 on one of the terraces of the East Fork Big Lost River. A preheat temperature of 240 °C was selected based on these results. (b) Recycling ratios for various preheat temperatures. Results shown are based on duplicate applied doses. (c) Results for recuperation at various preheat temperatures with a zero applied dose, shown as percent of the natural signal. (d) Results from dose recovery testing with a preheat temperature of 240 °C. Mean values shown are based on results from 10 aliquots for all samples except USU-251, for which only 8 aliquots were measured, and USU-651, which is based on 9 aliquots after elimination of one aliquot that did not meet criteria for inclusion.

per treatment step). For these measurements, cut-heat temperatures of 160 °C were used and optical measurements were at 125 °C at 90% LED power. Dose recovery tests followed similar procedures as the PH plateau tests and were performed using the most appropriate PH temperature identified in the PH plateau test.

Based on the results from the pre-heat plateau tests (Fig. 1.5), 240 °C was selected as the most appropriate pre-heat temperature for LRR samples. Mean recovered doses for each sample were acceptable for a PH temperature of 240 °C for 10 s, ranging from 93-107% of the given dose (Fig. 1.5a). Recycling ratios (based on the same regenerative dose given at the beginning and end of the SAR sequence) showed little dependence on temperature (Fig. 1.5b), suggesting that corrections for sensitivity changes were appropriate. In addition, recuperation values (determined through administration of a zero dose) were low, ~2-7% of natural, with a 240 °C pre-heat (Fig. 1.5c). Cut-heats applied before measurement of test doses were 160 °C with a 0 s pause. IR stimulation (at room temperature) was done at the end of each SAR cycle for all aliquots to detect for

residual feldspars and sample purity. Aliquots showing IR signals were rejected and not included within the final age calculation.

In dose recovery tests, mean recovered doses for the three alluvial fan samples (USU-251, USU-305, and USU-645) were within 10% of unity (Fig. 1.5d), suggesting that use of the 240 °C pre-heat in the SAR protocol is indeed suitable for LRR samples. Recovered doses showed greater variation for USU-651, the river terrace sample, ranging from 75-159% of the given dose for individual aliquots (mean of 103 ± 0.27%). This increased variability may reflect the different lithology of the terrace sediments as the E. Fork Big Lost River drains the Pioneer Mountains to the east. Only two of 34 total samples were collected from the E. Fork Big Lost River.

1.3.4 Calculation of Ages and Errors

OSL ages for each sample were calculated using the central age model (CAM; Galbraith et al., 1999) from a minimum of 21 aliquots of quartz sand that passed rejection criteria. Aliquots with recycling ratios or recuperation values >10 %, a low signal to background noise ratio (<3:1), feldspar contamination (infrared stimulation response), and a natural D_e value greater than the highest regenerative dose given were rejected and not included in age analysis. D_e values were obtained from dose response curves using saturating exponential and saturating exponential plus linear fits to the data. Uncertainty for sample D_e values was calculated at one standard deviation. Uncertainty in age estimates includes systematic and random errors from beta-source calibration, dose-rate estimation, and optical measurement errors according to the methods of Aitken and Alldred (1972) and Aitken (1976, 1985).

1.4 Results and Discussion

1.4.1 Dosimetry

Chemical data used to derive dose-rate values are shown in Table 1.1. Dose rates from traditional samples collected in metal pipes were derived from ICP-MS and ICP-AES analysis of a representative subsample of the sediment surrounding the sample. Of the 34 total samples, the two E. Fork Big Lost River samples and only four alluvial fan samples were collected by traditional methods. Dose rates from the traditional alluvial fan samples are in all cases greater than those for other samples from the same fan or same fan surface excavated from more coarse-grained portions of the deposit. The reasons for this will be discussed later.

For excavated samples, field inspection of the sampled deposits showed that both coarser grain sizes and the sandy matrix were primarily composed of carbonate lithologies, reflecting the overwhelming dominance of carbonate rocks in the drainage basins. To simplify sample processing, the < 2mm fraction was selected for initial dose-rate estimates as this was most similar to what would be collected while traditionally sampling a sand lens. To test the assumption that all grain sizes in LRR fan deposits would yield similar dose-rate results and that selecting only the < 2 mm fraction would produce accurate results, coarser grain sizes (>2 mm) were also analyzed as outlined in the methods (Section 2.2). Results from this analysis reveal that dose-rate results for LRR alluvial fan sediments are highly dependent on the grain size analyzed. When coarser grain sizes are analyzed separately or included with the bulk sediment samples, measured elemental concentrations almost always decrease for U, Th, Rb, and especially

Table 1.1 Sample chemistry and resulting dose rates. Footnotes indicate sample collection methods as well as grain-size fraction and method used to measure sediment chemistry. Site numbers refer to locations shown in Fig. 1.2.

Alluvial fan	Site No.	USU Lab No.	Burial depth (m)	In Situ H_20[f] (wt %)	U (ppm)	Th (ppm)	K_20 (wt %)	Rb_20 (ppm)	Cosmic (Gy/ka)	Dose Rate±1 standard error (Gy/ka)
Willow	1	USU-412[a,d]	1.4	1.7	4.0±0.3	4.9±0.4	1.53±0.05	66.8±4.0	0.25	2.70±0.18
Creek	2	USU-413[a,d]	2.0	2.9	3.8±0.3	4.9±0.4	1.60±0.05	70.9±5.4	0.24	2.67±0.18
Birch	3	USU-414[b]	2.0	6.5	1.2±0.1	2.4±0.2	0.67±0.02	25.4±1.0	0.23	1.13±0.06
Springs	4	USU-415[a,d]	1.5	0.3	1.2±0.1	1.6±0.2	0.52±0.08	19.2±1.3	0.25	1.01±0.08
	4	USU-645[a,d]	1.3	0.5	1.2±0.1	1.5±0.2	0.48±0.05	19.5±2.3	0.26	0.98±0.07
	4	USU-646[a,d]	1.5	1.5	1.2±0.2	1.5±0.4	0.49±0.10	17.8±3.4	0.25	0.98±0.10
	4	USU-647[a,d]	1.5	1.2	1.2±0.1	1.5±0.2	0.48±0.06	18.5±2.4	0.25	0.97±0.08
	5	USU-703[a,e]	1.8	2.4	1.1±0.1	1.3±0.2	0.48±0.02	17.3±0.7	0.25	0.94±0.06
	6	USU-704[a,e]	1.7	1.8	0.8±0.1	1.1±0.2	0.37±0.01	11.5±0.5	0.25	0.75±0.05
Upper	7	USU-251[b]	1.9	1.1	2.0±0.1	12.3±1.1	2.88±0.07	120.8±4.8	0.24	3.88±0.17
Cedar	8	USU-417[c,e]	5.0	1.9	3.1±0.2	4.2±0.4	1.33±0.03	56.5±2.5	0.16	2.23±0.10
Creek	9	USU-419[a,e]	1.2	3.5	2.8±0.2	5.2±1.3	1.28±0.06	60.3±2.4	0.27	2.27±0.14
	10	USU-652[c,e]	3.2	3.9	3.0±0.2	4.5±0.5	1.35±0.24	58.2±4.7	0.21	2.25±0.19
	11	USU-299[a,e]	2.3	1.8	2.5±0.2	1.6±0.4	0.42±0.10	17.5±0.7	0.22	1.19±0.10
	11	USU-300[a,e]	3.2	1.4	2.4±0.2	1.9±0.3	0.51±0.10	24.8±6.2	0.19	1.25±0.10
	12	USU-653[a,e]	1.6	1.2	2.1±0.2	1.7±0.4	0.46±0.08	19.1±0.8	0.24	1.18±0.09
	13	USU-301[a,e]	1.9	3.6	2.7±0.3	1.8±0.4	0.48±0.14	27.1±1.1	0.24	1.33±0.13
	14	USU-416[a,e,g]	15.0	1.8	2.7±0.6	1.6±0.5	0.40±0.11	14.7±0.6	0.06	1.06±0.15
	14	USU-302[a,e]	20.0	4.4	2.6±0.2	2.8±0.3	0.75±0.04	32.2±1.3	0.04	1.36±0.10
	15	USU-420[a,d]	1.7	2.2	3.3±0.4	3.4±0.7	1.02±0.03	45.7±8.7	0.24	1.95±0.21
	16	USU-250[b]	1.6 & 18[h]	0.3	3.2±0.2	4.9±0.4	1.49±0.04	69.1±2.8	0.24& 0.05	2.25±0.16
	17	USU-644[c,e]	3.5	0.5	2.4±0.4	2.1±0.8	0.61±0.15	33.7±1.3	0.18	1.31±0.15
Rams-	18	USU-305[a,d]	1.9	3.5	2.1±0.1	1.7±1.0	0.51±0.30	19.5±11.5	0.23	1.18±0.20
horn	19	USU-306[a,d]	2.0	3.2	2.5±0.3	2.2±1.1	0.66±0.35	24.7±13.3	0.23	1.45±0.24

Table 1.1 (continued) Sample chemistry and resulting dose rates. Footnotes indicate sample collection methods as well as grain-size fraction and method used to measure sediment chemistry. Site numbers refer to locations shown in Fig. 1.2.

Alluvial fan	Site No.	USU Lab No.	Burial depth (m)	In Situ H_20[f] (wt %)	U (ppm)	Th (ppm)	K_20 (wt %)	Rb_20 (ppm)	Cosmic (Gy/ka)	Dose Rate±1 standard error (Gy/ka)
Rams-	20	USU-307[a,d]	1.8	2.1	2.1±0.2	1.4±0.5	0.37±0.14	13.6±4.8	0.23	1.06±0.11
horn	21	USU-648[a,e]	1.6	3.2	2.0±0.1	3.2±1.1	0.81±0.14	46.4±16.7	0.24	1.53±0.14
	22	USU-649[a,e]	2.0	7.2	2.2±0.2	1.7±0.2	0.52±0.01	20.7±0.8	0.22	1.20±0.08
	22	USU-650[a,e]	1.6	3.0	1.9±0.1	1.4±0.6	0.41±0.13	20.2±0.8	0.24	1.06±0.11
King	23	USU-421b	1.0	0.6	3.2±0.2	9.7±0.9	1.84±0.05	73.6±2.9	0.25	3.09±0.14
Canyon	24	USU-422a,d	1.6	2.6	3.1±0.2	4.2±1.5	1.08±0.28	42.4±10.2	0.24	2.05±0.23
	25	USU-655a,e	1.9	2.0	2.8±0.4	4.1±0.4	1.19±0.11	42.3±1.7	0.23	2.09±0.16
	26	USU-656a,e	2.0	2.4	2.1±0.2	3.0±0.3	0.80±0.02	31.8±1.3	0.22	1.49±0.10
E. Fork	27	USU-304b	13.4	4.2	3.7±0.3	12.0±1.1	2.67±0.07	107.3±4.3	0.07	3.72±0.27
Big Lost terraces	28	USU-651b	1.1	2.2	3.9±0.3	13.5±1.2	3.06±0.08	125.8±5.0	0.26	4.55±0.21

a. Alluvial fan sheetflood deposits sampled at night or under tarps.
b. Tube sample from large sand lens.
c. Small sand lens sampled at night.
d. Chemistry based on average values from <2 mm grain size fraction and ~125-2000µm grain-size fraction.
e. Chemistry based on bulk sediment samples with all grain sizes in correct proportion.
f. If measured H2O content <3%, H2O content modeled as 3 ± 3% for the Holocene and 8 ± 8% for the late Pleistocene. If measured H2O content >3%, measured value used.
g. Signs of U/Th disequilibrium.
h. Burial depth modeled due to changes over time.

K, resulting in a lower dose rate (Fig. 1.6). This is due to the lower concentration of these elements in the predominately carbonate lithology source rocks.

Dose rates based on the inclusion of coarser grain sizes (>2 mm) were always less than dose rates based on the <2 mm grain-size fraction. However, the magnitude of this decrease with the inclusion of coarser grains varied widely, from ~0.4-40% with an average of 18%. In addition, the magnitude of change varied widely for a single alluvial fan or even a single surface of an alluvial fan despite homogenous rock type. As such, no average decrease due to inclusion of coarser grains could be assumed and applied to other

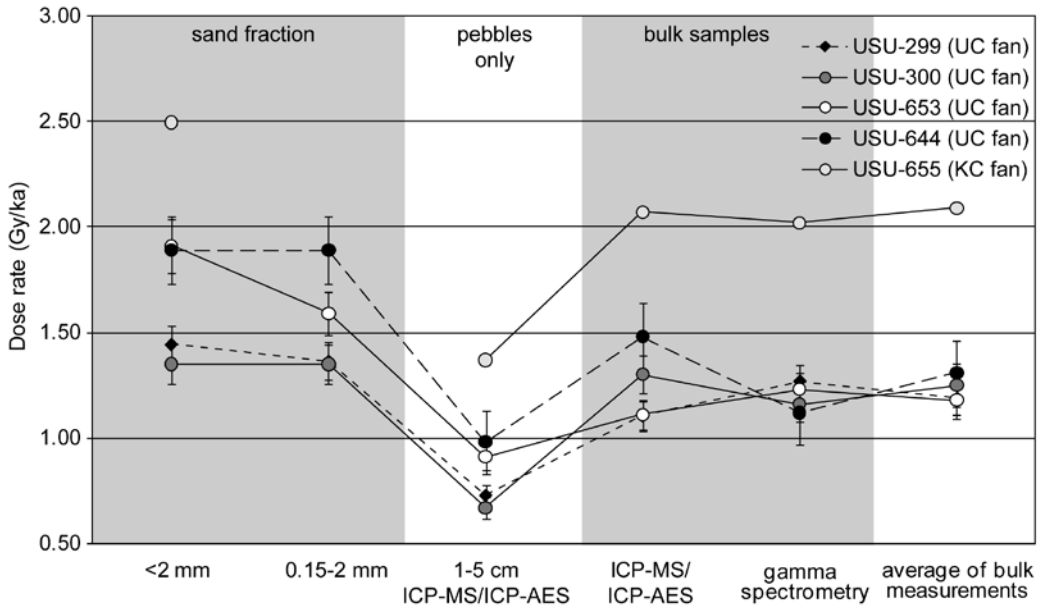

Figure 1.6 Dependence of dose rate on grain size fraction used for analysis as well as method used to measure sediment chemistry. Results are shown for five samples, all collected by excavation methods at night or under tarps from gravelly sheetflood deposits. Note that the fine grain fractions contribute higher dose rates than the predominately carbonate lithology pebble-size fractions. The average of bulk measurements were used to calculate age estimates for deposition.

sample sites, and each sample site had to be investigated individually. In general, analysis of the <2 mm fraction produced the highest dose rate estimates, while analysis of only coarser sizes (~0.15-2 mm and grains > 2 mm) generally produced the lowest dose-rate estimates (Fig. 1.6). Analysis of bulk samples generally produced dose-rate estimates somewhere between these two estimates (Fig. 1.6). The dose-rate estimates derived from bulk samples are assumed to provide the most accurate dose-rate estimates as they took into consideration the dose-rate contribution from all grain size fractions. Results from ICP-MS/ICP-AES analysis and gamma spectrometry of bulk samples were generally in agreement (Fig. 1.6). Chemistry results from these two methods were averaged, and the resulting dose rate used for age estimates.

We were unable to collect a bulk sediment sample for dose rate for some excavated samples from back-hoe trenches because of requirements to close trenches as quickly as possible. For these eleven samples, the dose rate is based on an average of the chemistry results from the <2 mm fraction and the 0.15-2 mm fraction. When including the 0.15-2 mm grain-size fraction, dose rate decreases for these samples ranged from 1-12% (average 8%), which falls within the lower end of the changes seen for samples with a bulk dose-rate sample. Comparison to bulk dose-rate estimates suggests that dose rates based on the average of analyses from the 0.15-2.0 mm and total <2 mm grain-size fractions may still overestimate dose rate by an average of ~10%. This is based on the ~18% average decrease in bulk sediment dose rate compared to the <2 mm fraction dose rate and the ~8% average decrease in 0.15-2.0 mm fraction dose rates compared to the <2 mm fraction dose rate. As such, we interpret sample ages based on an average of the two sand grain-size fraction dose rates as minimum ages that may be on average ~10% too

young. Despite this, the true age for many of these samples likely lie within error of the central age model (CAM; Galbraith et al., 1999) age reported, suggesting that this may still provide an appropriate way too estimate dose rate in these settings. Further, ages estimates for different samples from the same surface with dose rates estimated from different grain-size fractions do often show good agreement (see Table 1.2 and further discussion of this in Section 4.3).

The dependence of dose rate on the grain-size fraction analyzed likely results from slight differences in the lithology between the coarse (>2 mm) and fine (<2 mm) fractions. The majority of >2 mm grains in the fan deposits have carbonate lithologies, which produced a low dose due to lower concentrations of K, U, and Th, as seen in our analysis (rocks/pebbles in Fig. 1.6). While the <2 mm fraction is also predominately carbonate as determined by visual identification and reaction to HCl, slight differences in lithology for this fraction likely produce the increased K, U, Th, and Rb concentrations and thus increased dose rates. Some of the differences in lithology may be attributable to the incorporation of loess into the <2 mm fraction during deposition as thick loess deposits mantle alluvial surfaces throughout the basin. Concentration of heavy minerals during sediment transport along with concentration of minerals more resistant to weathering may also alter the lithology of the <2 mm fraction. The result of increased K, U, Th, and Rb concentrations in the fine fraction is a greater dose-rate contribution per volume from the fine sediment in comparison to the low dose-rate carbonate pebbles and cobbles within the deposit.

Errors in estimating dose rate lead to similar errors in estimating luminescence ages. While the true dose rate in any fluvial deposit is not homogenous, additional

heterogeneities in the dose rate may be introduced in coarse-grained deposits. Hülle et al. (2009) also encountered problems in how to best determine dose rates for heterogeneous sediment, even when *in situ* measurements were used. In addition, Nathan et al. (2003) showed that variability in grain size and composition in sediments could lead to significant heterogeneity in the portion of dose derived from beta radiation, and suggest that careful consideration is required in determining what portions of the sediment to include for analysis. Even relatively small inaccuracies in estimated dose rates and associated ages can have important implications when attempting to interpret ages in the context of centennial to millennial scale climate change. Older samples are more greatly affected by this problem as a 10% difference in dose rate can produce and age estimate for deposition during a very different climate regime. As a result, dose rates need to be examined more thoroughly to detect the presence of heterogeneity and how best to estimate the average dose rate.

Table 1.2 Optical ages for Lost River Range alluvial fans and terraces of the East Fork Big Lost River. Site numbers refer to Fig. 1.2. WC = Willow Creek Alluvial Fan. BS = Birch Springs Alluvial Fan. UC = Upper Cedar Creek Alluvial Fan. RH = Ramshorn Alluvial Fan. KC = King Canyon Alluvial Fan. EFBL = East Fork Big Lost River terraces.

Sample type	Site no.	Fan	USU Lab no.	No. of aliquots	Mean D_e	Median D_e	Mean D_e /median D_e	Skew	Kurtosis	Over-dispersion	Dose rate (Gy/ka)	D_e (Gy) ± 1σ	Optical age (ka) ± 1 standard error
Traditional	3	BS	USU-414	26	12.25	11.72	1.05	0.20	-0.68	18.2±4.8	1.13±0.06	12.17±3.06	10.78±0.92
	7	UC	USU-251	25	15.80	15.52	1.02	0.17	-0.42	23.3±4.7	3.88±0.17	15.51±3.62	4.00±0.35
	16	UC	USU-250	24	132.5 5	136.45	0.97	-0.04	-0.91	17.0±3.0	2.25±0.16	132.41±23.21	58.73±5.52
	23	KC	USU-421	25	25.30	25.86	0.98	0.11	-1.08[a]	6.7±2.6	3.09±0.14	25.65±3.27	8.29±0.58
	27	EFBL	USU-304	33	143.8 2	145.54	0.99	0.25	-0.49	27.4±4.2	3.72±0.27	141.68±41.02	38.12±3.86
	28	EFBL	USU-651	23	29.90	28.41	1.05	0.45	-1.13[a]	25.9±5.5	4.55±0.21	29.48±9.20	6.48±0.61
Excavated thin sand lens	8	UC	USU-417	23	16.11	15.92	1.01	0.21	-0.29	13.5±3.0	2.23±0.10	16.20±3.06	7.26±0.54
	17	UC	USU-644	21	129.5 7	124.13	1.04	-0.08	0.75	15.5±3.3	1.31±0.15	126.32±24.21	96.65±12.81
	10	UC	USU-652	24	18.17	17.97	1.01	0.69[a]	0.90	12.8±4.5	2.25±0.19	18.69±4.64	8.29±0.87
Excavated	1	WC	USU-412	24	36.95	37.32	0.99	-0.38	-0.65	12.7±2.7	2.70±0.18[b]	38.39±7.14	14.22±1.25
	2	WC	USU-413	22	38.63	39.13	0.99	0.52	0.40	26.8±4.6	2.67±0.18[b]	37.44±10.76	14.01±1.44
	4	BS	USU-415	23	31.74	31.75	1.00	0.38	0.33	14.7±2.6	1.01±0.08[b]	31.58±5.35	31.17±3.05
	4	BS	USU-645	27	27.44	26.88	1.02	0.36	-0.38	18.3±3.0	0.98±0.07[b]	26.90±5.63	27.33±2.60
	4	BS	USU-646	24	26.72	24.69	1.08	0.46	-0.88	26.4±4.8	0.98±0.10[b]	26.00±7.68	26.64±3.38
	4	BS	USU-647	22	28.39	28.36	1.00	0.57[a]	-0.06	14.5±3.1	0.97±0.08[b]	27.85±4.75	28.70±2.79
	5	BS	USU-703	24	44.79	46.44	0.96	0.65[a]	-0.13	19.4±3.1	0.94±0.06	44.25±8.31	47.19±4.27
	6	BS	USU-704	28	36.24	34.52	1.05	0.56[a]	-0.68	25.5±4.3	0.75±0.05	35.59±10.07	47.32±4.63
	9	UC	USU-419	24	21.73	20.99	1.04	0.49	0.14	17.3±3.7	2.27±0.14	21.50±5.08	9.47±0.83

Table 1.2 (continued) Optical ages for Lost River Range alluvial fans and terraces of the East Fork Big Lost River. Site numbers refer to Fig. 1.2. WC = Willow Creek Alluvial Fan. BS = Birch Springs Alluvial Fan. UC = Upper Cedar Creek Alluvial Fan. RH = Ramshorn Alluvial Fan. KC = King Canyon Alluvial Fan. EFBL = East Fork Big Lost River terraces.

Excavated	11	UC	USU-299	28	28.49	28.76	0.99	-0.15	-0.75	22.2±4.2	1.19±0.10	28.10±7.29	23.63±2.59
	12	UC	USU-653	31	25.81	27.70	0.93	-0.35	-0.84	33.0±4.8	1.18±0.09	24.91±8.61	21.07±2.33
	13	UC	USU-301	26	32.42	33.02	0.98	-0.23	-0.76	14.4±3.6	1.33±0.13	34.60±8.25	26.03±3.04
	14	UC	USU-416	24	120.24	117.61	1.02	0.16	-0.42	17.6±3.7	1.06±0.15	122.25±25.76	115.83±18.52
	14	UC	USU-302	22	132.17	126.42	1.05	0.32	-1.14[a]	13.0±3.8	1.36±0.10	132.08±25.71	97.08±9.63
	15	UC	USU-420	29	95.69	94.11	1.02	0.08	-0.16	13.6±3.0	1.95±0.21[b]	100.32±17.76	51.40±6.27
	18	RH	USU-305	37	46.91	42.46	1.10	0.30	-0.97[a]	25.6±3.6	1.18±0.20[b]	46.27±12.28	39.28±7.22
	19	RH	USU-306	26	21.46	21.82	0.98	0.19	-0.72	22.2±4.3	1.45±0.24[b]	21.49±5.79	15.12±2.75
	20	RH	USU-307	21	47.15	44.56	1.06	0.51	-0.25	23.8±5.5	1.06±0.11[b]	47.95±13.42	45.05±6.02
	21	RH	USU-648	23	25.92	24.72	1.05	0.01	-1.11[a]	12.3±3.0	1.53±0.14	27.11±5.33	17.69±1.95
	22	RH	USU-649	22	28.20	27.05	1.04	0.92[a]	0.37	18.6±3.5	1.20±0.08	28.01±6.43	23.36±2.18
	22	RH	USU-650	27	27.04	29.10	0.93	-0.30	-1.29[a]	20.8±3.4	1.06±0.11	26.61±5.95	25.01±3.03
	24	KC	USU-422	25	27.73	27.61	1.00	0.39	1.47[a]	13.1±3.5	2.05±0.23[b]	28.69±6.46	13.99±1.80
	25	KC	USU-655	27	29.22	29.60	0.99	-0.29	-0.59	34.3±5.6	2.09±0.16	27.76±9.14	13.29±1.53
	26	KC	USU-656	27	31.61	30.88	1.02	0.29	-0.65	22.7±3.9	1.49±0.10	31.35±8.65	21.10±2.00

Error on age includes random and systematic errors calculated in quadrature using 1 standard error for the D_e distribution.
a. significant values for kurtosis and skew
b. dose rate determined from the sand-sized fractions of excavated sheet flood deposits

1.4.2 Equivalent Dose Results

Fig. 1.7 shows five examples of D_e distributions represented as histograms, cumulative probability distributions, and radial plots. Examples were chosen to represent results from both traditional and excavated samples with a range of D_e distributions characteristics (skew, kurtosis, and overdispersion) as well as a range of resulting age estimates. In addition, various statistical metrics (mean:median ratio, skew, kurtosis, and overdispersion) for D_e distributions are shown in Table 1.2.

In order to detect partial bleaching, small aliquots of sand (~200 grains) were used during measurement of the natural signal as this decreases averaging of the signal from grains with different bleaching histories and increases the chances of identifying grains retaining residual signals (Olley et al., 1998,1999; Wallinga, 2002). Resulting D_e distributions were checked for significant positive skew as this can indicate the presence of poorly bleached grains (e.g., Olley et al., 1998, 1999; Lepper and McKeever, 2002). Resulting average skew values are 0.19 ± 0.34. None of the traditionally collected samples have significant skew, but three excavated samples have significant positive skew (USU-647, USU-704, USU-649; Table 1.2 and Fig. 1.7) and one has significant negative skew (USU-703; Table 1.2).

Analysis of $D_e(t)$ plots was also used to check for partial bleaching (Bailey et al., 2003). Poorly bleached grains are thought to retain more residual signal in their intermediate and slow components, producing greater D_e estimates if later portions of the signal decay curve are integrated. Results for $D_e(t)$ analysis of two samples, one collected from sheetflood gravels and with high positive skew (USU-652) and one a

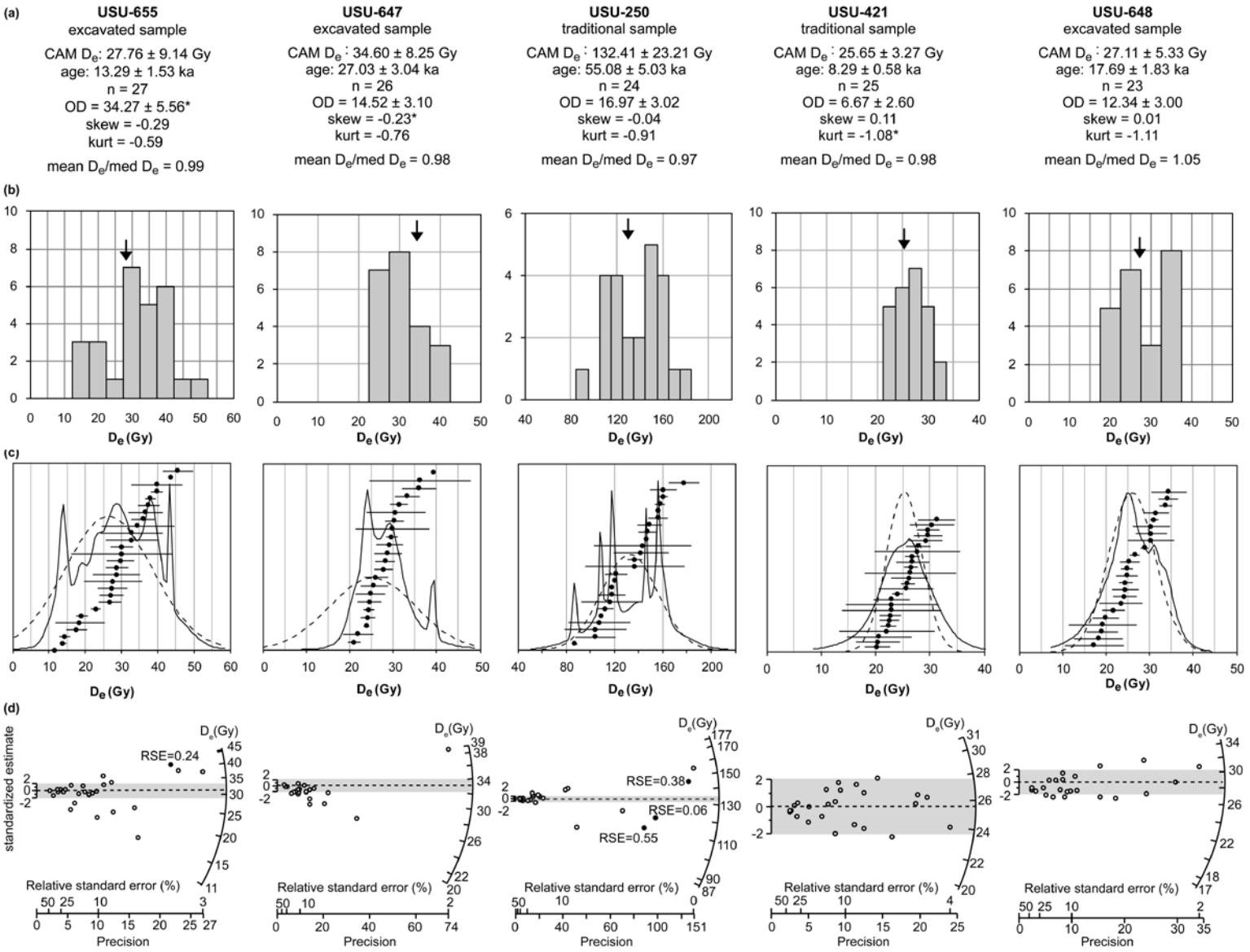
(a)
USU-655
excavated sample
CAM De: 27.76 ± 9.14 Gy
age: 13.29 ± 1.53 ka
n = 27
OD = 34.27 ± 5.56*
skew = -0.29
kurt = -0.59
mean De/med De = 0.99
USU-647
excavated sample
CAM De : 34.60 ± 8.25 Gy
age: 27.03 ± 3.04 ka
n = 26
OD = 14.52 ± 3.10
skew = -0.23*
kurt = -0.76
mean De/med De = 0.98
USU-250
traditional sample
CAM De : 132.41 ± 23.21 Gy
age: 55.08 ± 5.03 ka
n = 24
OD = 16.97 ± 3.02
skew = -0.04
kurt = -0.91
mean De/med De = 0.97
USU-421
traditional sample
CAM De : 25.65 ± 3.27 Gy
age: 8.29 ± 0.58 ka
n = 25
OD = 6.67 ± 2.60
skew = 0.11
kurt = -1.08*
mean De/med De = 0.98
USU-648
excavated sample
CAM De : 27.11 ± 5.33 Gy
age: 17.69 ± 1.83 ka
n = 23
OD = 12.34 ± 3.00
skew = 0.01
kurt = -1.11
mean De/med De = 1.05
(b)
De (Gy)
(c)
De (Gy)
(d)
standardized estimate
De(Gy)
RSE=0.24
RSE=0.38
RSE=0.06
RSE=0.55
Relative standard error (%)
Precision
a. significant skew or kurtosis value

Figure 1.7 (previous page) Examples of equivalent dose (D_e) distributions for Lost River Range alluvial fan samples of varying age and collection method. (a) Sample numbers are shown with their collection method. Excavated sample refers to samples collected by excavating sediment from sandy sheetflood deposits at night or under light-safe tarps. Traditional samples refers to samples collected from thick sand lenses by pounding a metal tube into the lens. Also shown are central age model D_e estimates (CAM; Galbraith et al., 1999) and the resulting age estimate as well as relevant statistics for the D_e distribution. Sample USU-655 provides an example of a distribution with significant overdispersion while USU-647 and USU-421 provide examples of distributions of significant skew and kurtosis, respectively. (b) D_e distributions shown as histograms. Arrow indicates D_e estimate from CAM. (c) D_e distributions shown as cumulative probability density plots. Black dots show D_e estimates ± 1σ. The solid line shows the sum of weighted distributions and the dashed line shows the average D_e. (d) Radial plots for D_e distributions. The relative standard error (RSE) has been changed for data points indicated by a closed circle in order to better display results. The calcualted RSE is shown next to the data point. Alluvial fan samples generally produce similar D_e distributions regardless of deposit sampled, sample collection method, or resulting age.

sample traditionally collected from a sand lens (USU-421) are shown in Fig. 1.8. D_e results for natural and regenerative doses are similar for all portions of the decay curve and do not show significant increase with integration time as would be expected for poorly bleached samples. However, other studies do suggest that this may not be a good indicator of partial bleaching as the stability of the medium component can influence results (Wallinga, 2002; Jain et al., 2003).

Error not attributable to partial bleaching or instrument error, such as sediment mixing after deposition or heterogeneity in the dose rate, may be indicated by D_e distributions that are broader than expected for a normal distribution (e.g., Kalchgruber et al., 2003). Significantly negative kurtosis (at the 1σ level) and overdispersion (OD) values greater than a critical value were interpreted as indicators of additional sources of

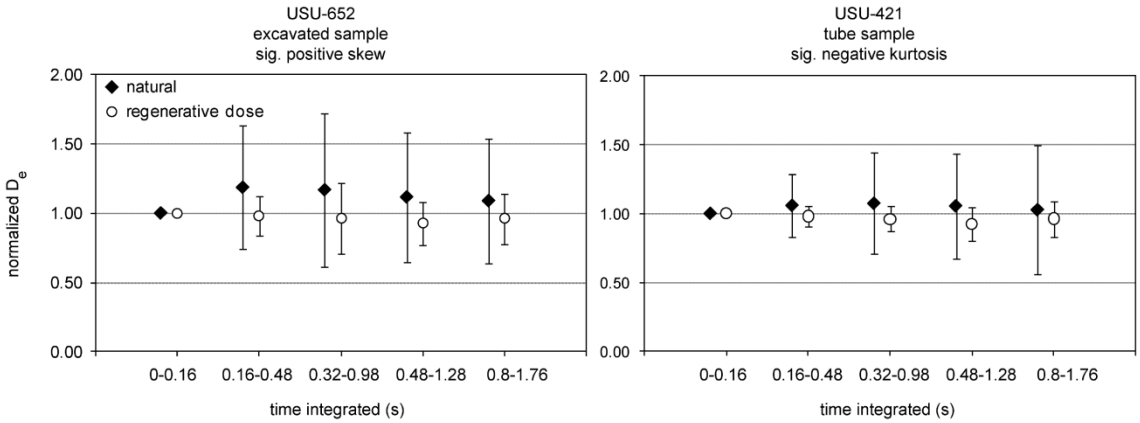

Figure 1.8 Examples of $D_e(t)$ plots used to check for partial bleaching (Bailey et al., 2003). USU-652 was collected by excavating sediment from a thin sand lens within a coarse grained sheetflood deposit and produced a Holocene age estimate (8.29 ± 0.87 ka) while USU-421 was collected by pounding a metal tube into a thick sand lens and also returned a Holocene age estimate (8.29 ± 0.58 ka). D_e estimates for natural and regenerated doses are similar for integration of various portions of the signal decay curve suggesting that the medium and slow components of the OSL sample are well bleached and partial bleaching is not a concern.

error. As overdispersion values up to 20% have been observed for well-bleached samples (e.g. Roberts et al., 1998; Jacobs et al., 2003 a,b, Olley et al., 2004 a,b; Galbraith et al., 2005), we have chosen 20% as our critical value for identifying samples that may have problems with dose-rate heterogeneity, partial bleaching, or other factors such as post-depositional mixing. Four of six traditionally collected samples had significantly negative kurtosis and/or OD >20% while 12 of 28 excavated samples have significant negative kurtosis and/or OD >20% (see Table 1.2). OD values from D_e distributions produced for age calculations were higher than OD values from dose recovery tests (18-26% vs. 5-25%). Kalchgruber et al. (2003) observed similar results with irradiated samples producing D_e distributions with smaller standard deviations than those produced by the natural sediment. This indicates that some portion of the OD for D_e distributions is attributable to partial bleaching, post-deposition mixing, or dose-rate heterogeneity.

Because samples do not show strong evidence for partial bleaching and were collected from >1 m in depth in deposits that appeared undisturbed, the most likely source of significant kurtosis and OD may be variability in the microdosimetry. Indeed, numerous studies using small or single-grain aliquots have suggested that heterogeneity in the dose contribution of the sediment, particularly in the beta dose, can produce greater variability in measured D_es (Olley et al., 1997; Murray and Roberts, 1997; Nathan et al., 2003; Vandenberghe et al., 2003; Mayya et al., 2006). Kalchgruber et al. (2003) also observed higher OD values for natural vs. laboratory radiated samples and attributed this to dose-rate heterogeneity within the sediment.

Samples collected from the fans by the traditional method of pounding a tube into a thick sand lens or by excavation of a thin sand lens are limited (3 and 4 samples, respectively), making any comparisons of the statistical metrics for different sample types less reliable. Nonetheless, results suggest that samples collected from sheetflood gravels are more likely to produce D_e distributions with significant skew, kurtosis, and OD (Fig. 1.9). The most probable explanation for this potential difference is the grain-size dependent heterogeneity in the dose rate detected for samples excavated from sheetflood gravels.

Accumulation of pedogenic $CaCO_3$ can also produce differences in microdosimetry for all types of sampled deposits (e.g., Nathan and Mauz, 2008). While care was taken to avoid collecting samples from locations with carbonate accumulation, the inclusion of clasts with thin, discontinuous coatings was often unavoidable as carbonate accumulation was observed to depths exceeding 3 meters at the bottom of

excavated trenches. Grains in areas with more significant carbonate accumulation would likely experience a decrease in dose rate through their burial history.

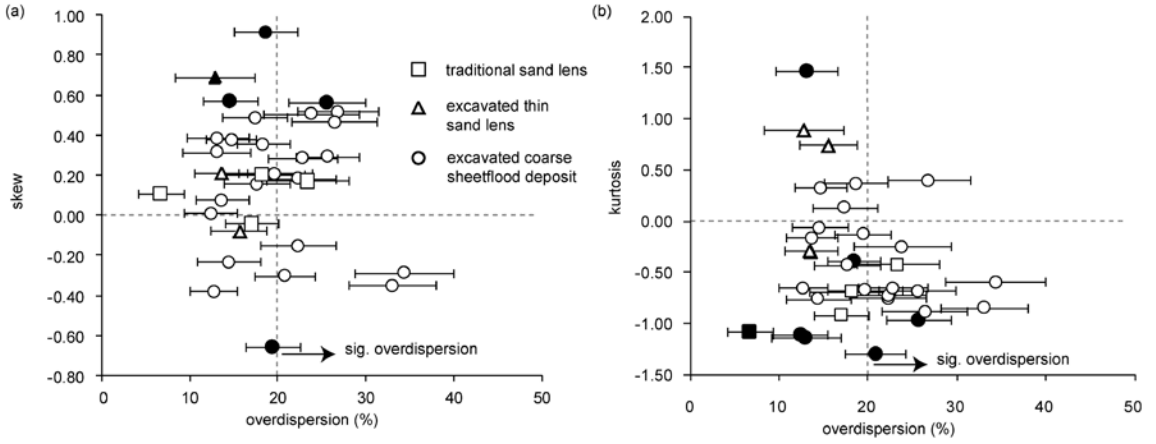

Figure 1.9 (a) Overdispersion (OD) values plotted against skew for D_e distributions of samples collected by traditional methods from thick sand lenses, samples excavated from thin sand lenses within coarse sheetflood deposits, and samples excavated from sandy sheetflood deposits. OD greater than 20% is considered significant and may suggest DR heterogeneity within the sampled sediment. This was a concern for samples from coarse-grained sheetflood deposits because of the greater range of grain sizes present and the dependence of DR estimates on grain-size fractions included in analyses. Significant skew values are shown by closed symbols with significant positive skew possibly symptomatic of partial bleaching (e.g., Olley et al., 1998, 1999; Lepper and McKeever, 2002). (b) Same as in (a) but with OD plotted against kurtosis. Significant negative kurtosis may be symptomatic of errors not attributable to instrumental error such as mixing of sediment after deposition or DR heterogeneity. Shaded symbols indicate significant kurtosis. All deposit types and their associated sampling method generally produce similar values for OD, skew, and kurtosis, indicating that the variability in results is not related to the depositional environment or greater DR heterogeneity for certain deposits.

Given the absence of strong evidence for partial bleaching, we did not use the minimum age model (MAM; Galbraith et al., 1999) to derive the D_e used in age calculations. Instead, a weighted mean using the central age model (CAM) of Galbraith et

al. (1999) was considered the most appropriate method for analysis of samples with broad D_e distributions with significant OD or kurtosis.

1.4.3 Analysis of Resulting Age Estimates

We obtained final age estimates for 32 samples from alluvial fans, and two samples from terraces of the E. Fork Big Lost River. OSL age estimates for the timing of deposition on LRR fans range from ~4-115 ka (Fig. 1.10), and the two samples from the E. Fork Big Lost River terraces return ages of 6.48 ± 0.61 ka and 38.12 ± 3.40 ka.

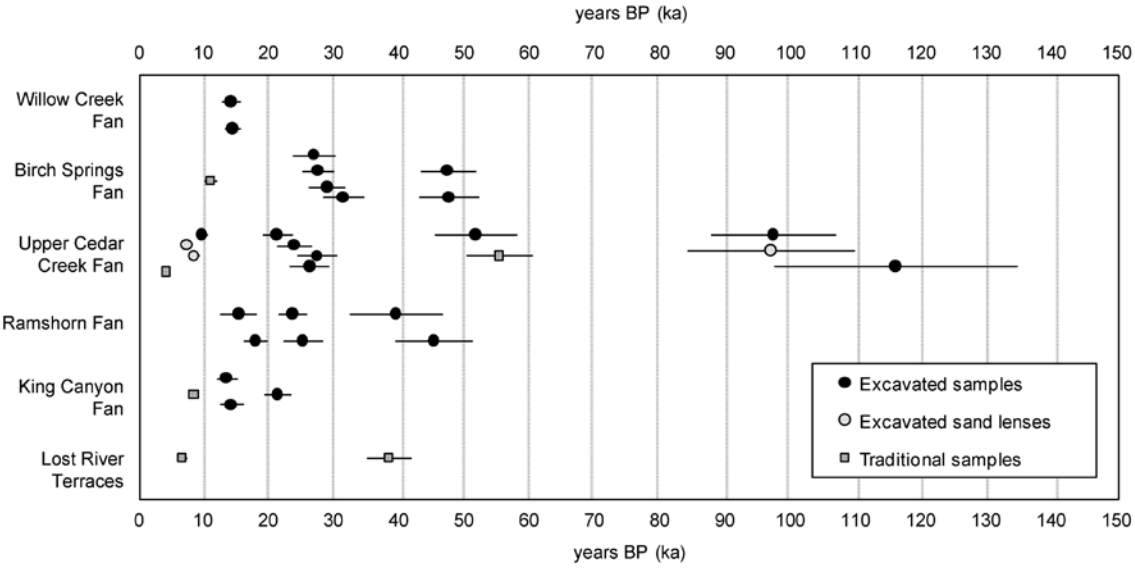

Figure 1.10 Graphical display of resulting optical age estimates for the timing of sediment deposition on Lost River Range alluvial fans and two terraces of the East Fork Big Lost River.

While there is little previous age control for comparison, there are several indications that dose-rate estimates and treatment of D_e distributions are producing accurate age estimates. First, good agreement was found between the age of a tephra

deposit and an OSL sample collected below the tephra (Fig. 1.11). The ~3-4 cm thick tephra deposit was found ~ 1 m below the surface within deposits exposed in an incised channel on Upper Cedar Creek Fan (site 9 in Fig. 1.2). The tephra was overlain by pebble and cobble gravel sheetflood deposits, which were capped by the modern soil with loess accumulation and infiltration to ~22 cm depth and stage II calcium carbonate accumulation. Immediately below the tephra was a probable buried soil, characterized by increased silt to fine sand that decreased with depth until sheetflood deposits were again visible. This resembles modern soils in which the accumulated loess at the surface has been mixed to some depth with the underlying fan gravels. Samples were collected from the tephra for identification by electron microprobe analysis at Washington State University's GeoAnalytical Lab as well as ICP-MS analysis at Boise State University. OSL sample USU-419 was excavated from this probable buried soil ~20 cm below the tephra. Both labs determined that the source of the tephra was Mt. Mazama, a stratovolcano whose eruption formed the present-day Crater Lake in Oregon, USA (~700 km west of the LRR). This eruption has been dated to 7627 ± 150 cal yr BP (Zdanowicz et al., 1999). An age of 9.47 ± 0.83 ka from the OSL sample is consistent with the tephra age, and the slightly older OSL age is consistent with its lower stratigraphic position. While the OSL sample from this site was collected from a probable buried soil rather than unaltered fan gravels (and therefore may provide an estimate of for the timing of

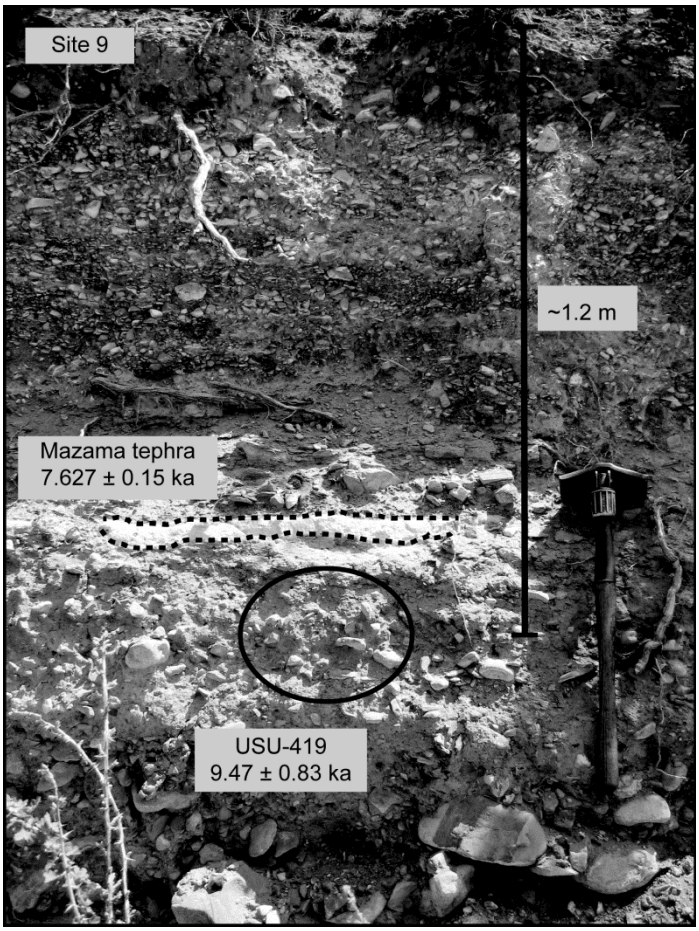

Figure 1.11 Close up of site 9 on Upper Cedar Creek Alluvial Fan where a deposit of Mazama tephra was identified and a sediment sample collected from the buried soil and alluvial gravels immediately below for optical dating (USU-419). Sample USU-419 was collected by excavating the sediment from the deposit at night, and the dose rate based on analysis of a bulk sediment sample collected from a 30 cm radius around the sample. The sample produces a reasonable age estimate (9.47 ± 0.83 ka) in relation to the age for the Mazama tephra above (7627 ± 150 cal yr BP; Zdanowicz et al., 1999).

loess deposition and surface stability rather than fan aggradation), it was still collected from a deposit with a highly heterogeneous grain-size distribution. As such, the results likely provide some measure of the ability of our methods to accurately estimate dose rate and thus age in sediments with a wide range of grain sizes.

Second, OSL ages correspond with other age estimates of LRR fan surfaces based on the thickness of pedogenic carbonate coats developed on the underside of clasts within fan surface soils (Pierce and Scott, 1982; Vincent et al., 1994; Patterson, 2006). With this method, Pierce and Scott (1982) and Patterson (2006) inferred that the late Pleistocene was a time of active aggradation for LRR fans. For example, Patterson (2006) estimated that surface stabilization occurred 28±20 ka for the surface of sites thirteen and eleven on Upper Cedar Creek Fan. This estimate shows reasonable agreement with our optical ages of 23.63 ± 2.59 ka, 27.16 ± 2.91 ka and 26.03 ± 3.04 ka. While the uncertainty on carbonate coat derived ages is too large to provide an accurate assessment of our OSL results, the two methods show a good first order agreement in age.

Third, multiple samples collected from the same trench return ages for deposition that are in good agreement. The trench at site 22 on Ramshorn Fan (Fig. 1.2b) provides the best example of this, with two samples excavated from depths of 1.6 m (USU-650) and 2 m (USU-649) as shown in Fig. 1.12a. Bulk samples for dose-rate estimation were collected for these samples, and final dose rates derived from an average of ICP-MS/ICP-AES and gamma spectrometry of these samples. The resulting central ages for these samples suggest a minor age reversal as the sample closer to the surface produces an age of 25.01 ± 3.03 ka (USU-650) and the deeper sample produces an age of 23.36 ± 2.18 ka (USU-649). However, these ages are within error, suggesting that they do indeed produce consistent ages as expected for samples from similar depths. These results indicate that our collection and analysis methods are appropriate for these deposits.

At site 4 on Birch Springs Fan (Fig. 1.2a), four samples collected from a single trench also show good agreement (Fig. 1.12b), despite the fact that bulk samples for

dose-rate analysis were not collected and dose-rate analysis was limited to the sand-size fractions. USU-415 and USU-647 were collected adjacent to each other at ~1.5 m depth on the northern end of the trench, while USU-645 and USU-646 were collected from depths of 1.25 and 1.5 m, respectively, in the center of the trench. Adjacent samples from the western end of the trench produced similar ages for deposition of 31.17 ± 3.05 ka (USU-415) and 28.70 ± 2.79 ka (USU-647). Similarly, the samples from the center of the trench agree, returning ages of 27.33 ± 2.41 ka (USU-645) and 26.64 ± 3.29 ka (USU-646). When considering all four samples collected within 0.5 m stratigraphic depth of each other, the results are within error and provide an estimate of 28.6± 2.0 ka for timing of deposition of this surface. However, as noted, dose-rate estimates for these four samples lack analysis of bulk samples. This, as well as pedogenic carbonate accumulation, could be contributing to the minor age reversals present at this site. Analysis of bulk dose-rate samples may improve results, but trenches were required to be filled before these samples could be collected.

Finally, multiple samples collected from different locations on the same geomorphic surface often return ages that are in good agreement. For example, Willow Creek Fan is composed almost entirely of one large surface that was sampled at two locations (USU-412 at site 1 and USU-413 at site 2; Fig. 1.2a). The resulting ages of 13.92 ± 1.32 ka and 13.86 ± 2.64 ka show very good agreement for the age of this surface (Table 1.2). Another significant surface on King Canyon Fan was sampled in two different locations (USU-422 at site 24 and USU-655 site 25; Fig. 1.2b), returning ages in good agreement of 13.99 ± 1.80 ka and 13.29 ± 1.53 ka (Table 1.2). Several surfaces of Upper Cedar Creek also produce multiple ages with good agreement (Fig. 1.2c). The

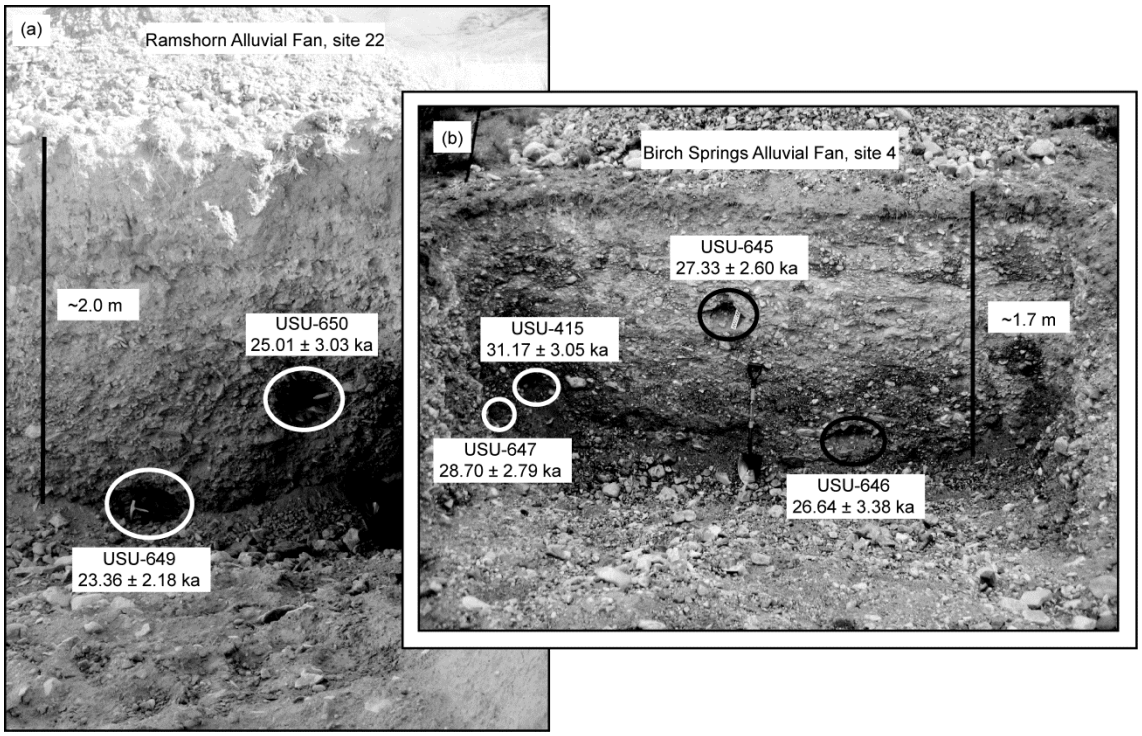

Figure 1.12 (a) Optical ages for two samples (USU-649 and USU-650) collected by excavating the sediment from the coarse-grained sheetflood deposit at night or under tarps at site 22 on Ramshorn Alluvial Fan. The resulting ages show good agreement. The minor reversal in the central ages for each sample may be due to factors such as DR heterogeneity, sediment mixing after deposition, or accumulation of pedogenic carbonate. (b) Optical ages for four samples (USU-647, USU-415, USU-645, and USU-646), also collected by excavating the sediment from the coarse-grained sheetflood deposit at night or under tarps at site 4 on Birch Springs Alluvial Fan. The resulting ages here also show good agreement and minor reversals in the central ages may result for similar reasons as in part (a).

youngest was sampled in four locations (USU-251 at site 7, USU- 421 at site 23, USU-417 at site 8, and USU-419 at site 9) with all samples returning Holocene ages from ~4-9 ka (Table 1.2). Another surface of Upper Cedar Creek Fan was sampled in 3 locations (USU-299 and USU-300 from site 11, and USU-301 at site 13) produced ages from ~23-26 ka.

Despite overall consistency of OSL ages with the geomorphic and stratigraphic relationships, at one location there is a significant age reversal. At site 14 on Upper Cedar Creek Fan, two samples, USU-416 and USU-302, were collected from a 30 m exposure from depths of approximately 15 m and 20 m, respectively (Fig. 1.13). Resulting ages of 115.83 ± 18.52 ka (USU-416) and 97.08 ± 9.63 ka (USU-302) show

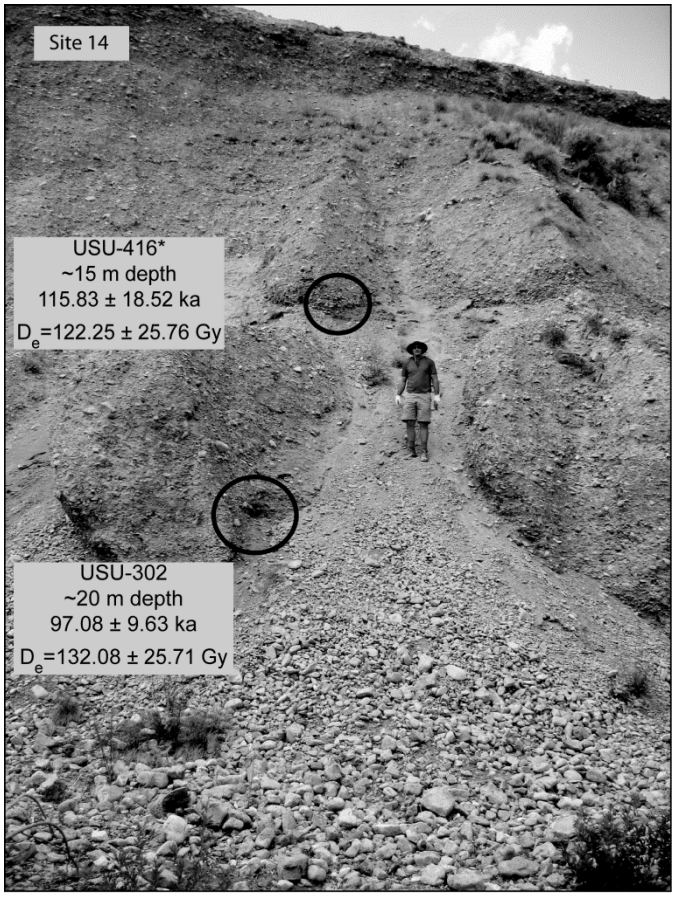

Figure 1.13 The ~30 m exposure at site 14 on Upper Cedar Creek Alluvial Fan with the locations of two OSL samples: USU-416 from ~15 m below the surface and USU-302 from ~20 m below the surface. The central age estimates of 115.83 ± 25.76 ka (USU-416) and 97.08 ± 9.63 ka show a reversal based on the locations of the samples in the stratigraphy. Though the equivalent doses are consistent with the stratigraphy, the age reversal likely results from U/Th disequilibrium in the dose rate as suggested by analysis of sediment chemistry showing an excess of U in relation to Th.

reasonable agreement but central ages are reversed based on the stratigraphic relationship. Analysis of sediment chemistry for dose-rate estimation suggests a problem with U/Th disequilibrium for USU-416. While the greater D_e of USU-302 is consistent with its stratigraphic position as the older sample, potential dose-rate disequilibrium in USU-416 produces the reversal in age estimates.

In three locations OSL ages from geomorphically lower/younger surfaces produces older ages than samples from geomorphically higher/older surfaces. These situations may be readily and most logically explained as instances of fill-cut terrace formation, or alluvial strath, in which vertically stacked deposits are incised (Fig. 1.14). Morphology of LRR fans indicates that these are indeed stacked fans where deposits have accumulated vertically rather than in a telescoping nature. One of the alluvial straths occurs on Ramshorn at sites 18, 19, and 22 (Fig.14a). The geomorphically higher/older surfaces of sites 19 and 22 produce OSL ages of 15.12 ± 2.75 ka (site 19), 23.26 ± 2.18 ka (site 22), and 25.01 ± 3.03 ka (site 22), but the geomorphically lower/younger surface of site 18 produces a much older OSL age of 39.28 ± 7.22 ka. After deposition of the ~39 ka sediment at site 18, the fan likely continued to aggrade vertically until deposition of the ~23-25 ka sediment at site 22. This surface was then incised and abandoned. Within the incised area, renewed deposition created an inset surface that includes the ~15 ka sediment at site 19. Finally, the most recent interval of erosion created the alluvial strath of site 18 with incision through the inset surface and into older deposits below, leaving the ~39 ka sediment buried under only a thin veneer of younger sediment.

A second alluvial strath surface occurs at sites 5 and 6 on Birch Springs Fan (Fig. 1.14b) where, despite a ~12 m height difference between these surfaces, OSL samples

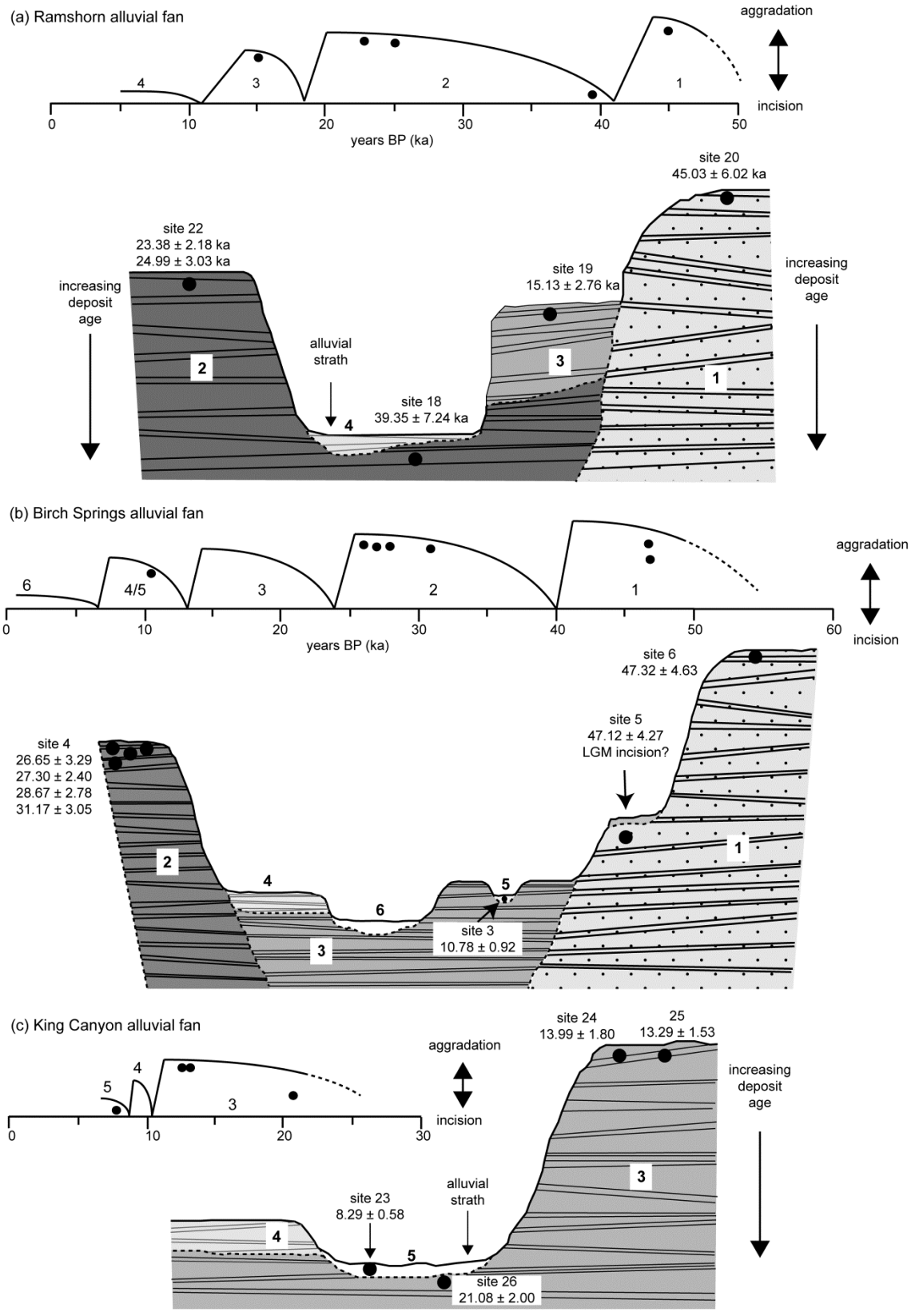
(a) Ramshorn alluvial fan
aggradation
incision
4
3
2
1
0
10
20
30
40
50
years BP (ka)
site 20
45.03 ± 6.02 ka
site 22
23.38 ± 2.18 ka
24.99 ± 3.03 ka
site 19
15.13 ± 2.76 ka
increasing
deposit
age
increasing
deposit
age
alluvial
strath
site 18
39.35 ± 7.24 ka
(b) Birch Springs alluvial fan
aggradation
incision
6
4/5
3
2
1
0
10
20
30
40
50
60
years BP (ka)
site 6
47.32 ± 4.63
site 5
47.12 ± 4.27
LGM incision?
site 4
26.65 ± 3.29
27.30 ± 2.40
28.67 ± 2.78
31.17 ± 3.05
site 3
10.78 ± 0.92
(c) King Canyon alluvial fan
site 24
13.99 ± 1.80
25
13.29 ± 1.53
aggradation
incision
increasing
deposit
age
4
5
3
0
10
20
30
alluvial
strath
site 23
8.29 ± 0.58
site 26
21.08 ± 2.00

Figure 1.14 (previous page) Illustration of the alluvial strath surfaces on (a) Ramshorn, (b) Birch Springs, and (c) King Canyon alluvial fans as inferred from OSL age estimates for timing of sediment deposition. Relative positions of surfaces are shown but illustrations are not to scale. These alluvial straths were formed through incision into older deposits that were subsequently sampled for OSL dating, producing an anomalously old age for a geomorphically lower and thus young surface.

produce similar ages of 47.19 ± 4.27 ka (site 5) and 47.32 ± 4.64 ka (site 6). The similar OSL ages for sites 5 and 6 suggest rapid fan aggradation ~47 ka with the resulting surface later incised to form the an alluvial strath that site 5 is located on. A third probable alluvial strath occurs on King Canyon Fan at sites 24, 25, and 26 (Fig. 1.14c). The geomorphically higher/older surface of sites 24 and 25 produce OSL ages of 13.99 ± 1.80 ka and 13.29 ± 1.53 ka, respectively, while the geomorphically lower/younger surface of site 26 produces an age of 21.10 ± 2.00 ka. Site 23 sits on the same probable alluvial strath of site 26 but produces an age of 8.29 ± 0.58 ka. This sample was collected at only ~1 m depth from a finer grained unit that interpret as minor younger deposition capping the alluvial strath.

Problems with OSL samples such as partial bleaching or dose-rate heterogeneity could potentially produce age reversals as well. However, as discussed in Section 1.4.2, D_e distributions do not indicate significant problems with partial bleaching (i.e., significant skew). Dose-rate heterogeneity would likely produce ages with more uncertainty due to increased variability in D_e estimates rather than entirely inaccurate ages. However, inaccurate ages may result for samples without bulk sediment samples for dose-rate estimation. At Ramshorn Fan, the OSL sample from site 18 on the alluvial strath does indeed lack a bulk sample for dose-rate estimation. As discussed in Section

1.4.1, dose rates based on bulk sediment samples produce lower dose-rate estimates and thus older age estimated than dose rate and age estimates based on only the <2 mm grain-size fraction (Fig. 1.6). This suggests that consideration of a bulk sediment sample for dose-rate estimation at site 18 would produce an age >39 ka, but an older age would not change our interpretation of this surface as an alluvial strath (Fig. 1.14a). At King Canyon Fan, we lack a bulk sediment sample for dose-rate estimation for site 25, suggesting that the OSL age of 13.29 ± 1.53 ka may be an underestimate. However, the OSL sample from site 24, located on the same surface as site 25 (Figs. 2b and 14a), produces an age in good agreement of 13.99 ± 1.80 ka that was calculated with a dose rate based on a bulk sediment sample. In our view, ages at these three locations with age reversals are most simply and logically explained by formation of alluvial strath surfaces.

1.5 Conclusions

The major goals of this study include, (1) investigating how best to sample predominately coarse-grained fluvial deposits that lack thick sand lenses for OSL dating and investigate how the range of grain sizes may influence dose-rate heterogeneity, and (2) from the resultinging age estimates, determine the timing of major episodes of aggradation on LRR alluvial fans. Addressing the first goal, our results suggest that optical dating can be accomplished for these types of fluvial deposits that lack sand lenses. Sampling strategies that don't involve tubes can easily be devised, but dose-rate estimates may require more consideration due to sediment heterogeneity. For LRR alluvial fan deposits, which have greater dose contribution from the <2 mm portion, dose-rate results from bulk samples with all sizes present in correct portions were considered to give the best estimates. Resulting ages for sediment deposition show good agreement

with a Mazama Ash and good reproducibility for individual exposures and fan surfaces. Other users who wish to apply optical dating to similar coarse-grained deposits may also want to analyze several grain sizes as well as bulk samples to identify any heterogeneity in dose rate that may be important to consider.

CHAPTER TWO: LATE PLEISTOCENE ALLUVIAL FAN AGGRADATION IN THE LOST RIVER RANGE, IDAHO – CLIMATE, GLACIATION, AND THE TIMING OF HILLSLOPE SEDIMENT PRODUCTION AND TRANSPORT

2.1 Abstract

Deciphering the role and importance of climate vs. tectonism in controlling rates and processes of erosion in mountainous regions remains an area of active research in geomorphology. Through dating of alluvial fan aggradation in the Lost River Range of Idaho, USA, we investigate the influence of Quaternary climate on hillslope sediment supply and transport capacity of mountain streams in this region. Fans along the normally-faulted western side of the Lost River Range extend ~2-6 km from the range front. Sediment is predominantly limestone-derived pebble to cobble gravels with a sandy matrix and is often sorted into coarse-fine couplets that suggest sheetflooding has been the dominant process transporting and depositing sediment. We selected five alluvial fans for correlation and mapping of similar-age surfaces using geomorphic positions of surfaces, optically stimulated luminescence (OSL) dating, soil development, and thickness of pedogenic $CaCO_3$ coats on clasts within soil profiles. Late Pleistocene glacial extent within alluvial fan contributing basins varied from 0-80% of catchment area, allowing investigation of the influence of glaciation versus regional climate on fan aggradation. OSL ages range from 4-115 ka and suggest synchronous fan aggradation regardless of the extent of past glaciation in catchments. Geomorphic maps of the fans suggests that approximately 10% of total fan area was constructed during the Holocene,

while ~80% was constructed during the late Pleistocene (undated/older fan surfaces account for the remaining ~10% of fan area). The more significant fan growth of the late Pleistocene may be divided into distinct periods at 10-20 ka, 20-35 ka, and 35-60 ka. Differences in the extent, facies, grain-size distributions, and average surface slopes between Holocene and late Pleistocene deposits suggest greater stream transport capacity and sediment delivery to fans during the late Pleistocene. These results suggest that the warmer and drier conditions of the Holocene (OIS 1) have promoted limited deposition and largely inactive fans. In contrast, the cold climate conditions throughout OIS 2-4 promoted aggradation and active fans in this region. While glaciers may have played a role in fan growth, deposition on fans with and without extensive glaciation in contributing basins suggests that glaciation was not required and that regional climate conditions drive other processes that result in fan aggradation. From these results, we infer that cold climate enhanced both stream transport capacity and sediment delivery to fans, resulting in aggradation. Greater stream transport capacity may have resulted from increased effective moisture as well as greater peak flows and total discharge during spring snowmelt. Greater sediment delivery to fans may have resulted from the direct effects of glaciers where present, but also through reduced vegetation density in contributing basins and more rapid weathering rates driven by greater effective moisture and temperature regimes that promoted more effective frost weathering processes. These findings suggest that in the Lost River Range and perhaps greater region, conditions during intervals of cold climate have most effectively driven denudation and subsequent alluvial fan growth.

2.2 Introduction

The spectacular topography of mountainous regions around the world invites questions regarding the influence of climatic and tectonic mechanisms on geomorphic processes (e.g., production and movement of sediment) that drive the evolution of these landscapes. Recent work has produced a variety of results regarding theoretical linkages between climate drivers (e.g., glaciation and frost weathering) and topographic relief of mountain ranges, as well as potential feedbacks among tectonics, climate and orographic development (e.g., Whipple et al., 1999; Snyder et al., 2000; Montgomery et al., 2001; Burbank et al., 2003; Reiners et al., 2003; Wobus et al., 2003; Densmore et al., 2004; 2005; Hales and Roering, 2005, 2007, 2009). Field-based studies combined with recent advances in Quaternary dating methods may provide further insight into the influence of climatic and tectonic mechanisms on geomorphic processes in mountainous regions.

Alluvial fans commonly develop in mountainous regions and may help establish links among climate, tectonic activity, and geomorphic response. In conceptual models of fan evolution, intervals of fan aggradation, stability, and incision have been attributed to (1) tectonics (e.g., Alexander and Leeder, 1987; Blair and Bildeau, 1988), (2) climate (e.g., Pierce and Scott, 1982; Bull, 1977, 1991; Ritter et al., 1995) and (3) autogenic behavior (e.g., Nicholas and Quine, 2007; Nicholas et al., 2009; Clarke et al., 2010). Studies of Quaternary alluvial fans in the western U.S. indicate that on million-year timescales, tectonic activity creates and maintains the accommodation space required for fan formation but that, on shorter timescales, climatic conditions drive intervals of aggradation and possibly incision (e.g., Ritter at al., 1995). Periods of alluvial fan aggradation are related to intervals of ample sediment availability coupled with adequate

transport capacity to move that sediment. Accurate ages for these intervals can allow alluvial fan deposition to be compared to global and regional climate records to help establish the conditions that enhance sediment production and transport.

Efforts to establish which climate conditions enhance fan aggradation have been impeded by a lack of dating methods that can accurately determine the timing of sediment deposition. Datable material such as organic carbon is rarely present or preserved in fan sediments, especially for fans dominated by alluvial rather than debris flow processes. Even if organic carbon is present, radiocarbon dating has an upper age limit of ~40 kyr that limits investigation of alluvial fan response over a glacial-interglacial cycle. Methods such as cosmogenic radionuclide dating or U/Th dating of pedogenic $CaCO_3$ coats developed in soils of fans surfaces can provide a minimum age for the timing of surface stabilization and abandonment, but do not provide a direct age of sediment deposition.

In many locations fan sediments can be accurately dated using optically stimulated luminescence (OSL) methods. In contrast to these other methods, OSL dating relies on commonly present quartz and feldspar sand grains to provide an age estimate for the timing of sediment deposition with an upper age limit of ~300 ka. Recent advances in OSL methodology (e.g., Murray and Wintle, 2000; Murray and Wintle, 2003; Duller, 2004; Lian and Roberts, 2006) and its application to fluvial sediments (e.g., Wallinga, 2002; Jain et al., 2004; Rittenour, 2008) have improved the accuracy of results for fluvial deposits. OSL dating has been successfully applied to alluvial fans in places such as the Kunlun Mountains of Tibet (Owen et al., 2006), the Black Mountains of Death Valley, USA (Sohn et al., 2007), and northwest Argentina (Spencer and Robinson, 2008).

The Lost River Range in east-central Idaho, USA (Fig. 2.1a) provides an ideal location to investigate climatically-driven alluvial fan aggradation. Along the western base of the range, numerous alluvial fans extend up to 6 km from the range front. Despite their geomorphic significance within the basin, these fans are almost entirely inactive under modern conditions. The main goals of this study are to (1) determine the timing of deposition on LRR alluvial fans and the areal extent of any distinct intervals of deposition; (2) describe deposit characteristics to make inferences about temporal changes in sediment supply and stream transport capacity; and (3) compare the timing of intervals of aggradation on LRR alluvial fans to records of regional climate and infer how regional climate and catchment glaciation influenced the timing of aggradation and evolution of LRR alluvial fans.

2.2.1 Background

The relative importance of tectonism, climate, and autogenic behavior in driving fan aggradation is still not entirely resolved (e.g., Ritter et al., 1995), and varies depending on the timescale of interest. On million-year timescales, tectonism drives fan formation (e.g., Blair, 1987; Ritter et al., 1995), but on shorter (100 kyr and less) timescales, individual offsets along range-front faults are unlikely to drive episodes of aggradation across the whole fan because the resulting changes in gradient diminish rapidly with distance from the scarp. For example, Fig. 2.2 shows how a ~3 m offset of a fan with an average slope of 3° changes local gradient by less than 5% at a distance of 1 km from the scarp and less than 2% at a distance of 2 km from the scarp. This demonstrates that on large radius fans, like those in the LRR, the influence of individual fault offsets is confined to the “near-fault, near-stream” environment.

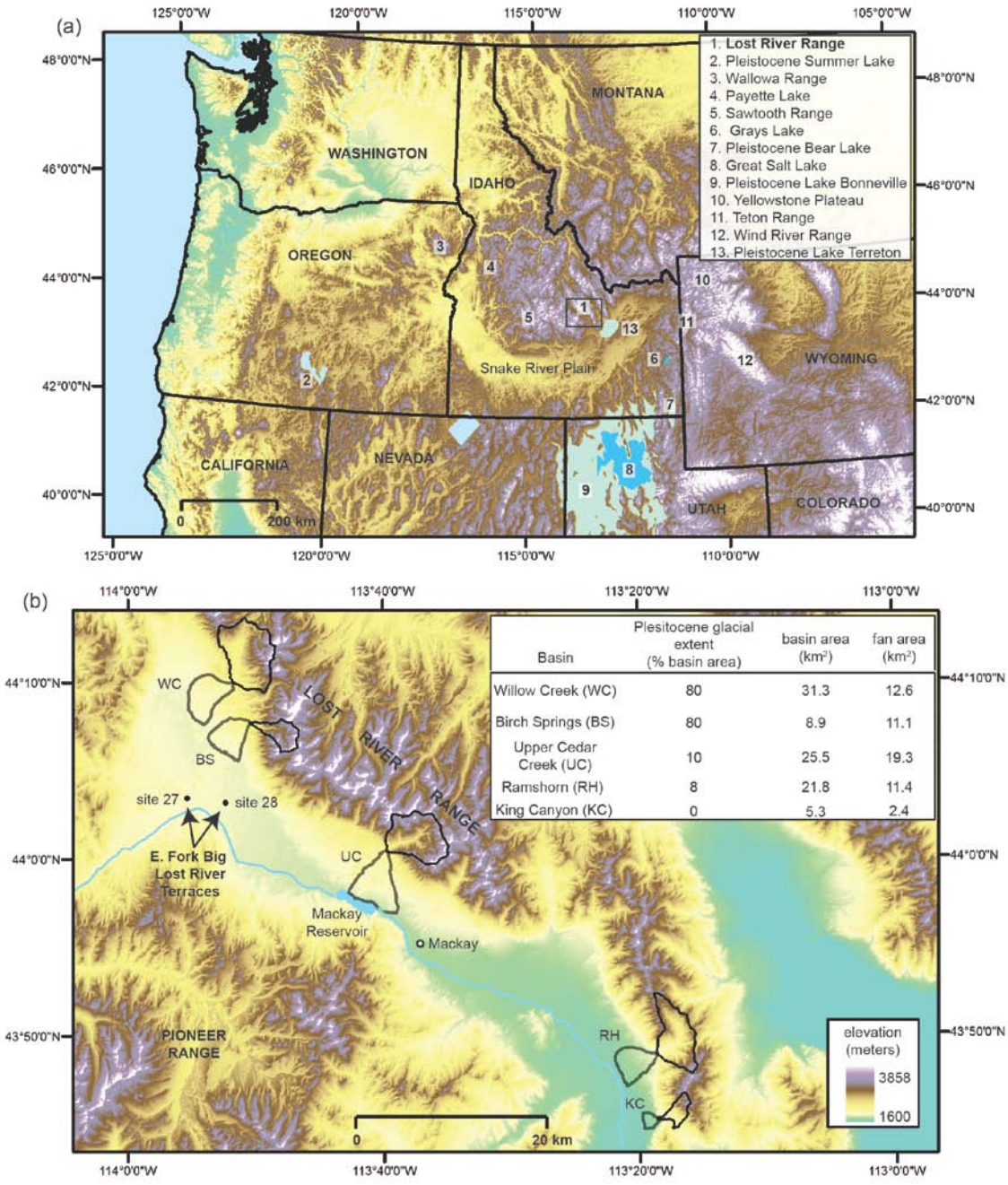

Figure 2.1 (a) Location of Lost River Range in the western U.S. and in relation to other ranges and locations of relevant paleoclimate records referenced in the text. (b) Location of the alluvial fan study sites in the Big Lost Valley and their contributing basins within the Lost River Range. The locations of OSL samples collected from two terraces of the E. Fork Big Lost River are also shown. Inset table shows the size of the alluvial fans and their contributing basins as well as the approximate area of contributing basins glaciated during the late Pleistocene.

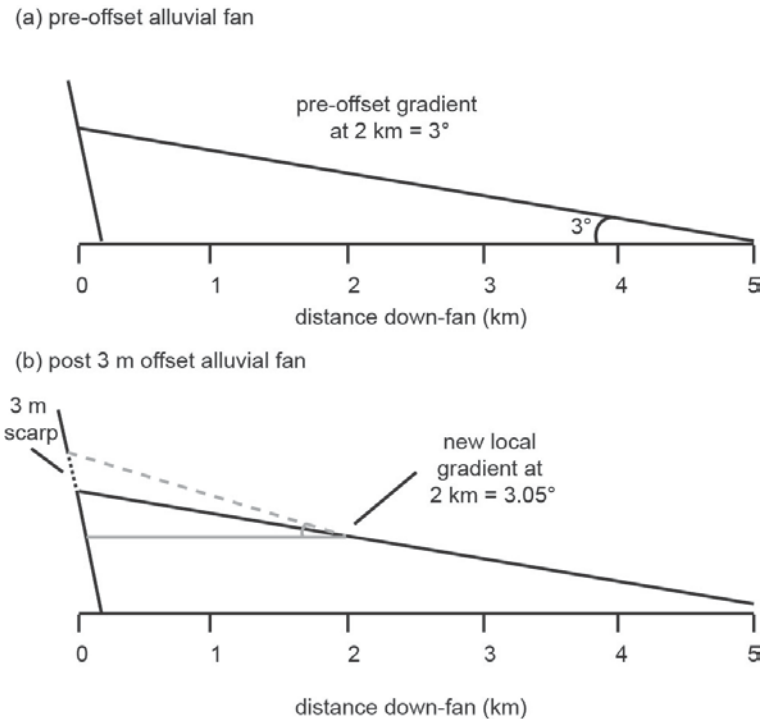

Figure 2.2 Illustration demonstrating minor changes in local gradient on large radius fans due to single faulting events. Figure not drawn to scale. (a) 5 km radius fan with average slope of 3° prior to faulting event. (b) Same alluvial fan after a 3 m offset. Though local slope changes drastically very near the fault scarp, the change in gradient 2 km from the scarp is only 0.05°. Such minor changes in local gradient are likely unable to drive significant fan aggradation or incision.

Autogenic mechanisms may also drive alluvial fan development on 100 kyr and shorter timescales or lead to complex responses to external forcing such as climate. Investigation of autogenic mechanisms has been largely restricted to numerical modeling (e.g., Coulthard et al., 2002; Nicholas and Quine, 2007; Nicholas et al., 2009) or alluvial fans generated in the laboratory (e.g., Clarke et al., 2010). Results from these studies indicate that fans can incise in the absence of external forcing, in response to intrinsic factors such as insufficient accommodation space for additional sediment, flow-width adjustment, or a shift from sheetflood to channelized flow as aggradation rates decrease with fan growth. Aggradation driven by autogenic mechanisms is poorly understood

since many of these studies assume that environmental conditions always generate adequate sediment supply and transport capacity for deposition. This assumption neglects environmental conditions producing the sediment supply and stream discharge. Numerical modeling by Coulthard et al. (2002) addresses this issue by investigating both catchment and fan response to Holocene climate and land use within the catchment. While the sediment supplied to the model fan from the basin closely followed the imposed climate signal, fan behavior did not, leading Coulthard et al. to suggest that internal thresholds and sediment storage and remobilization control fan activity rather than climate. This study suggests that autogenic mechanisms can indeed influence fan evolution during intervals in which environmental conditions are supplying adequate sediment and stream discharge to the fan.

Climate and changes in climate are likely the primary drivers of alluvial fan aggradation on 100 kyr and shorter timescales, likely influencing the changes in sediment delivery and transport capacity that produce deposition on fans (e.g., Pierce and Scott, 1982; Ritter et al., 1995). While many factors such as lithology and tectonic activity can vary significantly within a single mountain range or region, climatic conditions and timing of climate changes are more regional in scale. As such, climate forcing is expected to drive widespread and near-synchronous aggradation on fans within a single basin or even broader region as observed within the Madison River valley of southwestern Montana (Ritter et al., 1995) and the arid southwestern U.S. (e.g., Bull, 1991; McDonald et al., 2003). Factors that are variable over a region (i.e., lithology, histories of fault segments, extent of catchment glaciation and autogenic behavior) may cause asynchronous deposition on fans.

Entrenchment and incision on fans can be driven by climatically-altered sediment supplies and transport capacity within contributing basins. However, factors unrelated to the contributing basin may also trigger incision. These include base-level changes (which may be driven by tectonics or climate change; e.g., Harvey, 2002), fan-toe trimming by an axial stream, or autogenic mechanisms (e.g., Nicholas and Quine, 2007). This makes fan incision a less reliable indicator of climatically-altered conditions within contributing basins.

2.2.2 Conceptual Models of Alluvial Fan Aggradation

The exact climatic conditions that may enhance alluvial fan aggradation remain rather poorly understood, but two conceptual models provide examples of potential linkages between climate and fan aggradation. In the model often applied to the arid southwestern U.S., alluvial fan aggradation occurs during the climatic transition from cold glacial to warmer interglacial conditions (e.g., Bull, 1977, 1991). During glacial intervals, increased effective moisture, greater vegetation density, and enhance chemical and physical weathering of bedrock promotes the accumulation of a thick layer of sediment and regolith on hillslopes. As climate warms and effective moisture is reduced, vegetation density declines, leaving accumulated regolith more prone to erosion and subsequent deposition on alluvial fans. In addition, a stronger summer monsoon in the southwestern U.S. during warmer conditions may also produce more frequent, high-intensity precipitation events and Hortonian overland flow capable of mobilizing and transporting sediment to fans (Asmerom et al., 2007).

In the conceptual model often applied to more temperate zones like the northern Rockies of the U.S., where cold climate conditions promote cirque and valley glacier

growth at higher elevations, fan aggradation is hypothesized to occur during intervals of cold climate (Pierce and Scott, 1982; Ritter et al., 1995). This is thought to result from a simultaneous increase in transport capacity of streams feeding fans and the volume of sediment delivered to fans. Increased transport capacity results from colder temperatures that promote accumulation of a deeper winter snowpack and a delayed spring snowmelt that occurs when incoming solar radiation is greater. The result is rapid melting of a deep snowpack and large volume stream discharges with greater transport capacity. Simultaneously, sediment supply increases as a result of glacial erosion and also increased rates of bedrock weathering due to increased effective moisture and more effective frost weathering processes.

These hypotheses can be tested by comparing accurate numerical ages for intervals of sediment deposition on alluvial fans to regional climate records. Further, in mountain ranges where glacial climates promote cirque and valley glacier growth, the importance of glaciers in determining the timing of alluvial fan aggradation can be tested by comparing numerical ages for sediment deposition on fans with varying degrees of catchment glaciation.

2.2.3 Study Area

2.2.3.1 Geologic Setting

The Lost River Range (LRR) lies in east-central Idaho within the northernmost extent of the Basin and Range Province (Fig. 2.1a). Elevations in the Big Lost River Valley are approximately 1790 ± 130 masl while peak elevations reach 3861 masl at Borah Peak, the highest peak in Idaho. The axial Big Lost River is fed by the East Fork of the Big Lost River (a major tributary draining the Pioneer Range just to the west) as

well as springs within the basin and the small tributaries of the western side of the LRR. The Big Lost River flows southward toward the Snake River Plain, but high infiltration rates into fluvial gravels and basalt along with irrigation withdraws cause the river to become “lost” and not discharge to the Snake River. During times of greater discharges during the late Pleistocene, the Big Lost River was a primary water source for pluvial Lake Terreton in the Snake River Plain (Forman and Kaufman, 1997; Geslin et al., 1999; Gianniny et al., 2002; Fig. 2.1a).

Precambrian and Paleozoic sedimentary rocks (primarily limestone and quartzarenite) underlie the LRR and were folded and faulted from the Cretaceous and to the Eocene (Haller and Crone, 2004; Skipp and Hait, 1977). Regional extension leading to the development of the LRR began ~4-7 Ma (Haller and Crone, 2004) and may be related to passage of the Yellowstone hot spot (Pierce and Morgan, 1990). Relief of the LRR has resulted from movement along the Lost River Fault, a west-dipping normal fault that bounds the western flank of the range and can be divided into six distinct sections (Haller and Wheeler, 1995). Studies suggest a low long-term slip rate of 0.1-0.2 mm/yr on this fault (e.g Haller and Wheeler, 1995). The most recent activity along the Lost River fault occurred during the magnitude 7.3 Borah Peak earthquake of October, 1983. This event resulted in 34 km of surface rupture with new scarps averaging 0.8 m and reaching a maximum of 2.7 m (Crone and Machette, 1984).

Over longer timescales, the topographic relief generated on the Lost River extensional fault may be limited by climatic influences that determine how efficiently denudation occurs on the footwall (e.g., Densmore et al., 2004; Densmore et al, 2005). Small valley glaciers developed during Quaternary glacial intervals may be a main driver

of erosion and removal of sediment from catchment basins on the footwall, but Foster et al. (2008) found that the glacial signature is not as strong in the LRR as surrounding ranges such as Lemhi and Beaverhead-Bitterroot Ranges In addition, morainal evidence indicates that few glaciers make it down to the active footwall environment.

2.2.3.2 Alluvial Fans of the Lost River Range

The Lost River Fault on the western side of the LRR is crossed by numerous low gradient (~2-3°; Patterson, 2006) alluvial fans that extend ~2-5 km from the range front with surfaces of neighboring fans often coalescing to form a bajada. Because of their size, the typical ~1-3 m offsets of the Lost River Fault (Scott et al., 1985; Crone et al., 1987) are not likely to produce aggradation or incision over the length of the fan (see Section 2.1 and Fig. 2.2). Indeed, the geomorphic response to the 1983 Borah Peak Quake has been limited to minor ravel off the fault face and fault scarps are still near vertical due to the low precipitation rates and high cohesion in the calcium carbonate-cemented soils.

Fan morphology and deposits indicate very limited recent deposition on LRR fans, but older fan surfaces indicate significant aggradation and incision in the past. Modern deposition occurs primarily as small debris flows at fan apices. Active channels, where present, are narrow and entrenched through the length of the fan (Patterson, 2006). Fans typically have 2-4 large, distinct fan surfaces that suggest numerous past episodes of deposition and incision. Further, surface morphology and stratigraphy suggest that the fans have developed in a stacked rather than telescoping nature. LRR fan deposits are predominately clast-supported gravels with planar to subhorizontal bedding with a sandy matrix and little silt or clay content (Funk, 1976; Pierce and Scott, 1982; Pierce and

Colman, 1986; Patterson, 2006). Repeating, normally graded couplets are common and indicate deposition by sheetflooding (Pierce and Scott, 1982; Patterson, 2006). Large boulders and boulder levees sit on the surfaces of several northern fans and indicate deposition by debris flows rather than sheetflooding. Lithologic differences among basins likely control the dominant depositional processes on LRR fans (Poulos et al., 2008). However, fans dominated by debris flows are the exception within the Lost River basin and are thus not considered in this study.

Previous age estimates suggest that the LRR alluvial fans are primarily relicts of late Pleistocene conditions (Pierce and Scott, 1982; Patterson, 2006). Pierce and Scott (1982) inferred Pinedale (OIS 2) ages for many of the large fan surfaces based on their positions relative to glacial deposits thought to correlate to the regional Pinedale glacial advance. Most of the age estimates have been obtained through the use of pedogenic $CaCO_3$ coats that have formed on clasts within soils of fan and glacial deposits. Limited U-series dating of pedogenic $CaCO_3$ coats produced estimates for surface stabilization of ~160, ~30, and ~23 ka (Scott et al., 1985; Pierce, 1985). In addition, Patterson (2006) used the growth rate for pedogenic $CaCO_3$ coats developed by Pierce (1985) to estimate that many LRR fan surfaces in the valley stabilized between ~10-60 ka. However, this provides a minimum approximation for the timing of surface stabilization, not deposition.

2.2.3.3 Modern Regional Climate

Modern climate in the LRR ranges from arid on the valley floor to sub-humid at higher elevations on the peaks. Average annual precipitation in the Big Lost River valley is 246 ± 67 mm in the southern portion of the basin (Arco SW 3 weather station, 33 years of record between 1948-2006; Western Regional Climate Center, 2009) and 203 ± 61 mm

in the northern portion of the basin (Chilly Barton Flat weather station, 49 years of record between 1948-2006; Western Regional Climate Center, 2009). This potential precipitation gradient may result from the proximity of the southern portion of the valley to the SRP, which acts a conduit for moisture coming from the Pacific Ocean. Mean annual temperature on the basin floor ranges from 5.87 ± 1.03 °C in the south (ARCO SW 3 weather station, 26 years of record between 1948-2006; Western Regional Climate Center, 2009) and 4.08 ± 1.06 °C in the north (Chilly Barton Flat weather station, 43 years of record between 1948-2005; Western Regional Climate Center, 2009).

While there is little evidence to suggest that any of the permanent snow fields in the LRR are active glaciers, the LRR may contain rock glaciers that are active at present. Johnson et al. (2007) documented numerous active rock glaciers in the Lemhi Range, which sits ~20-30 km northeast of the LRR. The Lemhi mountains range in elevation from 2000-3718 m (Johnson, 2006), which is similar to the ~1790-3861 m elevation range in the LRR, and experiences similar climate conditions as the LRR. Aerial photography reveals morphological features within LRR basins that are consistent with rock glaciers, although we do not know if they are active under modern conditions.

2.2.3.4 Regional Glaciations and Paleoclimate

Despite the lack of modern glaciers in the LRR, past climate regimes produced glaciers within basins on both the eastern and western flanks of the range. On the western side of the range (the side this study is concerned with), the extent of late Pleistocene glaciation within basins varied from 0% of the area within southern basins to 80% of the area within northern basins (Fig. 2.1b). The location of moraines shows that during the most recent advances, glaciers in the majority of basins did not reach basin

outlets and extend onto alluvial fans (Birch Springs Fan is the exception to this, with moraines at its apex). The variation in areal extent of past glaciation extent within the five contributing basins presents a unique opportunity to investigate the influence of glaciers versus general glacial climate on alluvial fan aggradation.

The timing of glaciation in the LRR is not well constrained as there has been little numerical dating of glacial features within the range. Dates from nearby ranges suggest a probable time-frame for glaciation in the LRR, despite some regional variability in the timing of maximum advances (Gillespie and Molnar, 1995; Thackray, 2008). During the most recent glaciation in the western U.S., referred to as Pinedale and correlative with OIS 2, valley glacier advances have been documented between ~10-22 ka (Fig. 2.3e). Older Pinedale advances (~ 17-21 ka) are documented in the Wallowa Range, Oregon (Licciardi et al., 2004) and Wind River Range, Wyoming (Phillips et al., 1997; Licciardi and Pierce, 2008). Pinedale advances ~13-17 ka are most common in areas closest to the LRR, including Payette Lake, Idaho (Phillips et al., 2007), the Sawtooth Range, Idaho (Thackray, 2004), and in the Teton Range, Wyoming and Yellowstone Plateau (Licciardi and Pierce, 2008). Younger Dryas advances (~ 10-12 ka) are dated in the Wallowa Range (Licciardi et al., 2004) and Wind River Range (Gosse et al., 1995). There is also evidence for one or more glacial outburst flooding events emanating from the Pioneer Range to the northwest of the LRR ca. 17-21 ka. (Rathburn, 1993; Cerling et al., 1994; Gosse and Evenson, unpublished data).

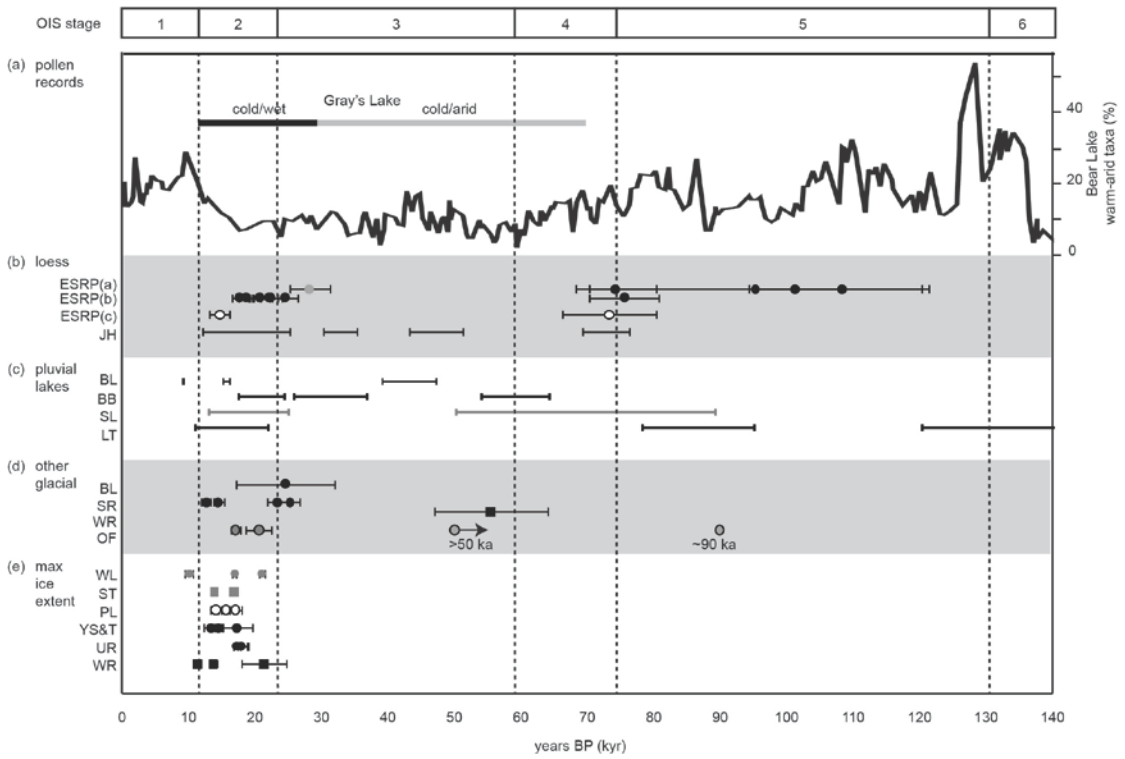

Figure 2.3 Paleoclimate records from the region surrounding the LRR for the last 140 ka. Locations of records are shown in Fig. 2.1a. (a) Pollen records from lake cores at Grays Lake, Idaho (Beiswenger, 1991) and Bear Lake, Idaho/Utah border (Jiménez-Moreno et al., 2007). (b) Ages for loess deposits in the region. Working downward, records are from the Eastern SRP, Idaho (ESRP; Forman et al., 1993; Phillips et al., 2009; and Dechert et al., 2006); and near Jackson Hole, Wyoming (JH; Pierce et al., 2011). (c) Timing of increased water levels in pluvial lakes. Working downward, records are Bear Lake, Idaho/Utah border (BL; Laabs and Kaufman, 2003); Bonneville Basin, Utah, (BB) with generally rising water levels beginning ~36 ka until highstand ~18 ka (Oviatt et al., 1992; Godsey et. al., 2005; Kaufman et al., 2001); Summer Lake, Oregon (SL; Cohen et al., 2000; Negrini at al., 2000); Lake Terreton, Idaho (LT; Forman and Kaufman, 1997; Gianniny et al., 2002). (d) Indicators of glacial activity. Working downward, records include glacial flour from the Uinta Range, Utah in Bear Lake cores (BL; Laabs et al., 2007); glacial outwash of the Snake River in the E. SRP, Idaho (SR; Phillips et al., 2009); Wind River, Wyoming glacio-fluvial terrace (WR; Sharp et al., 2003); glacial outburst flooding emanating from the Pioneer Range of Idaho and out the Big Lost River valley (OF; Cerling et al., 1994; Knudsen et al., 1999; Simpson et al., 1999; Gosse and Evenson, unpublished data); (e) Dates for timing of maximum glacial extent in ranges near the LRR. Working downward records include ages from Wallowa Lake, Oregon (WL; Licciardi et al., 2004); the Sawtooth Range, Idaho (ST; Thackray et al., 2004); Payette Lake, Idaho (PL; Phillips et al., 2007); Yellowstone Plateau and Teton Range, Wyoming (YS&T; Licciardi and Pierce, 2008); the Uinta Range, Utah (UR; Munroe et al., 2006; Refsnider et al., 2008); Wind River Range, Wyoming (WR; Gosse et al., 1995; Phillips et al., 1997).

Pre-Pinedale advances of valley glaciers in nearby ranges are not as well documented, due to the subdued morphology of older features and/or their destruction by later Pinedale advances rather than a lack of glacial activity. Evidence for pre-Pinedale glacial activity includes a glacio-fluvial terrace in the Wind River Range, WY with a minimum age of 55.5 ± 8.60 ka (Sharp et al., 2003) that may correlate to early Wisconsin time (OIS 4), and moraines and fluvial terraces that correlate to the Bull Lake (OIS 6) advance with ages of 140-160 ka (Phillips et al., 1997; Phillips et al., 1997; Sharp et al., 2003). A large moraine at Payette Lake, Idaho yields a mean age of 135.3 ± 3.0 (Phillips et al., 2007). In the Lost River basin, Simpson et al. (1999) estimate an age of ~90 ka from soil chronosequences for glacial outburst flooding from the Pioneers, draining through the LRR valley, while Knudsen et al. (1999) suggest an age >50 ka for the glacial outburst flooding based on correlations with thermoluminescence dated basalt flows.

Loess deposits are common throughout the region, and are often interpreted as indicators of cold climate conditions (e.g., Pierce et al., 2011). Cold climate conditions are thought to have accelerated loess accumulation because of greatly reduced winter discharges that leave larger areas of fine-grained floodplain and stream-bed deposits exposed to eolian erosion. Glacial erosion in the headwaters may also increase the amount of fine sediment deposited by streams. Loess deposits in the eastern Snake River Plain (Dechert et al., 2006; Phillips et al., 2009) and near Jackson Hole, WY (Pierce et al., 2011) date to ~12-25 ka, correlative with OIS 2 (Fig. 2.3b). Cold conditions during OIS 3-4 and late OIS 5 are suggested by loess accumulation near Jackson Hole from 30-35 ka, 43-51 ka, and 69-76 ka (Pierce et al., 2011), and in the eastern SRP between 25-31 ka, 68-80 ka, and 70-120 ka (Forman et al., 1993; Fig. 2.3b).

Lake levels of pluvial lakes throughout the Basin and Range Province of the western U.S. have fluctuated during the Pleistocene in response to changing climate, with high water levels indicative of increased effective moisture (Forman and Kaufman, 1997; Gianniny et al., 2002; Fig. 2.3c). Nearest to the LRR, Lake Terreton formed in the eastern Snake River Plain (Fig. 2.1a). The Big Lost River emptied into the Big Lost Trough sub-basin of Lake Terreton and was its primary source of sediment (and perhaps water) as indicated by detrital zircon ages and the petrography of sand within the basin (Geslin et al., 1999). Another sub-basin of Lake Terreton, Mud Lake, experienced high water levels from 160-120 ka, 95-78 ka, 22-11 ka, and also after 1 ka (Forman and Kaufman, 1997; Gianniny et al., 2002). The 160-120 ka highstand at Mud Lake can be correlated to sedimentary records from the Big Lost Trough (Gianniny et al., 2002), suggesting either a highstand in one large lake as sub-basins merged, or similarly timed high water levels in the separate sub-basins. Summer Lake, in south-central Oregon (west of the LRR) experienced high stands between 89-50 ka and 13- 25 ka (Negrini et al., 2000; Cohen et al., 2000). Highstands are suggested for 39-47 ka, 15-16 and ca. 9 ka in Bear Lake, on the Idaho-Utah border south of the LRR (Laabs and Kaufman, 2003). South of the LRR, water levels in the Lake Bonneville basin began to rise around 36.0 ± 0.8 ka, reached a temporary high between 25.8-24.3 ka during the Stansbury oscillation, then reached their highest levels between ~18.6 ka and ~17.5 ka before the lake catastrophically drained into the Snake River Plain in the Bonneville Flood (Oviatt et al., 1992; Godsey et. al., 2005). An older but lower highstand in the Bonneville Basin is suggested for 59 ± 5 ka (Kaufman et al., 2001). Study of high pluvial lake levels around the west suggests intervals of increased effective moisture correlative with OIS 2-4 and

OIS 6, driven by colder temperatures, greater precipitation, or a combination of both (e.g., Reheis, 1999).

Key pollen records of Pleistocene climate within the region include those from Bear Lake, Idaho (~200 km south of the LRR; Fig. 2.1a; Jiménez-Moreno et al., 2007) and Grays Lake, Idaho (~170 km southeast of the LRR; Fig. 2.1a; Beiswenger, 1991). The Bear Lake record indicates cooler temperatures through much of OIS 2-4, ~79-12 ka, and during OIS 6, ~128-186 ka (Fig. 2.3a; Jiménez-Moreno et al, 2007). The Grays Lake record (Beiswenger, 1991) suggests cold and dry conditions from ~70-30 ka, cold but with increased moisture ~30-11.5 ka, and the transition to warmer, more arid Holocene conditions ~11.5 ka (Fig. 2.3a).

Numerous records indicate that conditions in the LRR were likely warmer and drier throughout the Holocene. These records include peak fire activity in the Sawtooth Range, Idaho 7.6-8.5 ka (Svenson et al., 2009); pollen records from the Northern Rockies that indicate warm and dry conditions ~5-7 ka (Brunelle et al., 2005); very low lake levels in the Northern Rockies 4.5-7 ka (Shuman et al., 2009); low water levels at Hidden Lake, Colorado 1.3-4.2 ka (Shuman et al., 2009) and Foy Lake, Montana 1-2.2 ka (Stevens et al., 2006); and widespread droughts and more variable climate during the Medieval Climatic Anomaly 0.65-1.05 ka, as indicated by records such as a peak in high-severity fires and fire-related debris flows along the Southfork Payette River, Idaho (Pierce et al., 2004), pollen records from the Sawtooth Range, Idaho (e.g., Whitlock et al., 2011), and tree ring records throughout the western U.S. (e.g., Cook et al., 2004). However, some records indicate intervals of cooler and/or wetter climate during the Holocene, including floodplain widening and decreased fire-related sedimentation in

northern Yellowstone ~0.1-0.8, 1.3-2.0, 2.6-3.1, 5.6-7 ka (Meyer et al., 1995), glacier advances within the western U.S. ~3.4 ka (Konrad and Clark, 1998; Clark et al., 2005; Reyes et al., 2006; Menounos et al., 2009), and the Little Ice Age 0.1-0.65 ka. Despite these intervals of cooler and/or wetter conditions, Holocene conditions in the LRR were likely warmer and drier relative to the late Pleistocene.

2.3 Materials and Methods

Five sheetflood-dominated alluvial fans on the western side of the LRR were selected for geomorphic mapping and OSL dating. From north to south the fans are Willow Creek, Birch Springs, Upper Cedar Creek, Ramshorn, and King Canyon (Fig. 2.1b). Selected fans capture the variability in late Pleistocene glacial extent within contributing basins, which ranges from 0-80% of basin area (Fig. 2.1b). Major geomorphic surfaces of each alluvial fan were targeted for OSL dating, soil descriptions, measurement of pedogenic $CaCO_3$ coats, and characterization of deposits. Where possible, we used exposures in stream cut-banks or in abandoned gravel quarries. For surfaces that lacked exposures, trenches were dug by back-hoe tractor to a depth of 2-3 m, with sites located where the targeted surface appeared relatively intact and unaffected by secondary processes. We selected study sites on the fans as distally as possible from the Lost River Fault to ensure that we investigated intervals of widespread aggradation rather than localized deposition related to the fault scarp. In addition to the five alluvial fans, two terraces of the E. Fork Big Lost River were also dated using OSL.

2.3.1 Optically Stimulated Luminescence Dating

The following summarizes the OSL methodology and results relevant to the interpretation of age estimates for deposition on LRR alluvial fans. For a more detailed discussion of the optical dating methods and results, see Chapter 1.

Deposit types sampled for OSL dating included well-sorted fluvial sand lenses (nine samples; Figs. 2.4a and 2.4b) and clast-supported sheetflood gravels with a sandy matrix (25 samples; Figs. 2.4c and 2.4d). Thick sand lenses were sampled by pounding an opaque metal tube into the sediment, but thin lenses and sheetflood gravels were sampled under light-safe tarps or at night by excavating sediment from the deposit. Samples for moisture content were also collected, as well as a representative sample from a 30 cm radius around the sample site for dose-rate estimation.

All samples were sent to the Utah State University Luminescence Laboratory in Logan, Utah, USA for preparation and analysis. For samples collected by metal tube from thick sand lenses, elemental concentrations of U, Th, K, and Rb for dose-rate estimates were analyzed by ICP-MS/ICP-AES at ALS Chemex Labs. For excavated samples, analysis of sediment chemistry included ICP-MS/ICP-AES analysis (at ALS Chemex Labs) of two sand-size fractions (total <2 mm and 0.15-2.0 mm) and individual pebbles >2 mm. Bulk samples with all grain sizes present in correct proportions were also analyzed using geranium semiconductor gamma spectrometry and XRF at the USGS Luminescence Dating Laboratory in Denver, CO. These analyses show that the estimated dose rate depends on the grain sizes analyzed. As such, dose rates based on bulk sediment samples were preferred for excavated samples as they included all grain sizes in

correct proportions and thus were likely to produce the best estimate of the average dose-rate contribution from the sediment.

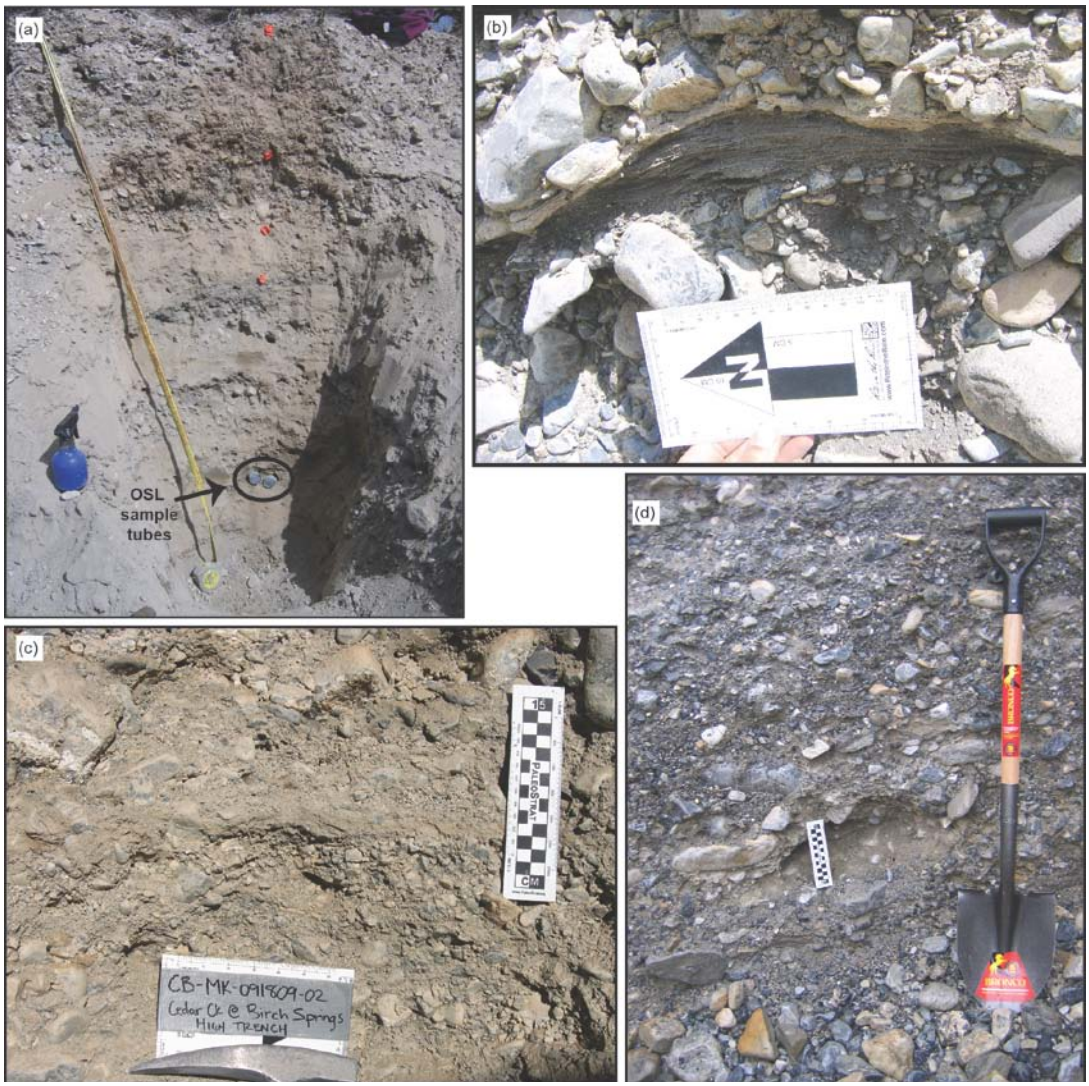

Figure 2.4 Examples of deposits sampled for OSL dating. (a) Thick sand lens sampled by pounding metal tubes into the sediment at site 3 (OSL sample USU-414). Thick sand lenses like this were rare, and found at only four alluvial fan sites and the two terraces of the East Fork Big Lost River. (b) One of three thin sand lens (site 8, USU-417) located and sampled for OSL dating by excavating sediment from the deposit under light-safe tarps or at night. (c) and (d) Pebble-to-cobble sheetflood gravels more typical of LRR fan deposits with (c) from site 6 (USU-704) and (d) from site 4 (USU-646). Site numbers refer those shown in Figures 2.5-2.9 sand sample numbers refer to those in Table 2.1

Equivalent dose (D_e) estimates for 2 mm quartz aliquots were determined using the single aliquot regenerative (SAR) dose protocol (Murray and Wintle, 2000), and resulting D_e distributions were similar for all deposit types sampled (Chapter 1, Section 1.4.2). In addition, D_e distributions indicate that incomplete solar resetting of the luminescence signal (partial bleaching) is not a significant problem, though the high overdispersion (OD) values (>20%) for many samples may be due to the heterogeneity in the sediment dose rate (Chapter 1, Section 1.4.2). The weighted mean (central age model, CAM; Galbraith et al., 1999) was used to calculate the D_e used in age calculations.

2.3.2 Mapping of Fan Surfaces

We correlated alluvial fan surfaces of similar age through use of OSL dating, geomorphic position, deposit characteristics, amount of loess accumulation, soil development, and the average thickness of pedogenic $CaCO_3$ coats on clasts within soil profiles. We mapped moraines at the apex of Birch Springs fan and inferred ages for the moraines based on their geomorphic position in relation to dated fan surfaces and the average thickness of pedogenic $CaCO_3$ coats. We then evaluated the relative geomorphic positions of fan surfaces and relevant moraines using aerial photographs, 10 m DEMs, and field verification. Elevation differences between fan surface treads were measured in the field using basic survey techniques.

General deposit characteristics were noted for major geomorphic surfaces, including style of sediment bedding, average grain size, and average surface slope. Samples for grain-size analysis were collected from at least one location on each fan, and average surface slopes estimated from a 10 m resolution DEM. At Birch Springs and

Upper Cedar Creek fans, additional samples were collected for grain-size analysis, local slopes measured, and cross-sections of the active channel surveyed by total station at two different locations.

Thickness of loess capping alluvial fan deposits was also noted at all sites. However, the thickness of the loess cap was often difficult to determine because the transition from loess to fluvial gravels was gradual, likely a result of mixing through bioturbation and frost action. For comparison between sites, we chose to use the depth where loess was no longer a significant component of the deposit.

Soil development was described according to the guidelines of Birkeland et al. (1991). The accumulation of pedogenic $CaCO_3$ in Bk horizons is the most prominent feature of soils in the basin so the stage of $CaCO_3$ accumulation at each soil description site was evaluated (Giles et al., 1966; Machette, 1985; Birkeland et al., 1991). In addition, the average thickness of pedogenic $CaCO_3$ coats developed on the underside of clasts within soil profiles was measured to use as a proxy for minimum surface age. Pedogenic $CaCO_3$ coats thicken with time as successive layers of $CaCO_3$ accumulate and a growth rate for these coats can be estimated with the aid of other numeric age control for the deposit (e.g., Vincent et al., 1994) or U-series dating of the coats themselves (e.g. Pierce, 1985). With the assumption of a similar growth rate for coats throughout a region of similar climate and lithology, and in the absence of features indicating older coats have become detached from clasts, the average coat thicknesses can then be used to estimate a minimum age for geomorphic surfaces (Pierce, 1985; Vincent et al., 1994). The average $CaCO_3$ coat thicknesses was determined by selecting approximately 20-30 clasts from the most significant Bk horizon, breaking the clasts open and measuring the thickest portion

of the carbonate coat that had laminar structure to the nearest tenth of a millimeter with a comparator (a small, handheld lens with measurement resolution of 0.1 mm). $CaCO_3$ coats were also collected for U-series dating that will provide minimum age estimates for the timing of surface stabilization, and results are pending.

Once geomorphic maps were complete, the approximate areal extent of similar age surfaces were estimated for individual fans and all five fans together. While volume estimates are often preferred and provide a better indication of the magnitude of a depositional event, this was not possible for LRR fans because exposures of deposits needed to estimate depths were often absent. As a result, we assume that deposit surface area provides a reasonable measure for comparing the extent of fan aggradation during different time periods.

2.4 Results

2.4.1 Geomorphic and Sedimentary Characteristics

Geomorphic mapping of the five study fans indicates that up to six distinct deposit groups are present on LRR fans. Where fans have active channels, Qa_1 denotes this surface. Qaf_1 denotes surfaces of Holocene age (<10 ka), while Qaf_2-Qaf_5 denotes deposits and surfaces of late Pleistocene age (Qaf_2 = 10-20ka; Qaf_3 = 20-35 ka; Qaf_4 = 35-60 ka; Qaf_5 = 90-120 ka). Qaf_2-Qaf_4 were expressed at fan surfaces and thus mapped, while older, buried Qaf_5 deposits were identified but not expressed at the current surface of any fan. Qaf_6 was used to denote surfaces and deposits on fans that are older than all other surfaces because of their higher geomorphic position but ages were not investigated.

In the northern portion of the LRR basin, surfaces Qa_1-Qaf_3 were present on the modern fan surface of the Willow Creek fan (Fig. 2.5), while surfaces Qa_1-Qaf_4 were present and mapped on the Birch Springs fan (Fig. 2.6). In addition, glacial outwash with inferred age >35 ka was mapped as Qo_4, glacial moraines with inferred ages of 10-35 ka were mapped as Qm_3 and glacial moraines with inferred ages >35 ka were mapped as Qm_4 (Fig. 2.6a). At the Upper Cedar Creek fan, Qa_1, Qaf_3-Qaf_4 and Qaf_6 were present while Qaf_2 surfaces or deposits appeared to be absent on this fan (Fig. 2.7a). In addition, Qaf_5 deposits were located on the Upper Cedar Creek fan through OSL dating but are buried and not expressed at the surface of the modern fan (Fig. 2.7c). In the southern portion of the basin, Qaf_1-Qaf_4 and Qaf_6 surfaces were mapped on the Ramshorn fan (Fig. 2.8), while Qaf_1-Qaf_2 and Qaf_6 surfaces were mapped on the King Canyon Fan (Fig. 2.9).

Average surface slopes also vary between Holocene and late Pleistocene deposits. Average surface slopes for similar age surfaces are not consistent between fans, but on individual fans late Pleistocene surfaces consistently have steeper average slopes than Holocene surfaces (Fig. 2.10). These differences in slope can often be observed in the field where height differences between surfaces diminish with distance down-fan until surfaces merge near the toe, becoming indistinguishable from each other.

Holocene and late Pleistocene fan deposits are generally similar; most deposits are composed of mainly subangular carbonate clasts that are poorly to moderately sorted, clast-supported gravels with approximately planar bedding and a sandy matrix. Couplets of alternating fine and coarse gravels suggest that aggradation on these five fans has been dominated by sheetflooding (e.g., Blair and McPherson, 1994). However, Holocene deposits more frequently contain preserved sand lenses while late Pleistocene deposits

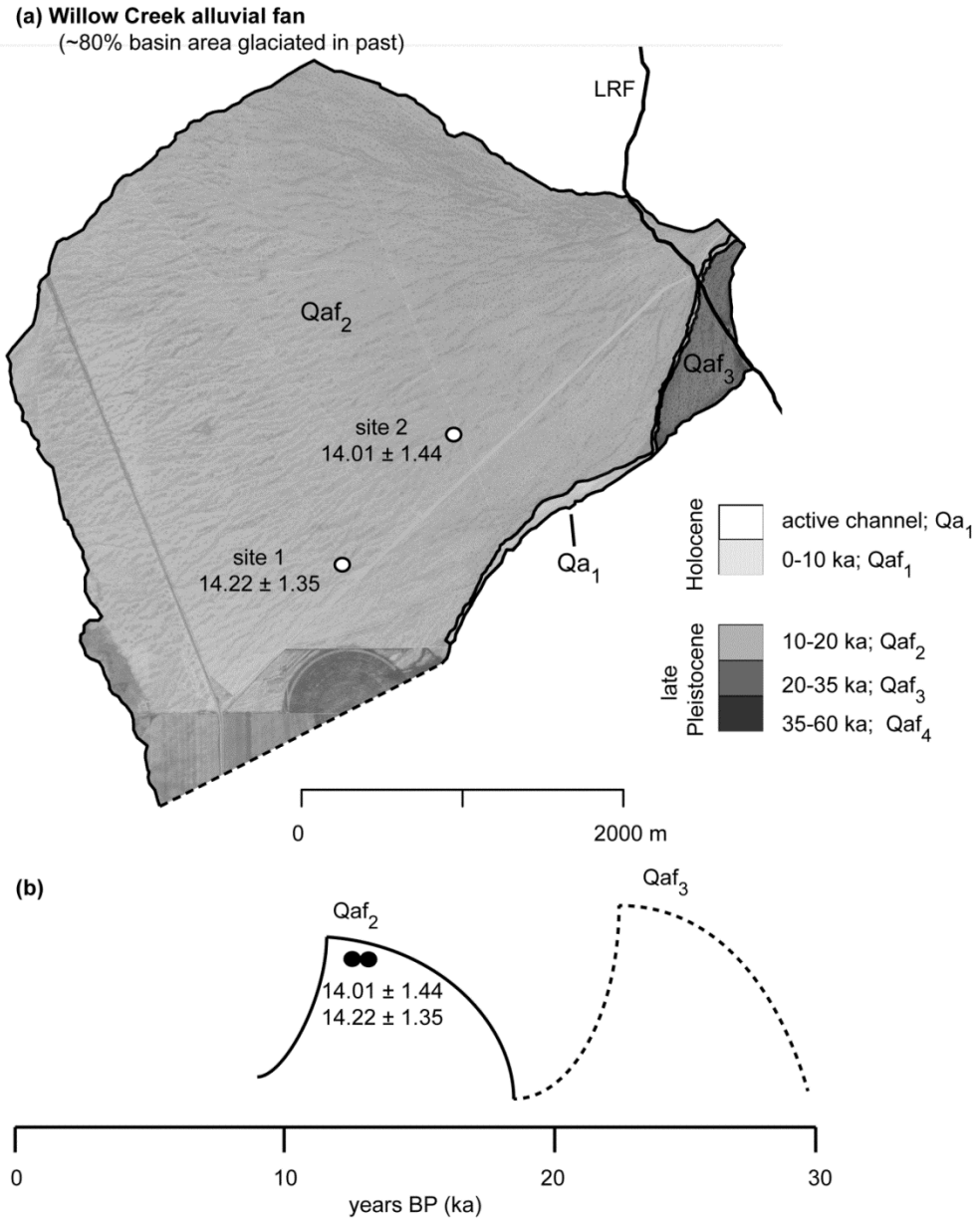

Figure 2.5 (a) Map showing surfaces of the Willow Creek alluvial fan. Surfaces are drawn over an aerial photo to show surface morphology. Roads and irrigated fields appear as darker patches on southern portion of fan. (b) Inferred timing of aggradation and incision on the Willow Creek fan. Black dots denote OSL samples.

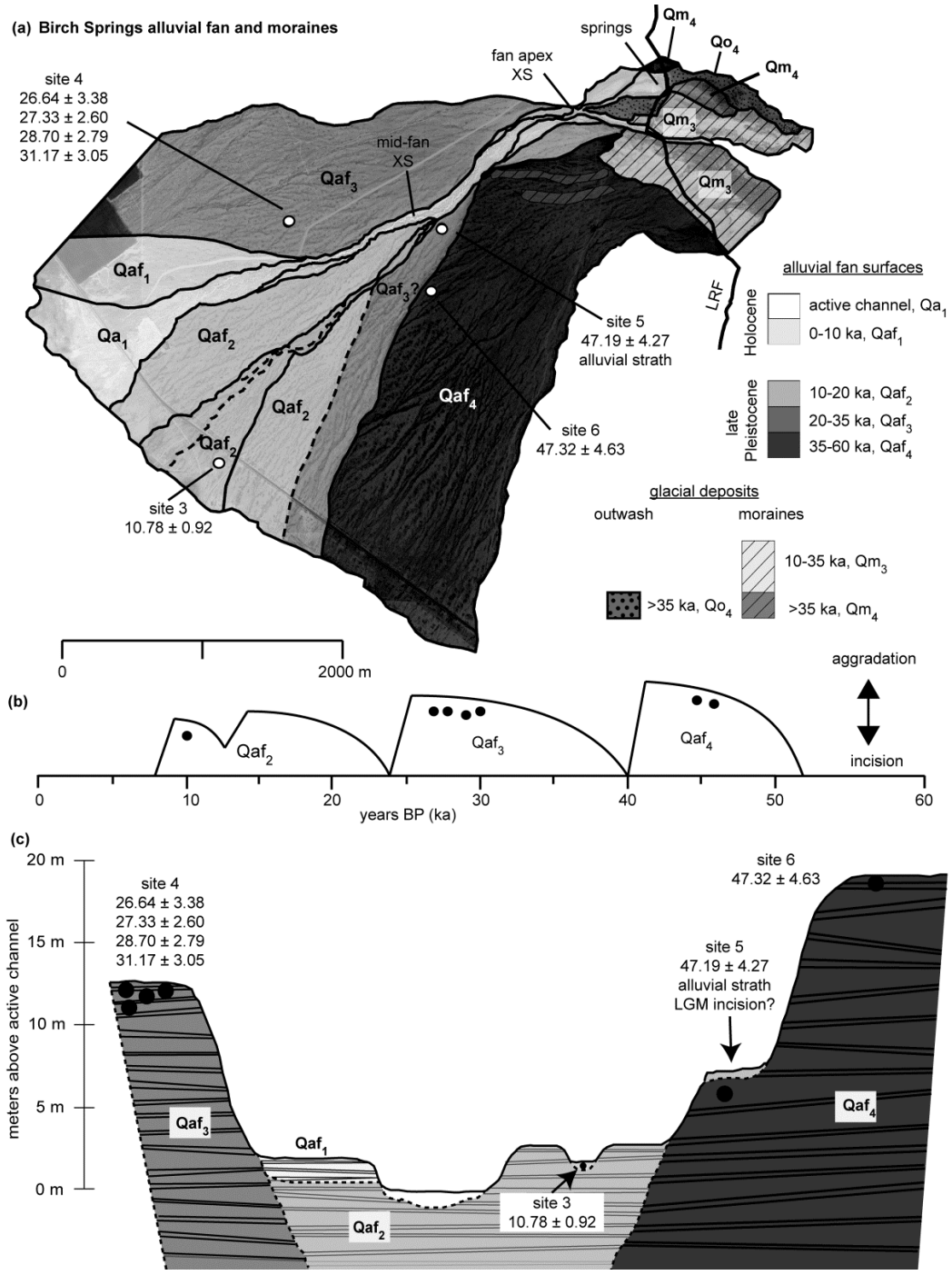

Figure 2.6 (a) Map of surfaces of the Birch Springs alluvial fan and associated glacial moraines. Surfaces are drawn over an aerial photo to show surface topography but roads and irrigated fields are also visible as darker squares. White circles show locations of OSL samples. (b) Inferred timing of aggradation and incision on the Birch Springs fan. Black dots denote OSL samples. (c) Generalized cross-section of fan showing locations of OSL samples with resulting ages estimates and inferred ages for non-dated deposits. Actual depth of fills is not known, and no horizontal scale is implied.

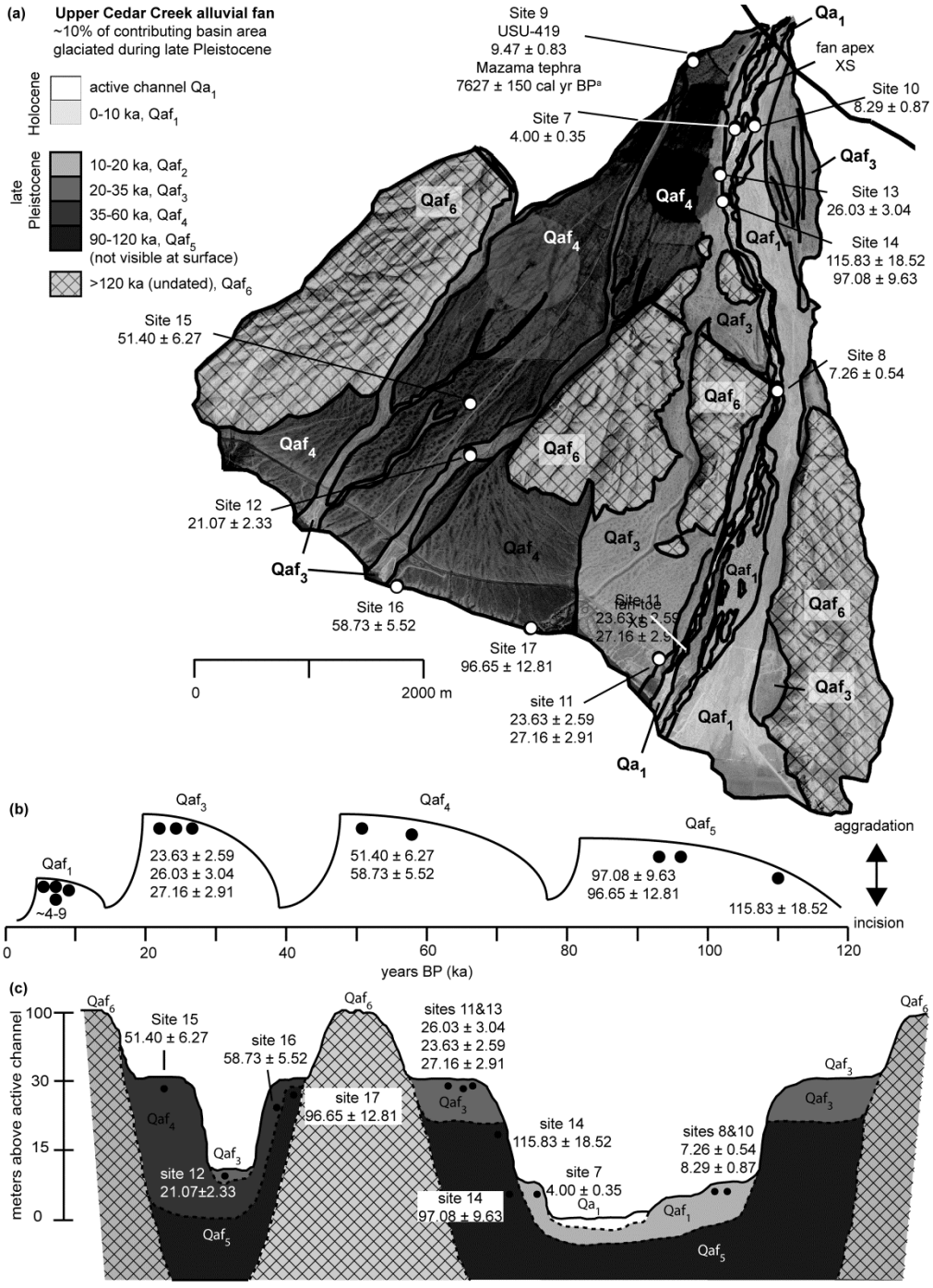

Figure 2.7 (a) Map of the Upper Cedar Creek alluvial fan. Surfaces are drawn over an aerial photo to show surface topography but roads and irrigated fields (lighter and darker circles) are also visible. White dots mark the locations of OSL samples, and yellow dots mark the general locations of sediment samples. (b) Inferred timing of aggradation and incision on the Upper Cedar Creek fan. Black dots denote OSL samples. (c) Representative cross-section of main surfaces and their inferred relationships with OSL sample locations and age estimates. Actual depth of fills is not known, and no horizontal scale is implied.

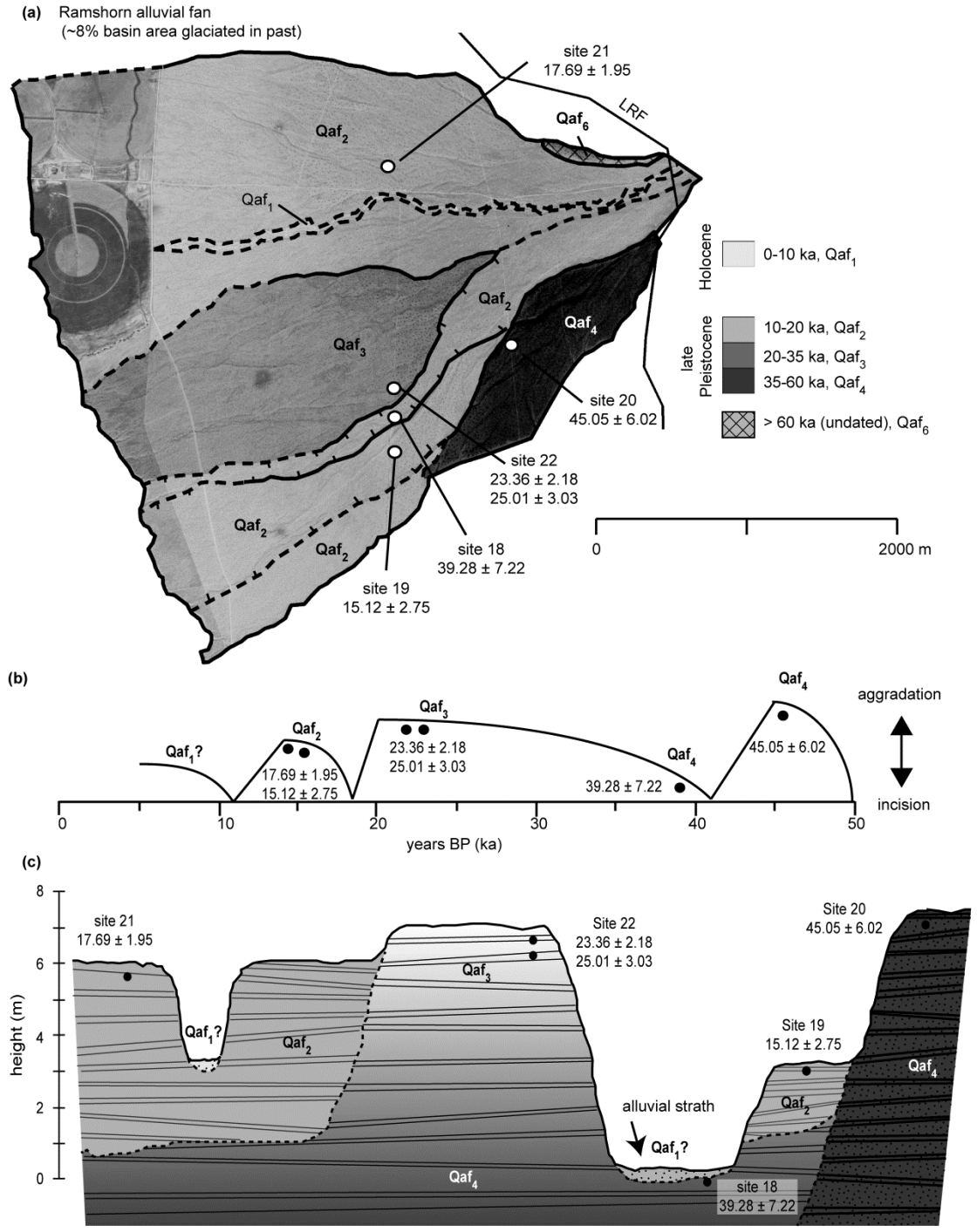

Figure 2.8 (a) Map of the Ramshorn alluvial fan. Surfaces are drawn over an aerial photo to show surface topography but roads and irrigated fields (darker circles) are also visible. Hash marks are drawn towards lower surface. (b) Inferred timing of aggradation and incision on the Ramshorn fan. Black dots denote OSL samples. (c) Generalized cross-section of the Ramshorn fan showing major surfaces and approximate locations of OSL samples with resulting age estimates. Actual depth of fills is not known, and no horizontal scale is implied.

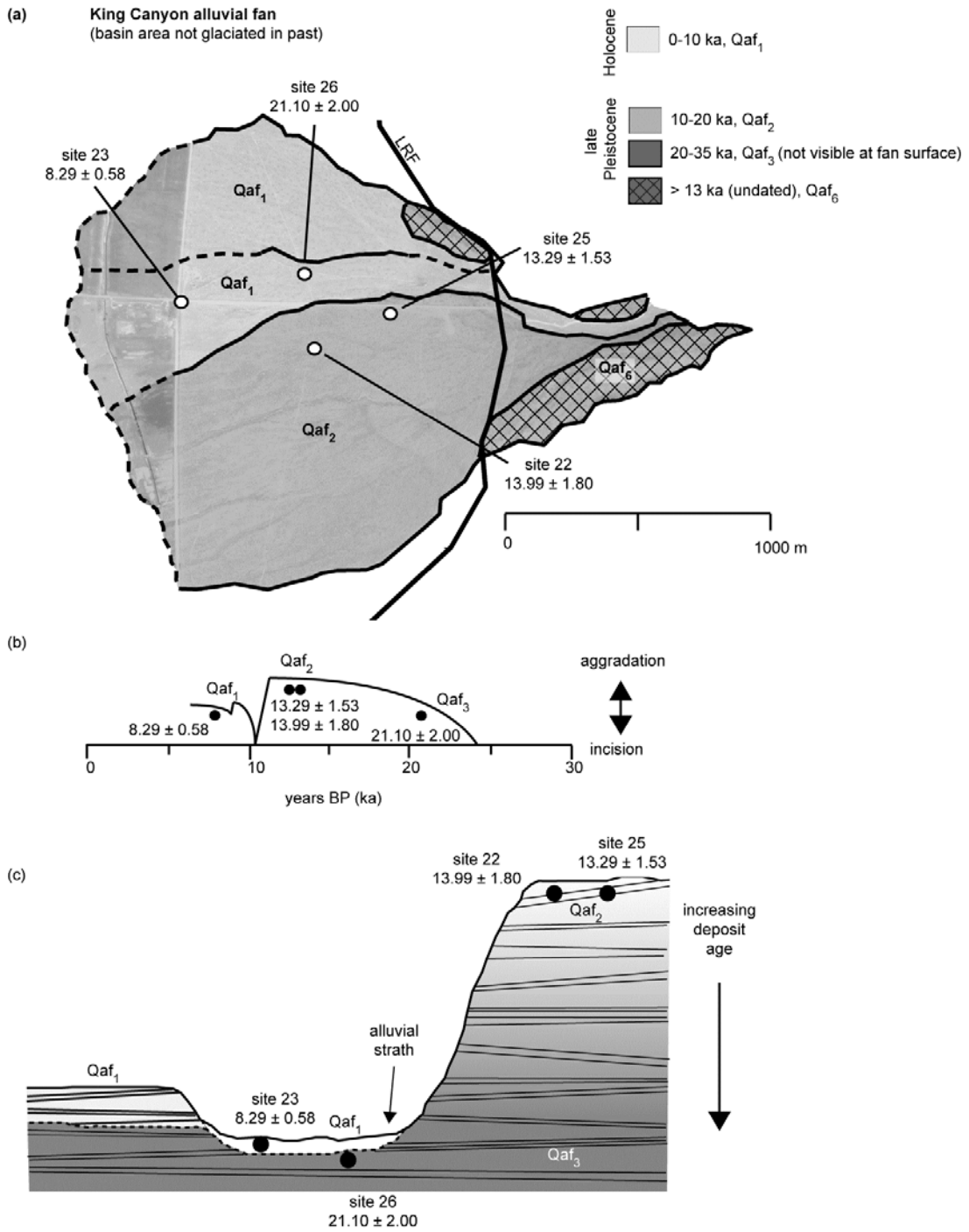

Figure 2.9 (a) Map of the King Canyon alluvial fan. Surfaces are drawn over an aerial photo to show surface topography but roads and irrigated fields (darker squares near fan toe) are also visible. (b) Inferred timing of aggradation and incision on the King Canyon fan. Black dots denote OSL samples. (c) Generalized cross-section showing the major surfaces of the King Canyon fan and the approximate locations of OSL samples with their resulting age estimates. Actual depth of fills is unknown and no horizontal scale is implied.

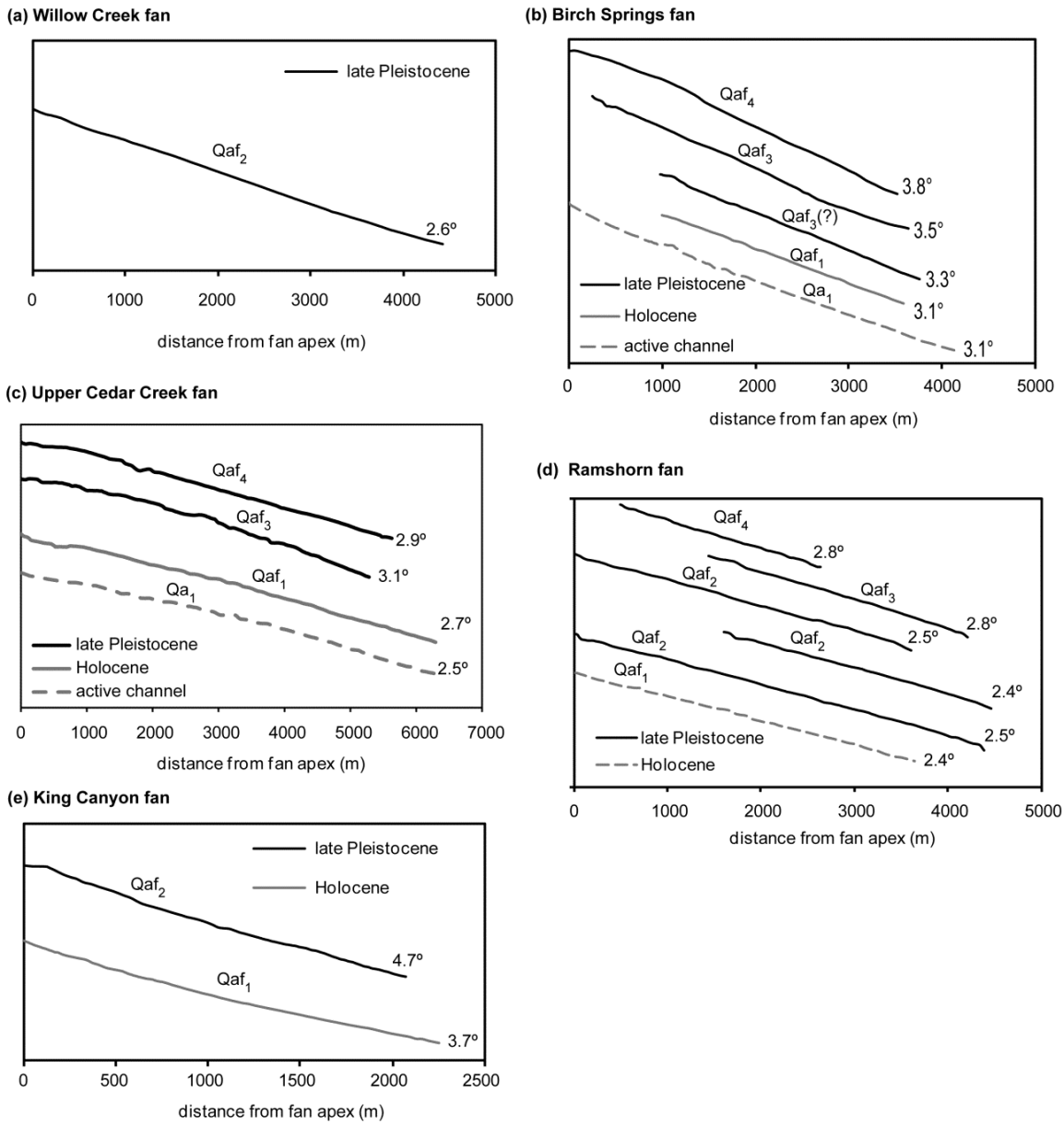

Figure 2.10 Longitudinal profiles for significant alluvial fan surfaces and average surface slope. While average surface slopes vary among fans for similar-age surfaces, late Pleistocene surfaces (Qaf_2-Qaf_4) are steeper than Holocene surfaces (Qaf_1) on individual fans. (a) Longitudinal profile for single major surface of the Willow Creek fan. (b) the Birch Springs fan. (c) the Upper Cedar Creek fan. (d) the Ramshorn fan. (e) the King Canyon fan.

rarely contain sand lenses. Patterson (2006) made similar observations and provides more detailed results of the facies assemblages for several LRR fans.

On the active surfaces of Birch Springs and Upper Cedar Creek fans, surface morphology indicates that flow occurs primarily in braided channels, though occasional sheetflooding may occur (Patterson, 2006). Depositional features such as ridges and mounds in the channel, as well as sediment and debris piled against the upstream side of trees indicate that transport capacity is at times capable of mobilizing sediment. It is not clear, however, whether this represents deposition of new material or reworking of old deposits. Because these active surfaces are entrenched through nearly the entire fan length, dominant depositional processes likely differ from those of the extensive late Pleistocene surfaces that likely aggraded predominantly through unconfined flow processes.

As observed in the field, results from grain-size analysis suggest that grain-size distributions for deposits of all ages are generally similar (Fig. 2.11). One exception is where a Holocene deposit containing a characteristic sand lens was sampled at UC fan, resulting in an increased proportion of <2 mm grain sizes (Fig. 2.11c, mid-fan graph). The gravel facies of Holocene and late Pleistocene deposits contained similar proportions of <2 mm grain-size fraction, ranging from approximately 14-22% by weight. The <2 mm grain-size portion for gravels of active surface deposits was approximately 1-21% by weight. However, patches of well-sorted sand were often observed within active channels, suggesting that the low percentages measured may reflect winnowing of the <2 mm grain-size fraction and better sorting by modern stream processes.

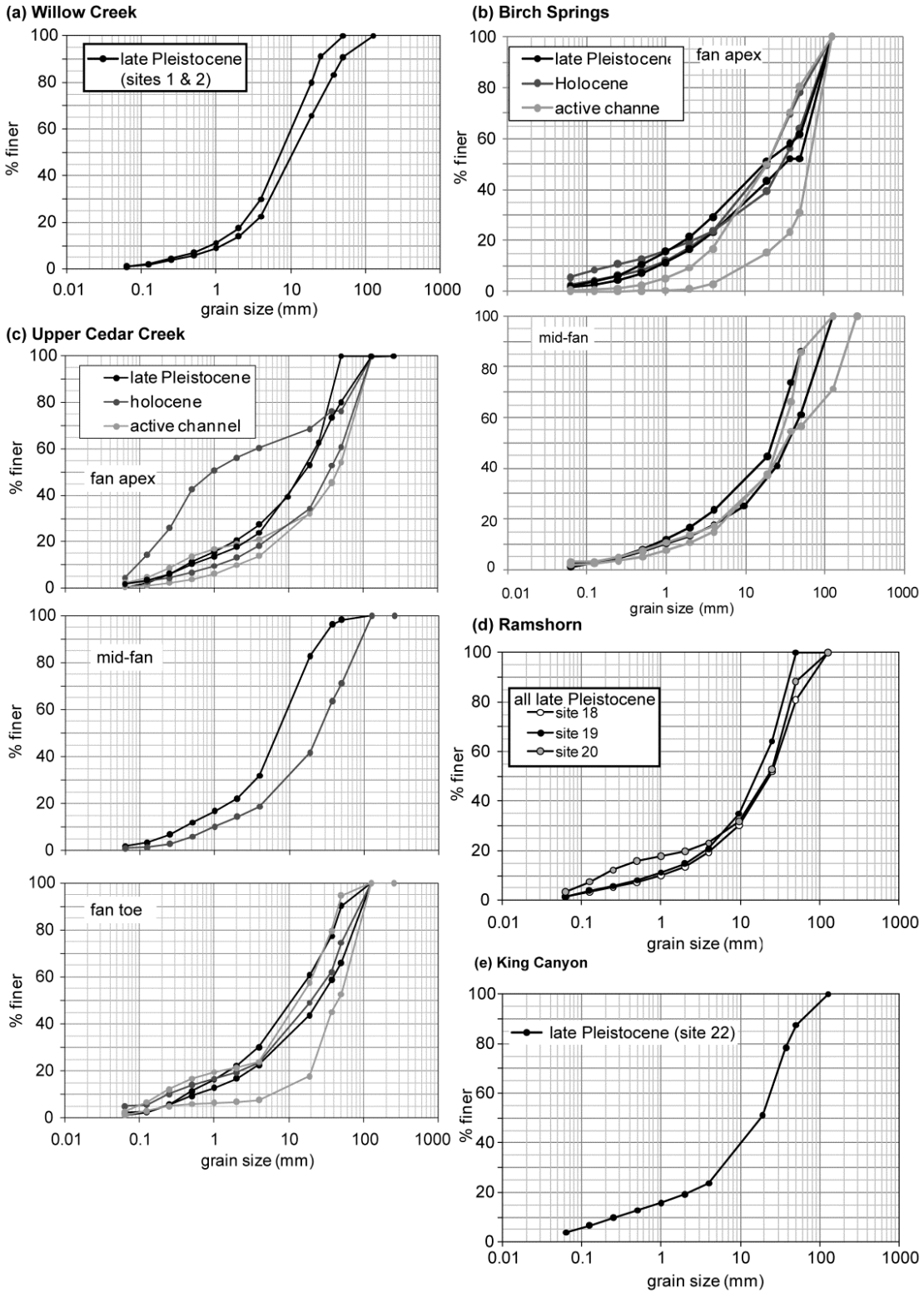
(a) Willow Creek
late Pleistocene (sites 1 & 2)
% finer
grain size (mm)
(b) Birch Springs
late Pleistocene
Holocene
active channe
fan apex
mid-fan
(c) Upper Cedar Creek
late Pleistocene
holocene
active channel
fan apex
mid-fan
fan toe
(d) Ramshorn
all late Pleistocene
site 18
site 19
site 20
(e) King Canyon
late Pleistocene (site 22)

Figure 2.11 (previous page) Grain-size distributions for sediment samples collected from LRR fan deposits of varying age. Late Pleistocene, Holocene, and modern deposits have generally similar grain-size distributions. (a) Grain-size distributions for samples taken from sites 1 and 2 on the Willow Creek fan. (b) Distributions for sediment samples collected in the vicinity of the fan apex and approximately half way down the length of the fan. (c) Distributions for deposits of varying age from the vicinities of the fan apex, mid-fan, and fan toe of the Upper Cedar Creek fan. (d) Distributions for sediment samples from late Pleistocene deposits at the Ramshorn fan. (e) Distribution for site 22 at the King Canyon fan.

2.4.2 OSL Age Estimates

Optical age estimates for LRR alluvial fan deposition range from approximately 4-115 ka (Fig. 2.12, Table 2.1). The six alluvial fan samples that return Holocene ages (~4-10 ka) were all collected from surfaces with smaller surface areas. The remaining 26 alluvial fan samples return late Pleistocene ages (~10-115 ka) with 24 of these collected from the extensive surfaces that comprise the majority of fan surface area. The final two fan samples were collected from an approximately 30 m exposure of fan gravels on Upper Cedar Creek Fan from depths of 15 m and 20 m below the modern surface (Fig. 2.13) and return some of the oldest age estimates (USU-416, 115.83 ± 18.52 ka; USU-302, 97.08 ± 9.63 ka). The two samples from terraces of the E. Fork Big Lost River return ages of 6.48 ± 0.61 ka (USU-651) and 38.12 ± 3.40 ka (USU-304).

For eleven of the samples excavated from coarse sheetflood deposits, bulk sediment samples for dose-rate estimates could not be collected as trenches were already closed (Table 2.1). Dose rates for these samples are based on an average of the two sand grain-size fractions. Results from other excavated samples indicate that true dose rates may be between 0.4-39.5% (average of 14.3%) lower than those estimated from the sand

grain-size fractions (Chapter 1, Section 1.4.1). As such, resulting ages may underestimate the timing of deposition by a similar percentage.

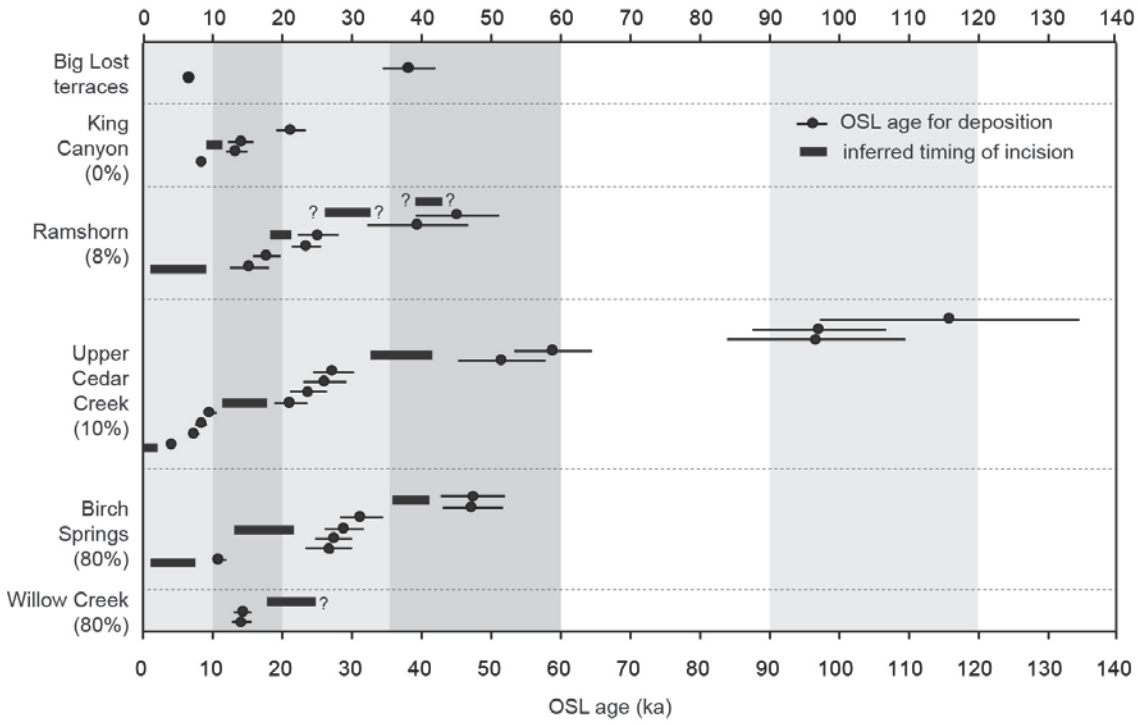

Figure 2.12 OSL age estimates for sediment deposition and inferred timing of incision for LRR alluvial fans and two terraces of the E. Fork Big Lost River. The number in parentheses following alluvial fan names refers to the extent of contributing basin area subject to late Pleistocene glaciation.

Table 2.1 OSL sample information and ages. Site numbers refer to locations shown in Figs. 2.5-2.9.

Location	Site no.	USU Lab no.	Deposit type	Sample depth (m)	No. of aliquots	Dose rate (Gy/ka)	D_e (Gy) ± 1σ	Optical age (ka) ± 1 standard error
Willow Creek Alluvial Fan	1	USU-412[b]	sheetflood gravels	1.4	24	2.7±0.18	38.39±7.14	14.22±1.25
	2	USU-413[b]	sheetflood gravels	2	22	2.67±0.18	37.44±10.76	14.01±1.44
Birch Springs Alluvial Fan	3	USU-414[a]	fluvial sand lens	2	26	1.13±0.06	12.17±3.06	10.78±0.92
	4	USU-415[b]	sheetflood gravels	1.5	23	1.01±0.08	31.58±5.35	31.17±3.05
	4	USU-645[b]	sheetflood gravels	1.3	27	0.98±0.07	26.9±5.63	27.33±2.60
	4	USU-646[b]	sheetflood gravels	1.5	24	0.98±0.10	26±7.68	26.64±3.38
	4	USU-647[b]	sheetflood gravels	1.5	22	0.97±0.08	27.85±4.75	28.70±2.79
	5	USU-703[c]	sheetflood gravels	1.8	24	0.94±0.06	44.25±8.31	47.19±4.27
	6	USU-704[c]	sheetflood gravels	1.7	28	0.75±0.05	35.59±10.07	47.32±4.63
Upper Cedar Creek Alluvial Fan	7	USU-251[a]	fluvial sand lens	1.9	25	3.88±0.17	15.51±3.62	4.00±0.35
	8	USU-417[c]	fluvial sand lens	5	23	2.23±0.10	16.2±3.06	7.26±0.54
	9	USU-419[c]	fluvial sands and gravels with loess in buried soil horizon	1.2	24	2.27±0.14	21.5±5.08	9.47±0.83
	10	USU-652[c]	fluvial sand lens	3.2	24	2.25±0.19	18.69±4.64	8.29±0.87
	11	USU-299[c]	sheetflood gravels	2.3	28	1.19±0.10	28.1±7.29	23.63±2.59
	11	USU-300[c]	sheetflood gravels	3.2	24	1.25±0.10	33.84±8.37	27.16±2.91
	12	USU-653[c]	sheetflood gravels	1.6	31	1.18±0.09	24.91±8.61	21.07±2.33
	13	USU-301[c]	sheetflood gravels	1.9	26	1.33±0.13	34.6±8.25	26.03±3.04
	14	USU-416[c]	sheetflood gravels	15	24	1.06±0.15[e]	122.25±25.76	115.83±18.52
	14	USU-302[c]	sheetflood gravels	20	22	1.36±0.10	132.08±25.71	97.08±9.63
	15	USU-420[b]	sheetflood gravels	1.7	29	1.95±0.21	100.32±17.76	51.40±6.27
	16	USU-250[a]	fluvial sand lens	1.6&18[d]	24	2.25±0.16	132.41±23.21	58.73±5.52
	17	USU-644[c]	fluvial sand lens	3.5	21	1.31±0.15	126.32±24.21	96.65±12.81

Table 2.1 (Continued.) OSL sample information and ages. Site numbers refer to locations shown in Figs. 2.5-2.9.

Location	Site no.	USU Lab no.	Deposit type	Sample depth (m)	No. of aliquots	Dose rate (Gy/ka)	D_e (Gy) ± 1σ	Optical age (ka) ± 1 standard error
Ramshorn Alluvial Fan	18	USU-305[b]	sheetflood gravels	1.9	37	1.18±0.20	46.27±12.28	39.28±7.22
	19	USU-306[b]	sheetflood gravels	2	26	1.45±0.24	21.49±5.79	15.12±2.75
	20	USU-307[b]	sheetflood gravels	1.8	21	1.06±0.11	47.95±13.42	45.05±6.02
	21	USU-648[c]	sheetflood gravels	1.6	23	1.53±0.14	27.11±5.33	17.69±1.95
	22	USU-649[c]	sheetflood gravels	2	22	1.2±0.08	28.01±6.43	23.36±2.18
	22	USU-650[c]	sheetflood gravels	1.6	27	1.06±0.11	26.61±5.95	25.01±3.03
King Canyon Alluvial Fan	23	USU-421[a]	fluvial sand lens	1	25	3.09±0.14	25.65±3.27	8.29±0.58
	24	USU-422[b]	sheetflood gravels	1.6	25	2.05±0.23	28.69±6.46	13.99±1.80
	25	USU-655[c]	sheetflood gravels	1.9	27	2.09±0.16	27.76±9.14	13.29±1.53
	26	USU-656[c]	sheetflood gravels	2	27	1.49±0.10	31.35±8.65	21.10±2.00
E. Fork Big Lost River Terraces	27	USU-304[a]	fluvial sand lens	13.4	33	3.72±0.27	141.68±41.02	38.12±3.86
	28	USU-651[a]	fluvial sand lens	1.1	23	4.55±0.21	29.48±9.20	6.48±0.61

a. Sample collected by pounding metal tube in sand lens. Dose rate based on total <2 mm grain-size fraction.
b. Sample excavated from deposit under light-safe tarps or at night. Dose rate based on sand grain-size fractions.
c. Sample excavated from deposit under light-safe tarps or at night. Dose rate based on bulk sediment samples.
d. Changes in burial depth through time due to erosion.
e. Signs of U/Th disequilibrium in dose-rate chemistry.

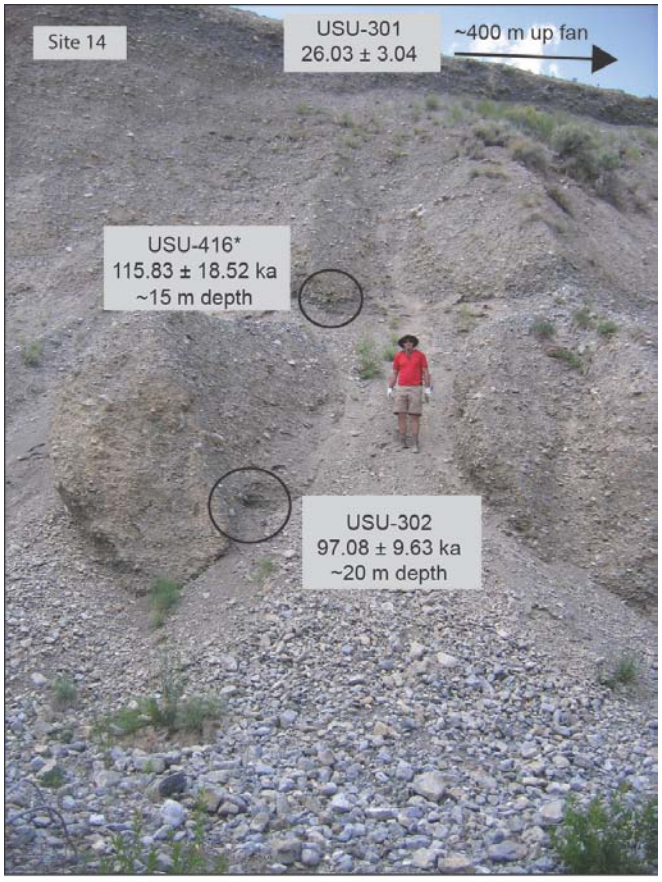

Figure 2.13 The ~30 m exposure of late Pleistocene deposits at site 14 on the Upper Cedar Creek fan with the locations and age estimates from 3 OSL samples.

A tephra deposit was found at Site 9 on the Upper Cedar Creek fan and sampled for identification (Fig. 2.14). The tephra was exposed within a small channel incised up to ~3 m within fluvial deposits, including sheetflood couplets and an old channel fill. Immediately under the tephra was a finer-grained unit interpreted as a buried soil surface due to its resemblance to modern soils in which upper horizons contain a greater component of buff-colored loess that decreases with depth as content of gray, limestone gravels increase, grading into unaltered sheetflood deposits. The tephra sample was analyzed at Washington State University's GeoAnalytical Lab by electron microprobe

and Boise State University by ICP-MS. Both labs determined that the source was the 7627 ± 150 cal yr BP (Zdanowicz et al., 1999) eruption of Mt. Mazama, a stratovolcano that formed present-day Crater Lake in Oregon, USA (~700 km west of the LRR). An OSL sample (USU-419) was collected from a gravelly portion of the deposit 20 cm below the ash. The slightly older age estimate of this sample (9.47 ± 0.83 ka) is appropriate given the relative positions of the tephra and OSL samples.

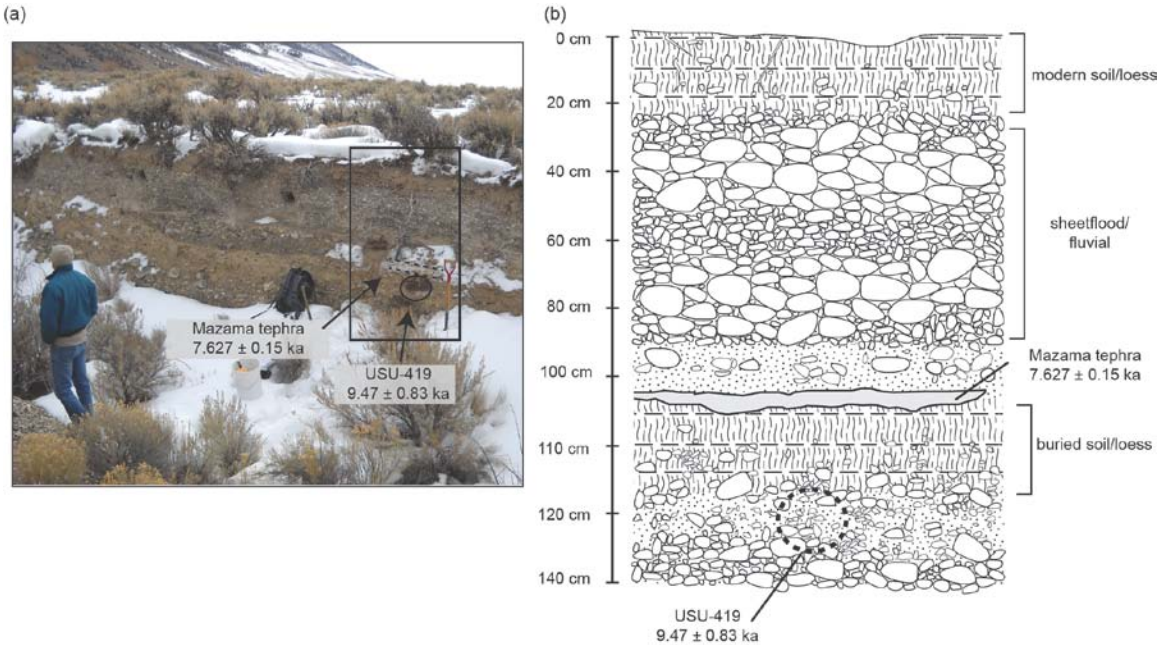

Figure 2.14 Illustration of site 9 on Upper Cedar Creek fan where Mazama tephra was identified and OSL sample USU-419, collected from below the tephra. The age of the tephra, 7.627 ± 0.15 ka (Zdanowicz et al., 1999) and age of the OSL sample, 9.47 ± 0.83 ka, show good agreement.

Geomorphic mapping and OSL dating of the five fans indicate that fan activity during the late Pleistocene (>10 ka) and Holocene (<10 ka) created distinct surface groups with more significant aggradation during the late Pleistocene. Fan deposits with an OSL or inferred late Pleistocene age account for a minimum of approximately 50%, a

maximum of nearly 100% of the area of individual fans (Fig. 2.15a), and over 80% of the total area of all five fans (Fig 2.15b). In contrast, surfaces with an OSL or inferred Holocene age account for a minimum of approximately 1% of fan, and a maximum of 20% for individual fans (Fig. 2.15a), and approximately 10% of the total fan area (Fig. 2.15b). (Geomorphically older surfaces not thoroughly investigated or uplifted remnant surfaces account for the remaining 10% of total fan area.)

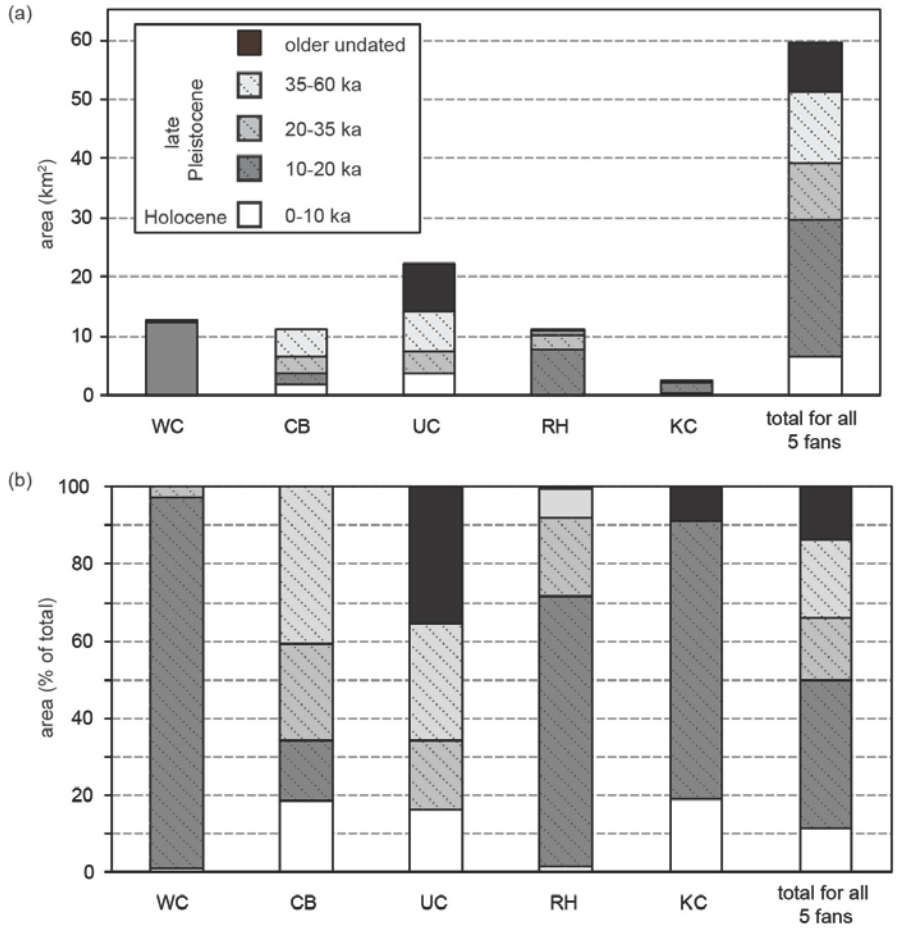

Figure 2.15 Summary of fan area for individual fans and total fan area composed of Holocene and late Pleistocene surfaces.

2.4.3 Pedogenic Carbonate and Loess Accumulation with Age

Soils developed within LRR alluvial fan deposits were similar throughout the range and typically displayed a sequence of buff-colored loess of varying thickness overlying sheetflood deposits of predominately gray, subangular limestone clasts (Fig. 2.16). In addition, soils display features common of semi-arid soils (Fig. 2.16). Sparse

(a) Upper Cedar Creek alluvial fan, site 15

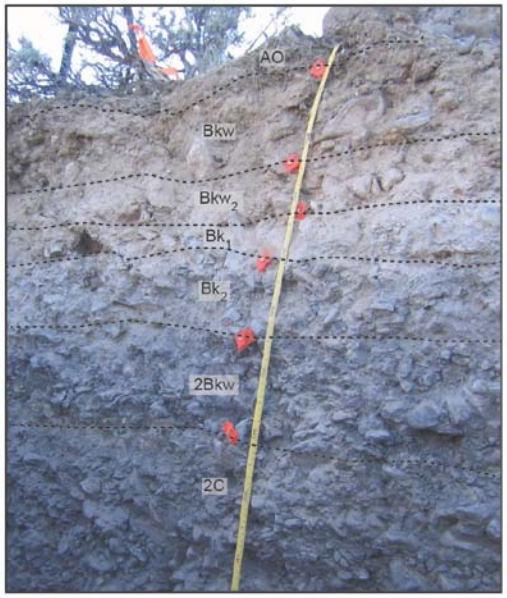

characteristics of soils on LRR alluvial fans

- thin or absent O horizon
- thin or absent A horizon
- loess accumulation
- mixed loess and alluvial gravels
- significant $CaCO_3$ accumulation
- unaltered alluvial gravels

(b)

depth (cm)	horizon or deposit	moist color	structure grade/ped type	gravel (%)	consistence (dry)	texture	boundary	parent material	$CaCO_3$ stage
0-5	AO	10YR 4/3	sg/gr	10	sh	SiL	abrupt and straight	loess	NA
5-24	Bkw	10YR 5/3	1/pl and sbk	15	sh	SiL	clear and wavy	loess	I+
24-33	Bkw_2	10YR 6/3	1/sbk	25	sh	SiL	clear and wavy	loess with some alluvial gravels	I+
33-41	Bk_1	10YR 6/2	2/sbk	35	h	SiL	abrupt and straight	alluvial gravels with some loess	III+to IV
41-55	Bk_2	10YR 4/2	1/sbk	40	sh	SiL	clear and straight	alluvial gravels with some loess	II+
55-71	2Bkw	10YR 3/1	m	50	lo	SL	gradual and straight	alluvial gravels	I
71-209	2C	10YR 3/1	m	75	lo	SL	bottom of trench	alluvial gravels	NA

Figure 2.16 Example of typical soil developed in LRR alluvial fan deposits. (a) Soil development at site 15 on the Upper Cedar Creek Alluvial fan. Typical characteristics found in all soils are listed to the right of the image. (b) Soil description for site 15 following methods outlined in Birkeland et al. (1991). sg = single grain, gr = granular, pl=platy, sbk=subangular blocky, m=massive, sh=slightly hard, h=hard, lo=loose, SiL=silty loam, SL=sandy loam.

vegetation cover produces thin to absent O horizons, while the low average annual precipitation produces a thin zone of leaching (A horizon) and significant accumulation of pedogenic $CaCO_3$ in one or more Bk horizons within both and alluvial gravel parent materials. Stable Holocene surfaces commonly had stage I-I+ carbonate accumulation, and late Pleistocene surfaces commonly had stage II-III, and rarely stage IV accumulation (see Appendix A). Based on comparison with OSL ages, the accumulation of pedogenic $CaCO_3$ generally increased with deposit age though there is variability in the observed stage for surfaces of similar age (Fig. 2.17a).

The average thickness of pedogenic carbonate coats also increased with deposit age (Fig. 2.17b). Coats were often thickest at the base of the loess layer, and average coat thicknesses ranged from a minimum of 0.46 ± 0.27 mm to a maximum of 2.81 ± 1.13 mm. A growth rate for pedogenic carbonate coats within the basin of 0.4 mm/10 ka (R^2=0.66) can be estimated from the relationship between average coat thickness and OSL ages (Fig. 2.17b).

The thickness of loess deposits on fan surfaces varied significantly from ~25-160 cm but did not show a strong relationship with deposit age (Fig. 2.17c). The greatest amount of loess was found on the southern fans, Ramshorn and King Canyon, with accumulation of >1 m on some surfaces. The relationship between OSL age and loess accumulation is also generally weak on individual fans, with the exception of the Ramshorn fan (Fig. 2.17c).

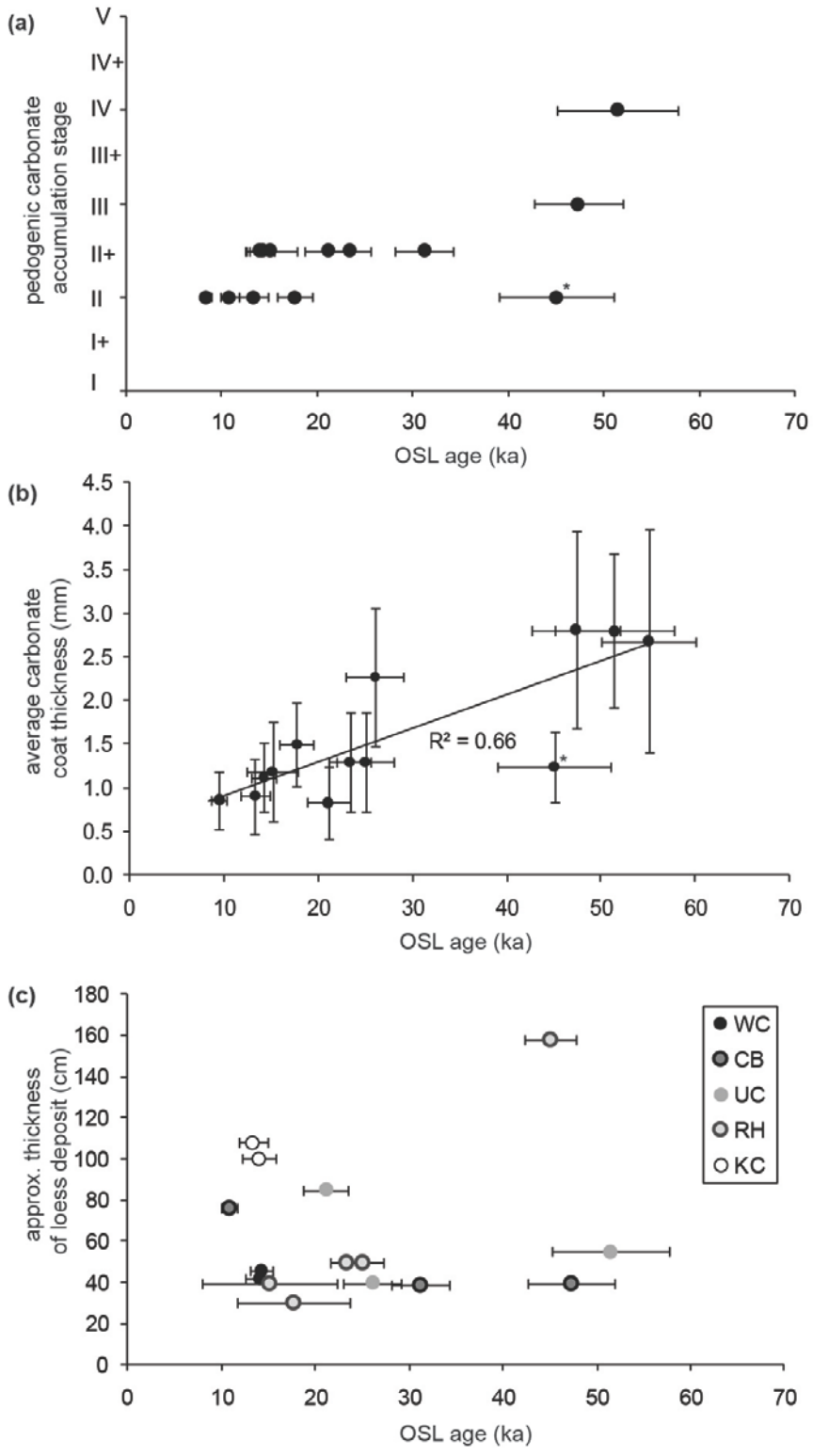
(a)
pedogenic carbonate accumulation stage
V
IV+
IV
III+
III
II+
II
I+
I
0
10
20
30
40
50
60
70
OSL age (ka)
(b)
average carbonate coat thickness (mm)
4.5
4.0
3.5
3.0
2.5
2.0
1.5
1.0
0.5
0.0
R² = 0.66
OSL age (ka)
(c)
approx. thickness of loess deposit (cm)
180
160
140
120
100
80
60
40
20
0
WC
CB
UC
RH
KC
OSL age (ka)

Figure 2.17 (previous page) Relationships among deposit age as indicated by OSL dating, observed pedogenic carbonate accumulation stage, average thickness of pedogenic carbonate coats, and loess deposits. (a) Observed stage of pedogenic carbonate accumulation (Birkeland et al., 1991) plotted with corresponding OSL age estimate. (b) Average pedogenic carbonate coat thickness plotted against OSL age for deposition from the same site. A growth rate of approximately 0.4 mm/10 ka for pedogenic carbonate coats within the basin is suggested (R^2=0.66). (c) Approximate depth of loess accumulation plotted against OSL age estimates for deposition, showing that loess accumulation for surfaces of similar age can vary significantly throughout the range. However, on individual fans, the relationship is sometimes stronger (for example Ramshorn fan). In both (a) and (b), outlying data points (marked by *) result from the same sample on the Ramshorn fan (site 20) with weak $CaCO_3$ accumulation and thin coats for OSL age. This may be due to the significant amount of loess accumulation at this site (~1.58 m).

2.5 Discussion

2.5.1 Surface Age Estimates from Loess and Pedogenic Carbonate Coats

OSL dating provides an opportunity to assess the reliability of other indicators of surface age, such as loess accumulation, pedogenic $CaCO_3$ stage, and the thickness of pedogenic $CaCO_3$ coats. First, the use of loess deposits to correlate fan surfaces of similar age throughout the basin proved problematic because of the weak relationship between the thickness of loess deposits and OSL age. A weak relationship would be expected for sites where fan morphology and OSL ages indicate younger incision into older, buried deposits (discussed further below). However, even with these locations removed, as in Fig. 2.17c, the relationship remains weak. Further, we observed a poor correlation between surface age and loess accumulation even on individual fans, with the exception of the Ramshorn fan. These findings may highlight that numerous factors influence the amount of apparent loess accumulation on an individual surface. These

factors include vegetation density, the orientation of the surface relative to prevailing wind direction, erosion by water and wind, and proximity to loess source areas. Proximity to loess source areas appears to influence loess accumulation in the LRR, as the thickest deposits are found on the southern fans, Ramshorn and King Canyon, which sit closest to the eastern Snake River Plain where thick loess sequences are common (e.g., Lewis et al., 1975).

We also observed considerable variability in the observed $CaCO_3$ accumulation stage in alluvial fan soils for deposits of similar age. For example, stage II+ accumulation was observed in soils developed on surfaces with depositional ages ranging from approximately 10-35 ka (Fig 2.17a; sites where fan morphology and OSL ages indicate incision into older, buried deposits have been removed). These results suggest that in this region, the difference in surface ages must approach ~20 kyr before $CaCO_3$ accumulation stage becomes a reliable indicator of age. Kluer (1988) also noted significant variability in $CaCO_3$ accumulation in the Willow Creek Area, and regarded it as an unreliable indicator of relative surface age. Some of this variability can likely be accounted for by the subjective nature of determining accumulation stage, but local differences in accumulation rates within the LRR also influence carbonate stage. The rate of pedogenic $CaCO_3$ accumulation within a soil can be influenced by many factors, including differences in vegetation type and density, amount of bioturbation, amount of loess accumulation, and variability in soil moisture related to elevation or aspect. For example, we noted weaker $CaCO_3$ accumulation both within the northern portion of the basin and at higher elevations, such as on moraines or glacial outwash surfaces north of the Willow Creek fan. With colder temperatures in the northern part of the basin and at

higher elevations, effective moisture is likely greater, reducing $CaCO_3$ accumulation. These observations suggest that the northern LRR is near the climate boundary for $CaCO_3$ accumulation, and that during past cooler and moister intervals, calcium carbonate would have been leached through these soils rather than deposited. Finally, $CaCO_3$ accumulation for surfaces may vary from OSL ages because OSL dating estimates timing of deposition, while carbonate accumulation stage estimates how long a surface has been stable for pedogenesis to occur. The lag time between deposition and soil formation likely varies from site to site, resulting in differences in carbonate accumulation for surfaces with similar depositional timing.

The correspondence of average $CaCO_3$ coat thickness and deposit age proved much stronger (Fig. 2.17b), providing a more reliable means of estimating surface age as others have previously demonstrated within the basin (Pierce, 1985; Vincent et al., 1994). In addition, the growth rate of 0.4 mm/10 ka (average for the period from 10-60 ka) for pedogenic $CaCO_3$ coats estimated in this study is reasonable when compared to previously estimated growth rates by Pierce (1985) and Vincent et al. (1994). Pierce (1985) estimated a long-term average growth rate of 0.6 mm/10 ka for the time period between 30-160 ka, while Vincent et al. (1994) estimated a growth rates ranging from 1.1 to 0.4 mm/ 10 ka, with an average of 0.56 mm/10 ka for the Holocene and 0.6-0.7 mm/10 ka for the last 25 ka. While reasonable, the predicted growth rate from this study is less than that of Pierce (1985), and falls into the low end of the range predicted by Vincent et al. (1994). Reasons for this may include (1) differences in methods used to estimate carbonate coat growth rates and (2) locations used to generate the growth-rate estimates. Pierce (1985) generated growth-rate estimates from U-series dating of the coats

themselves rather than relying on dating of other material within the same deposit. Further, the estimated growth rate from Pierce (1985) is based only on carbonate coats collected in the southern portion of the basin along the Arco segment of the Lost River Fault. Vincent et al. (1994) estimated their Holocene growth rates with radiocarbon dating of organic material within deposits, but their growth rate for the last 25 ka relies on assumed ages for LRR moraines. In addition, their study was restricted to the northern portion of the range. The growth rate from this study was generated through OSL dating and measurement of $CaCO_3$ coats throughout the basin, incorporating more of the potential variability in growth rates driven by the same factors that influence variability in overall accumulation of $CaCO_3$ in soils.

Comparisons between OSL ages for deposits and pedogenic $CaCO_3$ accumulation and coat thicknesses highlights the ability of OSL dating to detect alluvial strath surfaces. Such surfaces were identified on three of the five LRR alluvial fans, including the surface of site 5 on the Birch Springs fan (Fig. 2.6), the surface of site 18 on the Ramshorn fan (Fig. 2.8) and the surface of site 26 on the King Canyon fan (Fig. 2.9). At the King Canyon fan, the surface of site 26 is interpreted as an alluvial strath because the OSL age estimate here of 21.10 ± 2.00 ka significantly predates the age estimate of ~13-14 ka for the higher and geomorphically older surface of sites 22 and 25. Another OSL sample from this same strath surface (site 23), returns an age of 8.29 ± 0.58; however, we collected the site 23 sample from a sand lens at a depth of only 1 m. This suggests the deeper and older material is ~12.5 ka older than the younger loess cap. Partial bleaching of quartz grains could also produce these anomalously old ages for geomorphically young surfaces, but D_e distributions for OSL samples from these sites do not display

characteristics that suggest partial bleaching (see Chapter 1, Section.1.4.2). While alluvial strath surfaces make up a small portion of the fans, the distinction between surface formation through incision or deposition is often important in studies investigating links between climate and geomorphic response.

2.5.2 Episodes of Fan Aggradation

From OSL dating and geomorphic mapping, we have determined that LRR fans aggraded during several distinct episodes. However, two potential problems in interpreting OSL ages arise. First, the majority of OSL samples were collected from the top 1-3 m of deposits, resulting in age estimates that may most accurately represent the final stages of deposition on a surface. This interpretation assumes broadly concurrent deposition across much of the active fan surface due to rapid shifting of the active depositional lobe. If the active lobe of deposition on a surface did not shift rapidly, depositional ages would vary considerably across a surface and OSL ages may not represent final stage of deposition. Without samples from multiple depths in a deposit or numerous samples collected laterally across a single surface, we cannot determine if our OSL ages capture early, middle, or final stages of deposition. In the absence of such information, we assume that OSL ages likely represent later stages of aggradation but still indicate within uncertainty when environmental conditions enhanced fan building.

The second potential problem that arises while interpreting OSL ages comes from the eleven OSL samples excavated from sheetflood gravels that lack bulk sediment samples for dose-rate estimates. As discussed in Section 2.4.1, results from these samples may underestimate depositional ages between ~0.4-39.5% (average of 14.3%). However, in Chapter 1, Section 1.4.3 outlines an example in which two excavated

samples from the same surface, one with and one without a bulk sediment dose-rate sample, provide ages with good agreement (samples USU-422 and USU-655; Table 2.1). This suggests that in many cases, these samples still likely provide reasonable age control for fan aggradation.

2.5.3 Holocene Aggradation

Holocene fan activity and the resulting fan surfaces account for approximately 1-20% of the surface area of individual fans, and 10 % of the total fan area (Fig. 2.15). The actual area of Holocene aggradation is likely less as these percentages include modern channels on Birch Springs and Upper Cedar Creek fans that appear to be incising rather than depositing new sediment. Further, the volume of Holocene deposits is likely significantly less than late Pleistocene deposits as Holocene deposits are inset into late Pleistocene deposits, and probable alluvial strath surfaces indicate that Holocene deposits are very thin (see Figs. 2.6c, 2.8c, and 2.9c). In addition, the OSL age from one of the E. Fork Big Lost River terraces also suggests aggradation of this system during the Holocene.

2.5.4 Late Pleistocene Aggradation

OSL ages and geomorphic mapping suggest that Late Pleistocene aggradation occurred during distinct intervals from 10-20 ka, 20-35 ka, 35-60 ka, and possibly 90-120 ka. Dated or inferred deposition ~10-20 ka on four of the five fans accounts for roughly 40% of the total fan area. For the ~20-35 ka interval, dated or inferred deposition on four of the five fans accounts for roughly 20% of total fan area. Dated or inferred deposition ~35-60 ka on three of the five fans accounts for another approximately 20% of total fan

area. An age of 38.12 ± 3.40 ka from the higher E. Fork Lost River terrace (site 27; Fig. 2.1) suggests aggradation in the axial river system during this interval as well.

We tentatively suggest an older interval of fan aggradation ~90-120 ka based on ages produced by three OSL samples from two different sites (14 and 17) at the Upper Cedar Creek fan. However, we cannot estimate a surface area associated with these deposits because younger sediments overlie the sampled deposits at both sites, obscuring their extent. The two samples at site 14 (Fig. 2.7) were from depths of 15-20 m and overlying deposits return significantly younger ages (~23-27 ka; Fig. 2.7). The ~96 ka age from site 17 on the Upper Cedar Creek fan appears anomalously old in light of other OSL ages and $CaCO_3$ coat thickness from the same surface, suggesting that younger deposits overlie the ~96 ka deposit that we sampled (Fig. 2.7). However, in the absence of problems with the OSL sample from site 17, and its close correspondence with the ages from site 14, we infer that at site 17 we sampled a portion of an older, buried deposit.

2.5.5 Episodes of Inferred Fan Incision

Mapping of similar age fan surfaces also constrains ages for episodes of widespread alluvial fan incision throughout the basin. Three of the five fans likely incised in the last ~13 ka. OSL ages suggest that incision of the active surface of the Birch Springs fan began after ~10 ka (Fig. 2.6). The Upper Cedar Creek fan appears to have incised at least twice during the Holocene (Fig. 2.6). The approximately 4-8 ka surface incised up to ~7 m, followed by deposition of a minor, undated surface. This younger surface has subsequently been incised another ~3 m. Renewed incision in historic times is suggested by a minor surface near the fan toe that sits roughly 1 m above

the active channel. Dead cottonwoods still standing on this surface indicate recent abandonment, possibly related to reduced discharges after the onset of irrigation withdraws.

The King Canyon fan has no currently active channel, but surface morphology and OSL ages indicate two episodes of incision between approximately 8-13 ka (Fig. 2.9). First, the 13 ka surface incised, followed by an interval of stability or deposition that formed an undated surface. Incision of this undated surface to the level of the most recently active surface was complete at roughly 8 ka. The Ramshorn fan also likely incised twice during this period, first up to ~ 4 m into the 15 ka surface of site 19 (Fig. 2.8), followed by incision of a smaller channel on the northern portion of the fan. In Fig. 2.9, this young incised channel appears higher and thus older than other surfaces, but elevation differences shown are approximate for mid-fan. Near the apex, this most recently incised surface sits at the lowest elevation, making it the youngest surface.

We identified an older episode of widespread incision at roughly 10-30 ka on three of the five fans. On the Birch Springs fan, OSL ages from site 3 indicate that significant incision began sometime after 26-31 ka and was complete before deposition of the 10 ka surface of site 4 (Fig. 2.6). Similarly, at the Upper Cedar Creek fan, OSL ages from sites 13 and 11 suggest significant incision commenced after 23-27 ka but was complete before deposition of the 4-8 ka surface of sites 7, 8, and 10 (Fig. 2.7). Finally, at the Ramshorn fan, ages from site 22 suggest incision began after 23-25 ka and was finished before deposition of the 15 ka surface of site 19 (Fig. 2.8).

Additional evidence suggests widespread fan incision after ~45-50 ka as well, though younger deposits often obscure the location and extent of erosion. At the Birch

Springs, the roughly 6-7 m elevation difference between the surfaces of sites 6 and 4 resulted from incision between ~47-26 ka (Fig. 2.6). Similarly, the geomorphology of the Ramshorn fan suggests incision following the ~45 ka deposition at site 20. The Upper Cedar Creek fan may have also incised between deposition of the 51-58 ka surface of sites 15 and 16 and the approximately 21 ka surface of site 12 (Fig. 2.7). The converging pattern of the channel in which the 21 ka sediment of site 12 was deposited may suggest incision through headward erosion rather than from the contributing basin stream. However, creation of such a large channel through the length of the fan by headward erosion seems unlikely. Instead, the contributing basin stream likely incised the original channel and the converging pattern developed later as headward erosion started from the incised channel.

2.5.6 Temporal Changes in Transport Capacity and Sediment Supply

Differences in the characteristics of Holocene and late Pleistocene deposits, including differences in surface extents, average surface slopes, facies, and grain-size distributions indicate that the transport capacity of contributing basin streams and the volume of sediment delivered to the fans was greater under late Pleistocene conditions than during the Holocene.

Late Pleistocene deposits have much greater areal extent than Holocene deposits, indicating enhanced transport capacity and sediment delivery to fans during the late Pleistocene than during the Holocene. Late Pleistocene surfaces account for ~80% of total fan surface area while Holocene surfaces account for only ~10%. These calculations include probable alluvial strath surfaces, such as the active surfaces of the

Birch Springs and Upper Cedar Creek fans, so the actual extent of Holocene deposition is likely <10%.

Because the Holocene is the shortest period in the OSL chronology of deposition from this study, the smaller surfaces of this time period may simply be the result of less time for aggradation, rather than decreased aggradation rates. However, the lack of evidence for significant Holocene deposition on two fans, Willow Creek and Ramshorn, that do have extensive late Pleistocene surfaces suggests faster aggradation rates during the late Pleistocene on at least these fans. In addition, prior to the Holocene, the 10 kyr time period from ~10-20 ka accounts for ~40% of the total fan area. In contrast, the Holocene, which is a period of similar duration, has produced only ~10% of the total fan area.

Recent lack of activity on many fans also indicates conditions that are unable to generate adequate transport capacity in contributing basin streams to move available sediment to alluvial fans. Under modern conditions, three fans lack active surfaces (Willow Creek, Ramshorn, and King Canyon) despite extensive late Pleistocene deposits, and indicators of surface stability suggest negligible activity on these fans for much of the Holocene (Figs. 2.5, 2.8, 2.9; the small active channel on Willow Creek fan originates from springs on the Lost River Fault rather than the fan's contributing basin). For example, the absence of Holocene deposits on the Willow Creek fan, combined with evidence of surface stability from soils (e.g., stage II+ pedogenic $CaCO_3$ accumulation and an average coat thickness of 1.12 ± 0.29 mm on much of the fan area) is consistent with surface stability throughout the Holocene. The Ramshorn fan also lacks an active surface or other significant Holocene deposits (Fig. 2.8). A small channel on the northern

half of the fan likely incised during the Holocene, but soils on the larger alluvial strath surface on which site 18 is located exhibit stage II+ carbonate with an average coat thickness of 1.19 ± 0.57 mm, which is consistent with surface stability for much of the Holocene. At the King Canyon fan, the youngest dated deposit is ~8 ka at site 23 (Fig. 2.9), but stage III $CaCO_3$ and an average coat thickness of 0.46 ± 0.27 mm are consistent with surface stability shortly after ~8 ka. These three fans span the N-S extent of the LRR and suggest that Holocene transport capacity has been reduced throughout the range.

Differences in average fan surface slopes also suggest enhanced transport capacity and sediment supply to fans during the late Pleistocene. Though the exact controls on fan slope and longitudinal profiles are not well understood, modeling and flume work (e.g., Whipple et al., 1998; Parker et al., 1998) as well as field data from alluvial fans in the Mojave Desert, U.S. (Stock et al., 2008) suggest that the ratio of sediment supply to discharge delivered to the fan plays a key role in determining surface slope. Steeper slopes are the result of greater sediment supply relative to the volume of water, so fan slopes can provide information about relative changes in the volume of sediment supplied to the fan during different intervals of deposition (Stock et al., 2008). Further, Stock et al. (2008) hypothesize that steeper slopes of older deposits of Mojave Desert alluvial fans are a product of enhanced sediment delivery at the time, and gentler slopes of younger deposits are a product of reduced sediment delivery. In the LRR, the steeper slopes of late Pleistocene surfaces may also be a product of enhanced sediment yield, while gentler Holocene slopes suggest reduced sediment delivery. With evidence of greatly reduced transport capacity largely incapable of significant geomorphic work during the Holocene,

enhanced sediment delivery during the late Pleistocene would also require greater transport capacity to mobilize this sediment.

Finally, differences in facies assemblages and grain-size distributions also indicate greater transport capacity during the late Pleistocene. Mainly, the greater occurrence of sand lenses in Holocene deposits suggests reduced transport capacity during this period. In contrast, late Pleistocene deposits rarely contain sand lenses, suggesting that transport capacity was generally capable of mobilizing the sand grain-size fraction. Even on the Upper Cedar Creek fan, where exposures of late Pleistocene gravels are >1 km in length and up to 30 m in height, sand lenses are exceedingly rare. Moreover, Holocene deposits are generally found within incised channels that confine flow and thus allow lower volume discharges to reach the critical flow depth required to mobilize sand-sized sediment. Under this condition, the preservation of sand lenses suggests greatly reduced discharges during the Holocene.

With the exception of the sand lenses more often preserved in Holocene deposits, sieving of sediment samples indicated that the grain-size distributions of the pebble-to-cobble gravel facies in Holocene and late Pleistocene deposits are similar. Given the evidence of reduced transport capacity and sediment delivery to fans during the Holocene, one interpretation of these results is that in many locations, Holocene deposits are primarily reworked late Pleistocene sediment, rather than new material from the contributing basins. The location of Holocene deposits within incised channels supports this hypothesis as incision into older sediment could provide the sediment source for these younger deposits. In addition, more abundant sand lenses within Holocene deposits

could reflect the generally reduced transport capacity during this period, and flows that were capable of transporting sands but not he coarser material.

Using average deposit slopes and grain-size distribution data, we attempted to compare the required flow depths and discharges required to mobilize the median grain size for Holocene and late Pleistocene surfaces, but results proved problematic. This was due to (1) the rather similar grain-size distributions for the coarse-grained, gravelly portions of both Holocene and late Pleistocene deposits and (2) the assumption of channelized flow for late Pleistocene deposition in calculations. Given the similar grain-size distributions but steeper slopes of late Pleistocene deposits, the estimated flow depths and discharges to mobilize a given median grain size are smaller for late Pleistocene surfaces. This is problematic because it assumes channelized flow during the late Pleistocene though facies suggest deposition during dispersive sheetflooding events. Given the location of Holocene deposits within incised channels, channelized flow during this time period is likely more reasonable. Unchannelized flow during late Pleistocene sheetflooding would require greater discharges than channelized flow during the Holocene to reach the same critical flow depth for mobilization of a given grain size.

2.5.7 Caveats for Non-Climatic Influences on LRR Fans

OSL dating of alluvial fan sediments suggest that alluvial fan aggradation in the basin was in response to climatic conditions. Throughout the basin, the most significant aggradation on fans occurred between 10-60 ka during three distinct periods, and on all fans the last ~10 ka has produced largely stable fans with little to no deposition. This synchronous behavior suggests that fans aggraded in response to factors consistent over the spatial scale of the LRR basin, which is most likely climate. Additional mechanisms

hypothesized to drive fan development that would likely produce asynchronous aggradation and/or incision include tectonism, autogenic behavior, base-level lowering, and toe cutting by the axial river. The potential influence of each of these on LRR fan development will be considered.

Synchronous behavior among fans on different fault segments with disparate slip rates (e.g., Haller and Crone, 2004) indicates that tectonism is not driving sedimentation. Ages for offsets on segments of the Lost River Fault can be compared to OSL ages for sedimentation, but this age control is limited and linking sedimentation to faulting is often tenuous. Beginning in the north, Kluer (1988) constrained the most recent offset of the Thousand Springs segment between 0.53-6.85 ka. From OSL dating and fan morphology, we do not infer significant aggradation younger than ~7 ka that could suggest a tectonic driver of sedimentation (Fig. 2.5). The Upper Cedar Creek fan sits on the Mackay segment of the Lost River Fault, which Scott et al. (1985) estimate last ruptured ca. 4 ka, but the fan also lacks significant post-faulting deposits that could indicate a tectonic driver of sedimentation. The Ramshorn and King Canyon fans sit on the Arco segment of the Lost River Fault, which was estimated to have last ruptured ca. 30 ka (Pierce, 1985). OSL ages and fan morphology suggest more than one distinct episode of aggradation younger than 30 ka on both of these fans, indicating that the ca 30 ka offset is not responsible for driving most recent intervals of sedimentation. Even if there was strong temporal correlation between sedimentation and faulting events, offsets of ~2 m would not drive deposition or erosion except in the zone immediately adjacent to the fault scarp.

In many cases, age control intended to constrain the timing of the most recent fault offset may actually provide a date for timing of climatically-induced sedimentation. Without a means to directly date the rupture, age constraint is obtained by dating deposits believed to be in place prior to and after the faulting event. While thermoluminescence, radiocarbon, or OSL ages from deposits in the near-fault environment do indeed bracket the timing of faulting (e.g., Hemphill-Hailey, 2000; Kluer, 1988; Haller and Crone, 2004), with the exception of the colluvial wedge developed in the fault scarp, the timing of deposition below the scarp is likely driven by changes in climate. If in semi-arid areas, deposition in the near-fault environment is controlled by the frequency and magnitude of sediment transport events, this implies that many ages for fault offsets in these environments may reflect climatic rather than tectonic drivers. Indeed, thermoluminescence dating in the Lemhi Basin (just to the west of the LRR) that constrains the timing of faulting events produces many ages ranging from ~15-24 ka (Hemphill-Haley et al., 2000), which corresponds to significant fan aggradation throughout the LRR. These thermoluminescence ages may not only constrain faulting events but may also indicate that alluvial fans in the Lemhi Basin aggraded in response to the same climatic conditions as fans in the LRR.

Assessing the potential influence of autogenic processes on fan behavior through field-based studies is difficult. Like tectonism, autogenic behavior would likely result in largely asynchronous fan aggradation throughout the range, which is not shown by the OSL chronology for aggradation developed in this study. As such, we do not infer autogenic behavior as a primary driver of aggradation events on LRR fans.

While OSL dating provides some constraint on the timing of alluvial fan incision in the LRR and may suggest synchronous timing throughout the basin driven by late Pleistocene climate, constraint is not good enough to rule out asynchronous incision driven by other mechanisms (Fig. 2.12). Other than climate or changes in climate, potential drivers of fan incision include offsets of the Lost River Fault, base level lowering, toe cutting by the axial Big Lost River, and autogenic adjustment. We suggest that faulting is not likely to drive incision on LRR faults because, as discussed in Section 2.2.1, any aggradation or incision resulting from faulting is likely to be limited to the near-fault environment on such large large-radius, low-gradient alluvial fans. Base level for LRR fans is likely controlled by the Big Lost River, but without information or constraint on potential intervals of incision that would lower base level, we cannot confirm or rule out base-level lowering as a driver of fan incision in the LRR. However, toe-cutting of the fans by the Big Lost River may drive some amount of head-ward fan incision. This mechanism may be less likely for the more northern fans, Willow Creek and Birch Springs, as discharge of the river in this portion of the basin has likely always been much smaller because the major tributary of the E. Fork of the Big Lost River is not added until farther downstream. Morphology of the remaining fans, downstream of the confluence with the E. Fork Big Lost River, do however, show evidence of toe-cutting by the Big Lost River that may be a factor in incision. While Holocene incision is likely due to a decrease in the volume of sediment being supplied to fans from their catchment basins, an autogenic driver of incision may be more likely for the late Pleistocene when sediment supply was greater. Numerous studies show that fan incision can occur without external forcing, due to factors such as decreasing aggradation rates as fan area grows,

flow-width adjustment or a lack of accommodation space for sediment (Coulthard et al., 2002; Nicholas and Quine, 2007; Nicholas et al., 2009). As OSL dating, geomorphic maps, and deposit characteristics suggest, late Pleistocene fans were actively aggrading, resulting in increased fan area, decreased accommodation space, and possibly changes in flow-width that could have triggered an episode of incision.

2.5.8 Inferred Links Between Climate and Fan Aggradation

Global and regional climate records indicate generally warmer climate conditions during the Holocene, which corresponds with little aggradation and general stability on LRR alluvial fans (Fig. 2.18). In contrast, global and regional climate records indicate generally cold conditions between ~10-60 ka, when fans both with differing levels of glaciation within contributing basins (0-80%), were actively aggrading (and incising) in the LRR (Fig. 2.18). This highlights two of the main findings of this study: (1) the cold climate conditions of late Pleistocene promoted the enhanced transport capacity and sediment delivery to fans that resulted in the extensive fan aggradation in the basin between ~10-60 ka., and (2) general cold climate conditions, not glaciers, drive fan aggradation in the LRR as fans with varying degrees of late Pleistocene glaciation in contributing basins aggraded synchronously.

2.5.9 Climate Conditions During Late Pleistocene Aggradation

Dated regional moraines are lacking for the 60-35 ka period of aggradation, but many other types of records indicate that conditions were likely cold in the LRR through this period. First, in the Wind River Range, a minimum age of 55.5 ± 8.60 ka (Sharp et al., 2003) for a glacio-fluvial terrace of the Wind River suggests glacial activity prior to

or in the early part of OIS 3. The Bonneville Basin may have also been responding to cold conditions at this time, with high water levels dated to 59 ± 5 ka (Kaufman et al., 2001). Fossil woodrat middens suggest that this was followed by relatively cool and moist conditions ca. 46 ka, then cold and dry conditions in the northwestern portion of the basin between ~40-30 ka (Madsen et al., 2001). Near Jackson Hole, a loess unit dates to 47 ± 4 ka (Pierce et al., 2011), and high water levels in Bear Lake between 47-39 ka (Laabs and Kaufman, 2003) and Summer Lake between 89-50 ka (Cohen et al., 2000; Negrini et al., 2000) indicate wetter conditions, perhaps due to reduced evapotranspiration under cold climate conditions. Pollen records show agreement, with low percentages of warm-arid species present at Bear Lake during the 60-35 ka interval of fan aggradation, and cold-arid conditions between 70-30 ka suggested by the Grays Lake record (Beiswenger, 1991). These various records show good agreement that climate in the region was cold between 60-35 ka, but produce varying results regarding effective moisture.

There is also strong support for cold climate during the 35-20 ka episode of fan aggradation, which encompasses late OIS 3 and early OIS 2. Evidence of glacial activity during this period includes probable glacial flour deposited in Bear Lake between 32-17 ka (Laabs et al., 2007 and refs. therein). Maximum valley glacier extent in the Wallowa Range occurred 21.20 ± 0.40 ka (Licciardi et al., 2004) and in the Wind River Range 21.35 ± 3.35 ka (Phillips et al., 1997), suggesting cold conditions that promoted glacier growth for some time before these events. Additional evidence of glacial activity includes glacially-derived outwash of the Snake River in the eastern Snake River Plain between 25-12 ka (Phillips et al., 2009). Loess units near Jackson Hole are dated to 35-

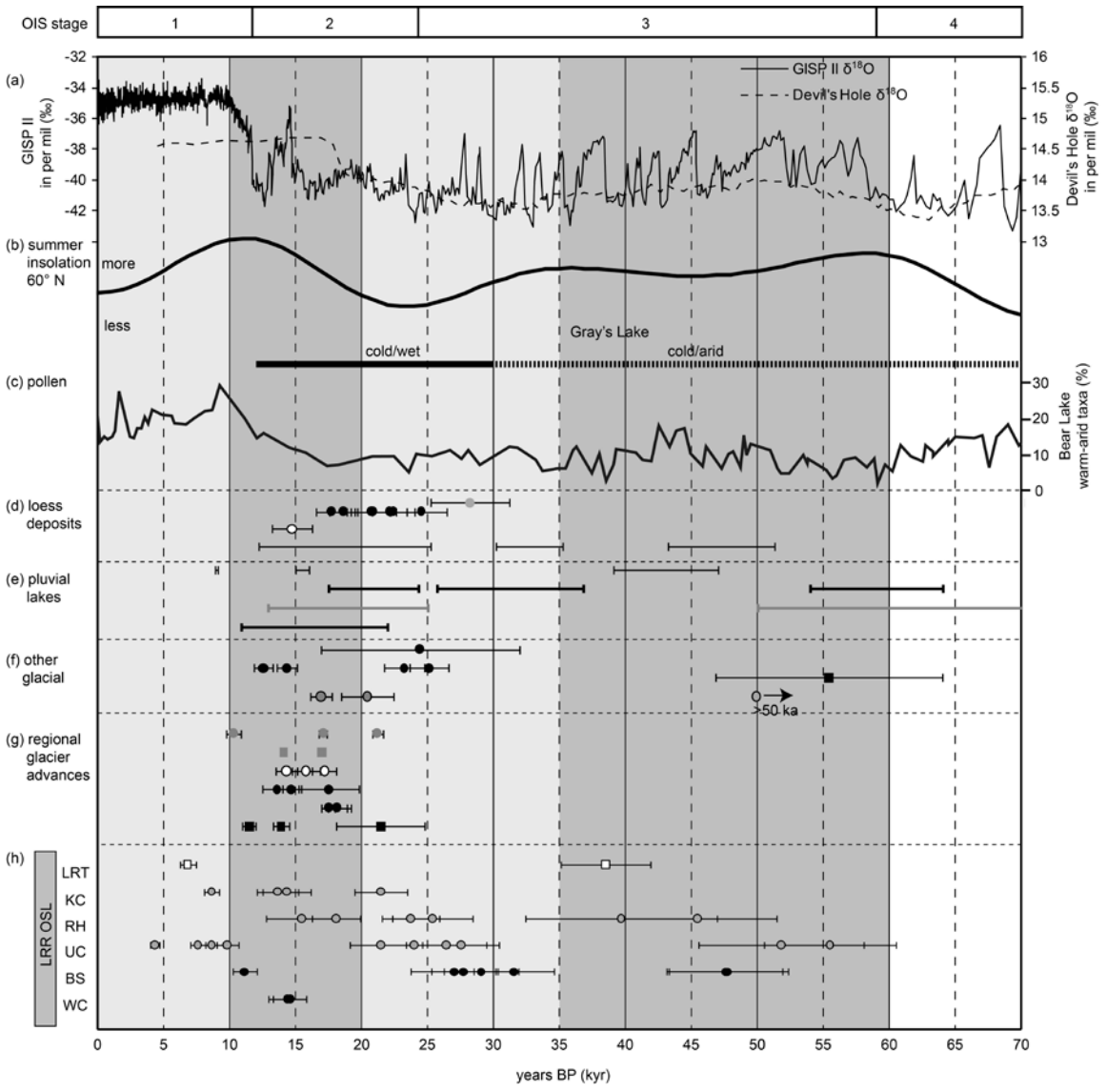

Figure 2.18 Comparison of climate records for the last 70 ka and OSL estimates for the timing of aggradation on the LRR fans. (a) Continuous, long-term $\delta^{18}O$ records from GISP II (e.g., Grootes and Stuvier, 1997) and Devil's Hole (Landwehr et al., 2011). (b) Insolation at 60° N for the last 70 kyr (Berger and Loutre, 1991). Climate records show in parts (c) through (g) are the same as those shown in Fig. 2.3. (h) OSL ages from this study for deposition on the LRR fans and Big Lost River terraces. WC= Willow Creek fan. BS=Birch Springs fan. UC=Upper Cedar Creek fan. RH= Ramshorn fan. KC=King Canyon fan.

30 ka and 25-17 ka (Pierce et al., 2011), and in the eastern Snake River Plain between ~25-17 ka (Phillips et al., 2009). Pluvial lakes were also likely responding to cold conditions between 35-20 ka with generally increasing water levels in the Bonneville Basin throughout this period (Benson et al., 2011 and refs. therein). The warm-arid taxa percentages from Bear Lake are very low between 35-20 ka (Jiménez-Moreno et a., 2007), and at Grays Lake pollen suggests the continuation of cold conditions but onset of increased moisture beginning ~30 ka and lasting until ~11.5 ka (Beiswenger, 1991).

Many of the same indicators of cold climate in the region between 35-20 ka also apply to the early portion of the 20-10 ka period of fan aggradation. There are many dated glacial advances in the region, including younger advances the Wallowa Range that reached maximum extents at 17.0 ± 0.3 ka and 10.2 ± 0.6 ka (Licciardi et al., 2004), and in the Wind River Range between 11-14 ka (Gosse et al., 1995). On the Yellowstone Plateau, the OIS 2 maximum advances were reached between approximately 14-18 ka and in the Teton Range between 13-15 ka (Licciardi and Pierce, 2008). The Alturas Valley glacier in the Sawtooth Range reached its maximum position shortly before ca. 16.9 ka with renewed advances in three valleys ca. 14 ka (Thackray et al., 2004). Maximum glacial extents in the Uinta Range at the North Fork Provo Valley were reached between 17-18 ka (Munroe et al., 2006; Refsnider et al., 2008). Numerous pluvial lakes had high water levels between 20-10 ka, including the Mud Lake sub-basin of Lake Terreton between 22-11 ka (Forman and Kaufman, 1997), Bear Lake at ~15-16 ka (Laabs and Kaufman, 2003), Summer Lake between 13-25 ka, and Lake Bonneville sometime between ~18.6-17.5 ka (Benson et al., 2011 and refs. therein) before the Bonneville flood. Loess deposits in the region also produce ages between ~14-20 ka

(Dechert et al., 2006; Phillips et al., 2009). At Bear Lake, the percentage of pollen from warm-arid taxa is low early in the 20-19 ka period, but quickly begins to increase to a peak value ca. 10 ka (Jiménez-Moreno et a., 2007). Similarly, the Grays Lake record shows a transition to warmer and drier Holocene conditions beginning ~11.5 ka (Beiswenger, 1991).

There are few regional climate records applicable to the possible 90-120 ka aggradation on LRR fans. The two younger ages from this period coincide with cooler conditions as suggested by the $\delta^{18}O$ Devil's Hole record (Winograd et al., 1997; Winograd et al., 2006; Landwehr et al., 2011), Bear Lake pollen record, and a probable high-stand in the Mud Lake sub-basin of Lake Terreton (Gianniny et al., 2002), but the older age from this period coincides with warmer conditions as suggested by the Devil's Hole and Bear Lake records. However, this oldest age estimate may be unreliable due to possible U/Th disequilibrium in the dose-rate estimate (site 4, USU-416 in Table 1). In addition, having only three dates older than ~80 ka (due to the paucity of exposure of older sediments) precludes much interpretation of how deposition during this time relates to past climate conditions.

The evidence is strong for cold conditions in the region surrounding the LRR between 10-60 ka, but potential changes in moisture delivery are not as clear. Colder temperatures may have been enough to increase effective moisture to drive glacial advances, changes in pollen assemblages, and pluvial lake highstands, but greater moisture delivery may have also played a role at times. Climate models and other studies suggest that the Laurentide Ice Sheet influenced atmospheric circulation and delivery of Pacific moisture to the western U.S. during the OIS 2 (e.g., Kutzbach et al., 1993). The

presence of such a large body of ice may have induced anti-cyclonic atmospheric flow that weakened westerly flow of moisture from the Pacific in addition to producing a region of high pressure that pushed the jet-stream south. The result would have been arid conditions in northwestern U.S. at the time of maximum glacial conditions (~21 ka). Thackray (2008) hypothesizes that ice sheet retreat and renewed moisture delivery may have in part driven the ~14-17 ka maximum advances of many valley glacier systems near the LRR. The ~11-22 ka Terreton Lake highstand and ~15-16 ka Bear Lake highstand may have been responding to this mechanism as well. Lake Bonneville reached its highstand following peak glacial conditions, and Madsen et al. (2001) infer from fossil woodrat middens that conditions in the basin were increasingly cold and moist by ~22 ka, very cold by ~17 ka, then warmer and moister than full glacial time from ~14-17 ka. However, Beiswenger (1991) suggests that the entire period from ~11.5-30 ka was relatively wet due to increases in winter and spring precipitation.

2.5.10 Climatic Drivers of Increased Transport Capacity

Pierce and Scott (1982) hypothesize that in the northern Rockies of the U.S., cold climate likely extends the portion of the year during which snow can accumulate, producing a snowpack with increased snow water equivalent. Increased moisture delivery during the months that snow accumulates is not required but would only enhance this effect. Cold temperatures would also delay the spring melt until the angle of the sun is higher. This increases incoming solar radiation, likely producing rapid melting and increased peak discharges. The overall result is proposed to increase the volume of peak and total discharges, resulting in contributing basin streams that have greater transport capacity for moving sediment out of basins and to the active fan surface (Fig. 2.19).

Transport capacity in the more extensively glaciated basins of Willow Creek and Birch Springs may have been further enhanced by meltwater as glaciers receded under warming climate. OSL dates and fan morphology from the Willow Creek fan support this hypothesis, suggesting that nearly the entire fan surface was deposited ca. 13-15 ka, concomitant with regional deglaciation that commenced ca. 17 ka (Licciardi et al., 2004). At the Birch Springs fan, glacial recession and increased availability of glacial till and outwash sediments may have been a factor contributing to the deposition of the large ~10-25 ka fan surface (Fig. 2.6). However, the contributing basins of the Ramshorn and King Canyon fans experienced very limited to no glaciation during the LGM but also recorded significant deposition between ~13-17 ka. This indicates that glaciers were not required for enhanced availability and transport of sediment to fan surfaces, and that general climate conditions were capable of enhancing fan deposition at this time.

In the above hypotheses, increased moisture delivery to the region is not required but is another potential driver of increased transport capacity. Despite potential changes in moisture delivery between 10-60 ka (see Section 2.5.10), LRR fans aggraded during times of both inferred arid and wetter climate. This suggests that potential increases in effective moisture from colder temperatures alone may enhance transport capacity, and that greater moisture delivery may not have been required.

2.5.11 Climatic Drivers of Sediment Production and Delivery

Deposit characteristics provide support for increased sediment delivery to fans concurrent with greater transport capacity and cold climate, but this does not necessarily indicate enhanced sediment production at the same time. Sediment supplied to fans during aggradation could be derived from material stored on basin hillslopes until the

onset of cold conditions that bring greater transport capacity. While stored sediment may have been one source during the late Pleistocene, the rather synchronous aggradation on fans both with and without extensively glaciated contributing basins suggests that glacial climate conditions enhanced sediment production. In the more extensively glaciated contributing basins (Willow Creek and Birch Springs), the direct effects of glaciation would almost certainly increase sediment production (Fig. 2.19). The similarly timed aggradation on the fans with little to no glaciation in their contributing basins indicates that cold conditions effectively enhance sediment production through mechanisms other than glaciation.

One possible mechanism is enhanced rates of chemical weathering of bedrock due to greater effective moisture, though the amount of time that this would be effective each year under a colder climate regime may be a limiting factor. More effective "frost wedging" of bedrock during cold climate could also enhance sediment production within the LRR (Fig. 2.19). Hales and Roering (2005, 2007, 2009) have hypothesized that topographic relief in mountainous regions may be limited by a "frost buzzsaw," that is, erosion of bedrock through segregation ice growth. This idea is similar to the "glacial buzzsaw" hypothesis (e.g., Whipple et al., 1999; Mitchell and Montgomery, 2006), but the "frost buzzsaw" does not require the presence of glaciers. This "frost buzzsaw" is most effective under specific temperature and moisture regimes, so that the elevation at which the process is most effective shifts as climate changes. Hales and Roering (2005) have shown for New Zealand's Southern Alps, past changes in temperature moved this elevational band where the frost buzzsaw was most effective, and increased the area subject to frost weathering under colder conditions. A similar mechanism is possible for

the LRR. Cold climate between 10-60 ka may have lowered and expanded the elevational band of most effective weathering, potentially subjecting a greater area to this mechanism and producing more sediment. Studies suggest that late Pleistocene equilibrium-line altitudes (ELAs) in the Western U.S. were ~450-1000 m than at present (e.g., Porter et al., 1983; Locke, 1990), and in the LRR sat at about 2600-2900 m (Meyer et al., 2004). While ELAs are determined by factors in addition to air temperature, late Pleistocene decreases in ELAs may provide an approximation for the magnitude of change in the temperature-dependent lower limit of the zone of most effective frost weathering. This would suggest that the lower limit of the zone of most effective frost weathering in the LRR may have been 450-1000 m lower during the late Pleistocene than at present.

Vegetation cover on basin hillslopes can also influence when sediment is available within contributing basins for transport to and deposition on alluvial fans. In the southwestern U.S., alluvial fan aggradation is often hypothesized to occur during transitions to warmer and drier interglacial climate when vegetation density decreases, increasing erosion from hillslopes (e.g. Bull, 1991). However, in alpine areas like the LRR, the timing of sedimentation would likely coincide with the transition to glacial climate, rather than the transition to interglacial climate. This is because in higher elevation, alpine areas like the LRR, vegetation cover on basin hillslopes would likely be denser during warmer climate when tree lines moved up in elevation. Under modern climate conditions, the upper tree-line is ~2800 m throughout the LRR and the lower tree-line is between ~2100-2400 m and often controlled by the location of alluvial fans that are currently too dry to support tree growth. The effect is a very limited elevation

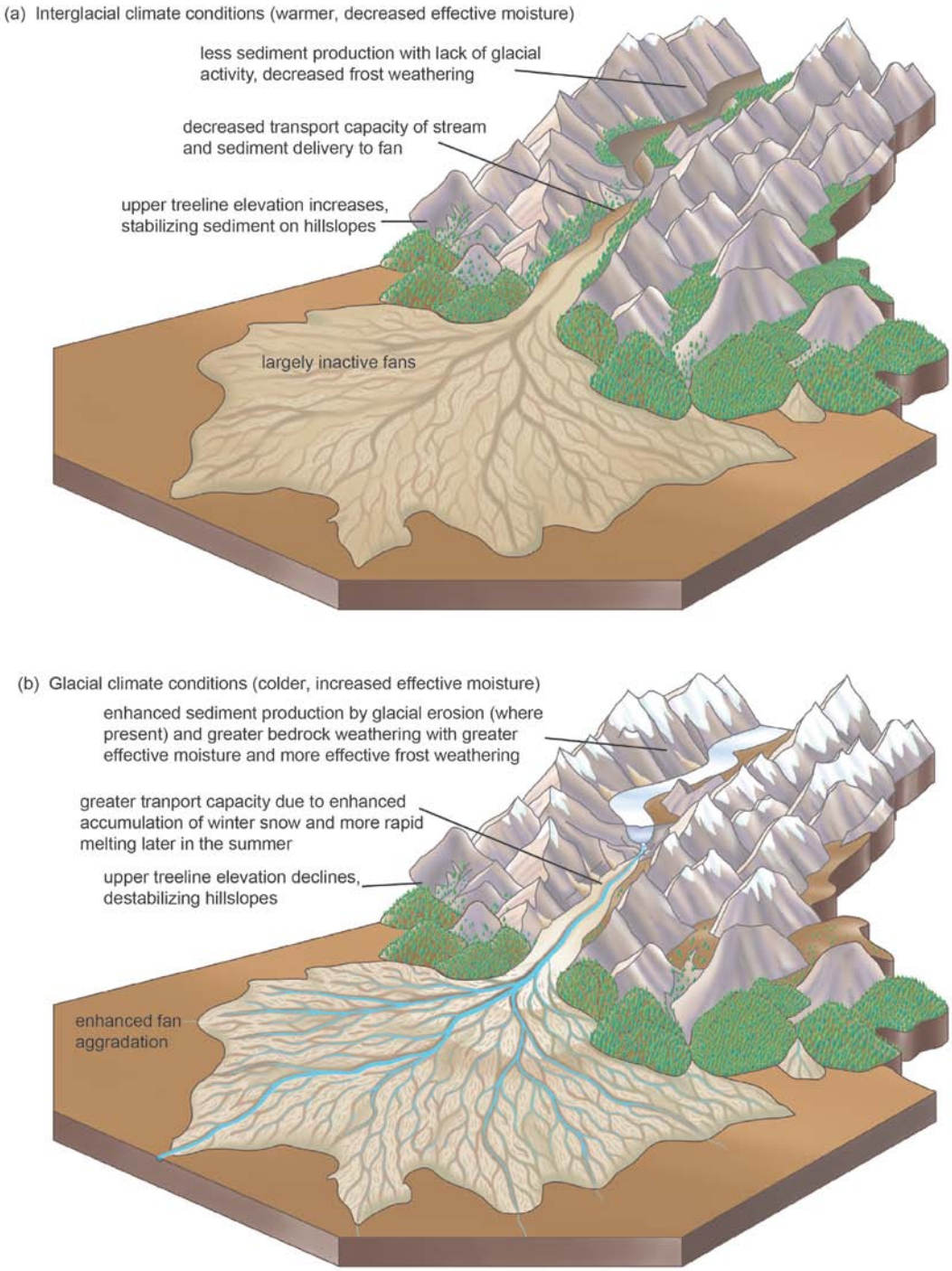

Figure 2.19 Conceptual illustration of inferred links between climate and alluvial fan aggradation in the Lost River Range. (a) Largely inactive fan during warm and dry climate conditions that promote reduced stream transport capacity and sediment delivery to fans. (b) Enhanced fan aggradation under cold climate conditions, the result of increased stream transport capacity and sediment delivery to fans. Illustration by David Robertson, used with permission.

band of more dense vegetation, leaving most basins only partially vegetated under modern climatic conditions. The onset of cold climate would have caused tree-line elevation to decline on steep upper-basin slopes, reducing stabilizing vegetation cover and freeing accumulated sediment for transport. Additionally, vegetation density on fans themselves may have increased, further promoting deposition of sediment on fan surfaces.

2.5.12 Reexamining Pinedale and Bull Lake Ages

Throughout the western U.S., significant but undated alluvial and fluvial deposits are often assigned Pinedale or Bull Lake ages under the assumption that, like many glacial systems throughout the western U.S., alluvial and fluvial systems also responded most significantly to climate conditions during these periods. Significant alluvial fan aggradation in the LRR between ~24-120 ka, as indicated by OSL dating, suggests that assigning Bull Lake ages to pre-Pinedale alluvial and fluvial deposits may not be appropriate in this region. Similarly, more recent dating has shown that in the southwestern U.S., significant alluvial fan aggradation previously assumed to be OIS 6 (Bull Lake) in age is actually OIS 4 in age (Gosse, 2010). In addition, significant fluvial activity during OIS 5-3 has been documented throughout the Grand Canyon and its tributaries in the eastern portion of the Grand Canyon and the Grand Wash (Anders et al., 2005; Rittenour and Pederson, 2010).

Findings from the LRR suggest that within the range and perhaps throughout the western U.S., (1) climate conditions that do not promote extensive growth of glaciers may still promote deposition of significant alluvial and/or fluvial deposits, or (2) glacier advances and alluvial/fluvial deposition do indeed result from similar climate conditions,

but OIS 2 advances erased evidence of previous glacial activity. In either case, alluvial deposits may thus provide a more sensitive and/or complete record of geomorphic response to climate than glacial features. Further, it suggests that alluvial and fluvial deposits may prove useful as paleoclimate proxies in regions where glacial evidence or other evidence is lacking. As Gosse (2010) suggests, the finding of younger than previously assumed ages for significant geomorphic features also has implications for rates of weathering, soil development, and landscape evolution based on incorrectly assumed OIS 6 ages.

2.6 Conclusions

In our efforts to correlate similar-aged alluvial fan surfaces in the LRR, we found that OSL dating is indeed applicable to gravelly deposits lacking sand lenses through a modified sampling strategy and careful consideration of the dose-rate contribution from the sediment. Further, we found that the average thickness of pedogenic $CaCO_3$ coats, commonly used in semi-arid regions to estimate surface age, do indeed correlate well with OSL age on dated surfaces. However, correlations between $CaCO_3$ accumulation stage and OSL age were not convincing. The thickness of overlying loess deposits proved less reliable for correlating similar-aged surfaces as the relationship with OSL age was very poor.

OSL dating and geomorphic mapping of LRR fans confirm previous inferences by workers such as Pierce and Scott (1982) and Patterson (2006) that LRR fans are primarily relicts of late Pleistocene climates. Approximately 80% of the current surface area of LRR fans was deposited under cold, late Pleistocene climate conditions in distinct intervals from 10-20 ka, 20-35 ka, and 35-60 ka, and only ~10% of total fan area

deposited during warmer and drier Holocene conditions. Further, late Pleistocene deposits often have steeper surface slopes and a coarser grain-size distribution than Holocene deposits that more often contain thick sand lenses.

In addition, the synchronous aggradation of LRR fans both with and without extensive late Pleistocene glaciation indicates that glaciers are not required to drive a significant geomorphic response to cold climate. This surprising result suggests that while the direct effects of glaciation may contribute to enhanced fan aggradation, general conditions during intervals of cold climate promote other processes that may even more effectively produce and move sediment, such as the "frost buzzsaw" (Hales and Roering, 2005, 2007, 2009). Further, this finding is contradictory to other studies citing glaciers as the most important "buzzsaws" limiting topographic relief (e.g., Whipple et al., 1999; Mitchell and Montgomery, 2006).

Deposit characteristics suggest that cold conditions ~10-60 ka enhanced both transport capacity of contributing basin streams and sediment delivery to fans. Greater effective moisture at this time as well as larger peak discharges during the spring snowmelt may have driven enhanced transport capacity. At the same time, increased sediment delivery to fans likely resulted from faster rates of sediment production within contributing basins through glacial erosion where present, as well as enhanced frost weathering (e.g., Hales and Roering, 2005) or accelerated rates of bedrock weathering with greater effective moisture. In addition, changes in vegetation density may have altered hillslope stability, leaving stored sediment more prone to erosion.

While the conditions of OIS 2 promoted extensive glacial advances throughout the western U.S. as well as aggradation on LRR fans (~40% of total fan area), significant

fan aggradation also occurred during OIS 3 when climate was generally cold though perhaps more arid than OIS 2. This finding suggests that assuming Pinedale or Bull Lake ages for significant but undated alluvial and fluvial deposits in the western U.S. needs re-examination. The conditions that promote maximum glacial advances are not the only climate conditions that promote significant fan aggradation within the LRR. Further, alluvial/fluvial systems may contain more detailed records of geomorphic response to climate than glacial systems that often record only the most recent or most significant responses. As such, alluvial/fluvial records may prove useful as proxies for paleoclimate in locations where glacial records are absent or limited, or for intervals between recorded maximum ice advances.

This investigation of fan aggradation suggests that in the Lost River Range and perhaps greater region, cold climate conditions most effectively drive denudation that may limit topographic relief or interact in longer-term feedbacks with tectonism to drive topographic development. Further, results indicate that while glaciers may be one "buzzsaw" operating during cold conditions, they are not required to drive effective denudation and may not even be the most effective drivers of denudation. Instead, conditions during intervals of cold climate may very effectively enhance denudation in other ways such as changes in hillslope stability with changes in vegetation density or enhanced weathering rates through greater effective moisture and more effective frost weathering processes.

REFERENCES

Adamiec, G., and Aitken, M. 1998. Dose-rate conversion factors: update. Ancient TL 16, 37-50.

Aitken, M. 1998. An Introduction to Optical Dating. Oxford, Oxford Science Publications.

Aitken, M.J. 1976. Thermoluminescent age evaluation and assessment of error limits: revised system. Archaeometry 18, 233-238.

Aitken, M.J. 1985. Thermoluminescence Dating. London, Academic Press 359 p.

Aitken, M.J., and Allred, J.C. 1972. The assessment of error limits in thermoluminescent dating. Archaeometry 14, 257-267.

Alexander, J., and Leeder, M.R. 1987. Active tectonic control on alluvial architecture. In: Ethridge, F.G., Flores, R.M., Harvey, M.D. (Eds.). Recent Developments in Fluvial Sedimentology. Society of Economic Paleontologists and Mineralogists Special Publication 39, 243-252.

Anders, M. D., Pederson, J. L., Rittenour, T. M., Sharp, W . D., Gosse, J. C., Karlstrom, K. E., Crossey, L. J., Goble, R. J., Stockli, L. and Yang, G. 2005. Pleistocene geomorphology and geochronology of eastern Grand Canyon: linkages of landscape components during climate changes. Quaternary Science Reviews 24, 2428-2448.

Asmerom, Y., Polyak, V., Burns, S., and Rassmussen, J. 2007. Solar forcing of Holocene climate: New insights from a speleothem record, southwestern United States. Geology 35, 1-4.

Bailey, R.M., Singarayer, J.S., Ward, S., and Stokes, S. 2003. Identification of partial resetting using De as a function of illumination time. Radiation Measurements 37, 511-518.

Beiswenger, J.M. 1991. Late Quaternary Vegetational History of Grays Lake, Idaho. Ecological Monographs 61, 165-182.

Benson, L. V., Lund, S. P., Smoot, J. P., Rhode, D. E., Spencer, R. J., Verosub, K. L.,. Louderback, L. A, Johnson, C. A., Rye, R. O., and Negrini, R. M. 2011. The rise

and fall of Lake Bonneville between 45 and 10.5 ka. Quaternary International 235, 57-69.

Berger, A., and Loutre, M.F. 1991. Insolation values for the climate of the last 10 million years. Quaternary Science Reviews 10, 297-317.

Birkeland, P.W., Machette, M.N., and Haller, K.M.. 1991. Soils as a tool for applied Quaternary geology. Utah Geological and Mineral Survey Miscellaneous publication 91-3, 44 p.

Blair, T. C.. 1987. Tectonic and hydrologic controls on cyclic alluvial fan, fluvial, and lacustrine rift-basin sedimentation, Jurassic-Lowermost Cretaceous Todos Santos Formation, Chiapas, Mexico. Journal of Sedimentary Research 57, 845-862.

Blair, T.C., and Bilodeau. 1998. Development of tectonic cyclothems in rift, pull-apart, and foreland basins: Sedimentary response to episodic tectonism. Geology 16, 517-520.

Blair, T.C., and McPherson, J.G. 1994. Alluvial fans and their natural distinction from rivers based on morphology, hydraulic processes, sedimentary processes, and facies assemblages. Journal of Sedimentary Research 64, 450-489.

Brennan, B.J. 2003. Beta doses to spherical grains. Radiation Measurements 37, 299-303.

Brunelle, A., Whitlock, C., Bartlein, P., and Kipfmueller, K. 2005. Holocene fire and vegetation along environmental gradients in the Northern Rocky Mountains. Quaternary Science Reviews 24, 2281-2300.

Bull, W.B. 1977. The alluvial-fan environment. Progress in Physical Geography 1, 220-270.

Bull, W.B. 1991. Geomorphic Response to Climate Change. New York, Oxford University Press, 326 p.

Burbank, D.W., Blythe, A.E., Putkonen, J., Pratt-Sitaula, B., Gabet, E., Oskin, M., Barros, A., and Ojha, T.P. 2003. Decoupling of erosion and precipitation in the Himalayas. Nature 426, 652-655.

Cerling, T.E., Poreda, R.J., and Rathburn, S.L. 1994. Cosmogenic 3He and 21Ne age of the Big Lost River flood, Snake River Plain, Idaho. Geology 22, 227-230.

Clark, D.H., Bowerman, N.D., Bilderback, E., Chasman, B., and Burrows, R. 2005. Regional timing of neoglaciation in the maritime ranges of the western U.S.: Constrains from glacial and lacustrine records. Geological Society of America Abstracts with Programs 37, 121.

Clarke, L., Quine, T.A., and Nicholas, A.. 2010. An experimental investigation of autogenic behaviour during alluvial fan evolution. Geomorphology 115, 278-285.

Cohen, A., Palacios-Fest, M., Negrini, R., Wigand, P., and Erbes, D. 2000. A paleoclimate record for the past 250,000 years from Summer Lake, Oregon, USA: II. Sedimentology, paleontology and geochemistry. Journal of Paleolimnology 24, 151-182.

Colls, A.E., Stokes, S., Blum, M.D., and Straffin, E. 2001. Age limits on the Late Quaternary evolution of the upper Loire River. Quaternary Science Reviews 20, 743-750.

Cook, E. R., Woodhouse, C. A., Eakin, C. M., Meko, D. M. and Stahle, D.W. 2004. Long-Term Aridity Changes in the Western United States. Science 306, 1015-1018.

Coulthard, T.J., Macklin, M.G., and Kirkby, M.J. 2002. A cellular model of Holocene upland river basin and alluvial fan evolution. Earth Surface Processes and Landforms 27, 269-288.

Crone, A.J., Machette, M.N., Bonilla, M.G., Lienkaemper, J.J., Pierce, K.L., Scott, W.E., and Bucknam, R.C. 1987. Surface faulting accompanying the Borah Peak earthquake and segmentation of the lost river fault, central Idaho. Bulletin of the Seismological Society of America 77, 739-770.

Crone, A.J., and Machette, M.N. 1984. Surface faulting accompanying the Borah Peak earthquake, central Idaho. Geology 12, 664-667.

Dechert, T.V., McDaniel, P.A., Pierce, K.L., Falen, A.L., and Fosberg, M.A. 2006. Late Quaternary Stratigraphy, Idaho National Laboratory, Eastern Snake River Plain, Idaho. Idaho Geological Survey Technical Report 06-01.

Densmore, A.L., Dawers, N.H., Gupta, S., and Guidon, R. 2005. What sets topographic relief in extensional footwalls? Geology 33, 453-456.

Densmore, A.L., Dawers, N.H., Gupta, S., Guidon, R., and Goldin, T. 2004. Footwall topographic development during continental extension. J. Geophys. Res. 109, F03001.

Duller, G.A.T. 2004. Luminescence dating of quaternary sediments: recent advances. Journal of Quaternary Science 19, 183-192.

Duller, G.A.T. 2008. Single-grain optical dating of Quaternary sediments: why aliquot size matters in luminescence dating. Boreas 37, 589-612.

Forman, S.L., and Kaufman, D.S. 1997. Late Quaternary oscillations of Lake Terreton, Eastern Snake River Plain, Idaho. Geological Society of America Abstracts with Programs 29, A253.

Forman, S.L., Smith, R.P., Hackett, W.R., Tullis, J.A., and McDaniel, P.A. 1993. Timing of Late Quaternary Glaciations in the Western United States Based on the Age of Loess on the Eastern Snake River Plain, Idaho. Quaternary Research 40, 30-37.

Foster, D., Brocklehurst, S.H., and Gawthorpe, R.L. 2008. Small valley glaciers and the effectiveness of the glacial buzzsaw in the northern Basin and Range, USA. Geomorphology 102, 624-639.

Funk, J.M. 1976. Climatic and tectonic effects on alluvial fan systems, Birch Creek Valley, east central Idaho [Ph.D. thesis], University of Kansas.

Galbraith, R.F., Roberts, R.G., Laslett, G.M., Yoshida, H., and Olley, J.M. 1999. Optical dating of single and multiple grains of quartz from Jinmium Rock Shelter, northern Australia: part I, experimental design and statistical models. Archaeometry 41, 339-364.

Galbraith, R.F., Roberts, R.G., and Yoshida, H. 2005. Error variation in OSL palaeodose estimates from single aliquots of quartz: a factorial experiment. Radiation Measurements 39, 289-307.

Geslin, J.K., Karl Link, P., and Mark Fanning, C. 1999. High-precision provenance determination using detrital-zircon ages and petrography of Quaternary sands on the eastern Snake River Plain, Idaho. Geology 27, 295-298.

Gianniny, G.L., Thackray, G.D., Kaufman, D.S., Forman, S.L., Sherbondy, M.J., and Findeisen, D. 2002. Late Quaternary highstands in the Mud Lake and Big Lost Trough subbasins of Lake Terreton, Idaho.Geological Society of America Special Paper 353 , p. 77-90.

Giles, L.H., Peterson, F.F., and Grossman, R.B. 1966. Morphological and genetic sequences of carbonate accumulation in desert soils. Soil Science 101, 347-360.

Gillespie, A., and Molnar, P. 1995. Asynchronous Maximum Advances of Mountain and Continental Glaciers. Rev. Geophys. 33, 311-364.

Goble, R.J., Mason, J.A., Loope, D.B., and Swinehart, J.B. 2004. Optical and radiocarbon ages of stacked paleosols and dune sands in the Nebraska Sand Hills, USA. Quaternary Science Reviews 23, 1173-1182.

Godsey, H.S., Currey, D.R., and Chan, M.A. 2005. New evidence for an extended occupation of the Provo shoreline and implications for regional climate change, Pleistocene Lake Bonneville, Utah, USA. Quaternary Research 63, 212-223.

Gosse, J.C. 2010. The OIS 4 glacial-alluvial dichotomy. Geological Society of America Abstracts with Programs 42, 74.

Gosse, J.C., Evenson, E.B., Klein, J., Lawn, B., and Middleton, R. 1995. Precise cosmogenic 10Be measurements in western North America: Support for a global Younger Dryas cooling event. Geology 23, 877-880.

Gosse, J., and Phillips, F.M.,2001. Terrestrial in situ cosmogenic nuclides: theory and application. Quaternary Science Reviews 20, 1475-1560.

Granger, D.E. 2006. A review of burial dating methods using 26Al and 10Be. Geological Society of America Special Papers 415, 1-16.

Granger, D.E., and Muzikar, P.F. 2001. Dating sediment burial with in situ-produced cosmogenic nuclides: theory, techniques, and limitations. Earth and Planetary Science Letters 188, 269-281.

Grootes, P.M., and Stuiver, M. 1997. Oxygen 18/16 variability in Greenland snow and ice with 10^3 to 10^5-year time resolution. Journal of Geophysical Research 102.

Hales, T.C., and Roering, J.J. 2005. Climate-controlled variations in scree production, Southern Alps, New Zealand. Geology 33, 701-704.

Hales, T.C., and Roering, J.J. 2007. Climatic controls on frost cracking and implications for the evolution of bedrock landscapes. J. Geophys. Res. 112, F02033.

Hales, T.C., and Roering, J.J. 2009. A frost "buzzsaw" mechanism for erosion of the eastern Southern Alps, New Zealand. Geomorphology 107, 241-253.

Haller, K.M., and Crone, A.J. 2004. Twenty Years After the Borah Peak Earthquake—Field Guide to Surface-Faulting Earthquakes Along the Lost River Fault, Idaho, *in* Haller, K.M., and Wood, S.H., eds., Geological Field Trips in Southern Idaho, Eastern Oregon, and Northern Nevada. U.S. Geological Survey Open File Report 2004-1222, 119-135.

Haller, K.M., and Wheeler, R.L. 1995. Fault number 601e, Lost River fault, Pass Creek section. Quaternary fault and fold database of the United States, U.S. Geological Survey.

Harvey, A.M. 2002. The role of base-level change in the dissection of alluvial fans: case studies from southeast Spain and Nevada. Geomorphology 45, 67-87.

Hemphill-Haley, M. A., Sawyer, T. L., Knuepfer, P. L. K., Forman, S. L., and Wong, I. G. 2000. Timing of faulting events from thermoluminescence dating of scarp-related deposits, Lemhi fault, southeastern Idaho, *in* Noller, J. S., Sowers, J. M.

and Lettis, W. R., eds., Quaternary Geochronology, Methods and Applications. 541-548.

Hülle, D., Hilgers, A., Kühn, P., and Radtke, U. 2009. The potential of optically stimulated luminescence for dating periglacial slope deposits -- A case study from the Taunus area, Germany. Geomorphology 109, 66-78.

Huntley, D.J., McMullan, W.G., Godfrey-Smith, D.I., and Thewalt, M.L.W. 1989. Time-dependent recombination spectra arising from optical ejection of trapped charges in feldspars. Journal of Luminescence 44, 41-46.

Jacobs, Z., Duller, G.A.T., and Wintle, A.G. 2003a. Optical dating of dune sand from Blombos Cave, South Africa: II--single grain data. Journal of Human Evolution 44, 613-625.

Jacobs, Z., Wintle, A.G., and Duller, G.A.T. 2003b. Optical dating of dune sand from Blombos Cave, South Africa: I--multiple grain data. Journal of Human Evolution 44, 599-612.

Jain, M., Murray, A.S., and Botter-Jensen, L. 2004. Optically stimulated luminescence dating: how significant is incomplete light exposure in fluvial environments? [Datation par luminescence stimulée optiquement : quelle signification en cas de blanchiment incomplet des sédiments fluviatiles ?] Quaternaire 15, 143-157.

Jain, M., Murray, A.S., and Bøtter-Jensen, L. 2003. Characterisation of blue-light stimulated luminescence components in different quartz samples: implications for dose measurement. Radiation Measurements 37, 441-449.

Jiménez-Moreno, G., Scott Anderson, R., and Fawcett, P.J. 2007. Orbital- and millennial-scale vegetation and climate changes of the past 225 ka from Bear Lake, Utah-Idaho (USA). Quaternary Science Reviews 26, 1713-1724.

Johnson, B.G. 2006. The effect of topography, latitude and lithology on the distribution of rock glaciers in the Lemhi Range, central Idaho. M.S. thesis, Idaho State University.

Johnson, B.G., Thackray, G.D., and Van Kirk, R. 2007. The effect of topography, latitude, and lithology on rock glacier distribution in the Lemhi Range, central Idaho, USA. Geomorphology 91, 38-50.

Kalchgruber, R., Fuchs, M., Murray, A.S., and Wagner, G.A. 2003. Evaluating dose-rate distributions in natural sediments using [alpha]-Al2O3:C grains. Radiation Measurements 37, 293-297.

Kock, S., Kramers, J.D., Preusser, F., and Wetzel, A. 2009. Dating of Late Pleistocene terrace deposits of the River Rhine using Uranium series and luminescence methods: Potential and limitations. Quaternary Geochronology 4, 363-373.

Kaufman, D.S., Forman, S.L., and Bright, J. 2001. Age of the Cutler Dam Alloformation (Late Pleistocene), Bonneville Basin, Utah. Quaternary Research 56, 322-334.

Kluer, J.K. 1988. Quaternary geology of Willow Creek and some age constraints on prehistoric faulting, Lost River Range, east-central Idaho. Bulletin of the Seismological Society of America 78, 946-955.

Knudsen, K.L., Sowers, J.M., Ostenna, D.A., and Levish, D.R. 1999. Examination of evidence for, and timing of, a late Pleistocene outburst flood along the upper big Lost River, central Idaho. Geological Society of America Abstracts with Programs 31, A-19.

Konrad, S.K., and Clark, D.H. 1998. Evidence for an early Neoglaciol glacier advance from rock glaciers Rind Lake sediments in the Sierra Nevada, California, USA. Arctic and Alpine Research 30, 272-284.

Kutzbach, J., Guetter, P., Behling, P., and Selin, R. 1993. Simulated climatic changes: results of the COHMAP climate-model experiments, *in* Wright, H., Kutzbach, J., Webb, T.I., Ruddiman, W., Street-Perrott, F., and Bartlein, P., eds., Global Climates Since the Last Glacial Maximum: Minneapolis, Univeristy of Minnesota Press, 24-93.

Laabs, B.J.C., and Kaufman, D.S. 2003. Quaternary highstands in Bear Lake Valley, Utah and Idaho. Geological Society of America Bulletin 115, 463-478.

Laabs, B. J. C., J. S. Munroe, J. G. Rosenbaum, K. A. Refsnider, D. M. Mickelson, B. S. Singer, and M. W. Caffee. 2007. Chronology of the Last Glacial Maximum in the Upper Bear River Basin, Utah, Arctic, Antarctic, and Alpine Research 39, 537-543.

Landwehr, J.M., Sharp, W.D., Coplen, T.B., Ludwig, K.R., and Winograd, I.J. 2011. The chronology for the δ18O record from Devils Hole, Nevada, extended into the mid-Holocene. U.S. Geological Survey Open-File Report 2011-1082, 5 p.

Lepper, K., and W. S. McKeever, S. 2002. An Objective Methodology for Dose Distribution Analysis: Radiation Protection Dosimetry 101, 349-352.

Lewis, G.C., Fosberg, M.A., McDole, R.E., and Chugg, J.C. 1975. Distribution and Some Properties of Loess in Southeentral and Southeastern Idaho. Soil Sci Soc Am J 39, 1165-1168.

Lian, O.B., and Roberts, R.G. 2006. Dating the Quaternary: progress in luminescence dating of sediments. Quaternary Science Reviews 25, 2449-2468.

Licciardi, J.M., Clark, P.U., Brook, E.J., Elmore, D., and Sharma, P. 2004. Variable responses of western U.S. glaciers during the last deglaciation. Geology 32, 81-84.

Licciardi, J.M., and Pierce, K.L. 2008. Cosmogenic exposure-age chronologies of Pinedale and Bull Lake glaciations in greater Yellowstone and the Teton Range, USA. Quaternary Science Reviews 27, 814-831.

Locke, W. W. 1990. Late Pleistocene glaciers and the climate of western Montana, U.S.A. Arctic and Alpine Research 22, pp. 1-13.

Machette, M.N. 1985. Calcic soils of the southwestern United States, *in* Weide, D.L., ed., Soils and Quaternary geology of the southwestern United States. Geological Society of America Special Paper 203, 1-21.

Madsen, D. B., D. Rhode, D. K. Grayson, J. M. Broughton, S. D. Livingston, J. Hunt, J. Quade, D. N. Schmitt, and M. W. Shaver III. 2001. Late Quaternary environmental change in the Bonneville basin, western USA. Palaeogeography, Palaeoclimatology, Palaeoecology 167, 243-271.

Mayya, Y.S., Morthekai, P., Murari, M.K., and Singhvi, A.K. 2006. Towards quantifying beta microdosimetric effects in single-grain quartz dose distribution. Radiation Measurements 41, 1032-1039.

McDonald, E.V., McFadden, L.D., and Wells, S.G. 2003. Regional response of alluvial fans to the Pleistocene-Holocene climatic transition, Mojave Desert, California, *in* Enzel, Y., Wells, S.G., and Lancaster, N., eds., Paleoenvironments and paleohydrology of the Mojave and southern Great Basin Deserts. Boulder, CO, Geological Society of America, p. 189-205.

Menounos, B., Osborn, G., Clague, J.J., and Luckman, B.H. 2009. Latest Pleistocene and Holocene glacier fluctuations in western Canada. Quaternary Science Reviews 28, 2049-2074.

Meyer, G.A., Fawcett, P.F., and Locke, W.W. 2004. Late-Pleistocene equilibrium-line altitudes, atmospheric circulation, and timing of mountain glacier advances in the interior northwestern United States, *in* Haller, K., and Wood, S.H., eds., Geological Field Trips in Southern Idaho, Eastern Oregon, and Northern Nevada. Geological Society of America Field Guide, 61-66.

Meyer, G.A., Wells, S.G., and Timothy Jull, A.J. 1995. Fire and alluvial chronology in Yellowstone National Park. Climatic and intrinsic controls on Holocene geomorphic processes. Geological Society of America Bulletin 107, 1211-1230.

Mitchell, S.G., and Montgomery, D.R. 2006. Influence of a glacial buzzsaw on the height and morphology of the Cascade Range in central Washington State, USA. Quaternary Research 65, 96-107.

Montgomery, D.R., Balco, G., and Willett, S.D. 2001. Climate, tectonics, and the morphology of the Andes. Geology 29, 579-582.

Munroe, J. S., B. J. C. Laabs, J. D. Shakun, B. S. Singer, D. M. Mickelson, K. A. Refsnider, and M. W. Caffee. 2006. Latest Pleistocene advance of alpine glaciers in the southwestern Uinta Mountains, Utah, USA. evidence for the influence of local moisture sources. Geology 34, 841-844.

Murray, A.S., and Olley, J.M. 2002. Precision and accuracy in the optically stimulated luminescence dating of sedimentary quartz: A status review. Geochronometria 21, 1-16.

Murray, A.S., and Roberts, R.G. 1997. Determining the burial time of single grains of quartz using optically stimulated luminescence. Earth and Planetary Science Letters 152, 163-180.

Murray, A.S., and Wintle, A.G. 2000. Luminescence dating of quartz using an improved single-aliquot regenerative-dose protocol. Radiation Measurements 32, 57-73.

Murray, A.S., and Wintle, A.G. 2003. The single aliquot regenerative dose protocol: potential for improvements in reliability. Radiation Measurements 37, 377-381.

Nathan, R.P., and Mauz, B. 2008. On the dose-rate estimate of carbonate-rich sediments for trapped charge dating. Radiation Measurements 43, 14-25.

Nathan, R.P., Thomas, P.J., Jain, M., Murray, A.S., and Rhodes, E.J. 2003. Environmental dose rate heterogeneity of beta radiation and its implications for luminescence dating: Monte Carlo modelling and experimental validation. Radiation Measurements 37, 305-313.

Negrini, R., Erbes, D., Faber, K., Herrera, A., Roberts, A., Cohen, A., Wigand, P., and Foit, F. 2000 A paleoclimate record for the past 250,000 years from Summer Lake, Oregon, USA. 1. chronology and magnetic proxies for lake level. Journal of Paleolimnology 24, 125-149.

Nicholas, A.P., Clarke, L., and Quine, T.A. 2009. A numerical modelling and experimental study of flow width dynamics on alluvial fans. Earth Surface Processes and Landforms 15, 1985-1993.

Nicholas, A.P., and Quine, T.A. 2007. Modeling alluvial landform change in the absence of external environmental forcing. Geology 35, 527-530.

Olley, J., Caitcheon, G., and Murray, A. 1998. The distribution of apparent dose as determined by Optically Stimulated Luminescence in small aliquots of fluvial quartz: Implications for dating young sediments. Quaternary Science Reviews 17, 1033-1040.

Olley, J.M., Caitcheon, G.G., and Roberts, R.G. 1999. The origin of dose distributions in fluvial sediments, and the prospect of dating single grains from fluvial deposits using optically stimulated luminescence. Radiation Measurements 30, 207-217.

Olley, J.M., De Deckker, P., Roberts, R.G., Fifield, L.K., Yoshida, H., and Hancock, G. 2004. Optical dating of deep-sea sediments using single grains of quartz: a comparison with radiocarbon: Sedimentary Geology, v. 169, p. 175-189.

Olley, J.M., Pietsch, T., and Roberts, R.G. 2004. Optical dating of Holocene sediments from a variety of geomorphic settings using single grains of quartz. Geomorphology 60, 337-358.

Olley, J.M., Roberts, R.G., and Murray, A.S. 1997. Disequilibria in the uranium decay series in sedimentary deposits at Allen's cave, nullarbor plain, Australia: Implications for dose rate determinations. Radiation Measurements 27, 433-443.

Oviatt, C.G., Currey, D.R., and Sack, D. 1992. Radiocarbon chronology of Lake Bonneville, Eastern Great Basin, USA. Palaeogeography, Palaeoclimatology, Palaeoecology 99, 225-241.

Owen, L.A., Finkel, R.C., Haizhou, M., and Barnard, P.L. 2006. Late Quaternary landscape evolution in the Kunlun Mountains and Qaidam Basin, Northern Tibet: A framework for examining the links between glaciation, lake level changes and alluvial fan formation. Quaternary International 154-155, 73-86.

Parker, G., Paola, C., Whipple, K.X., Mohrig, D., Toro-Escobar, C.M., Halverson, M., and Skoglund, T.W. 1998. Alluvial fans formed by channelized fluvial and sheet flow II: Application. Journal of Hydraulic Engineering 124, 996-1004.

Patterson, S.J. 2006. Sedimentology and geomorphology of quaternary alluvial fans with implications to growth strata, Lost River Range [M.S. thesis], Montana State University.

Phillips, F.M., Zreda, M.G., Gosse, J.C., Klein, J., Evenson, E.B., Hall, R.D., Chadwick, O.A., and Sharma, P. 1997. Cosmogenic 36Cl and 10Be ages of Quaternary glacial and fluvial deposits of the Wind River Range, Wyoming. Geological Society of America Bulletin 109, 1453-1463.

Phillips, W.M., Breckenridge, R.M., Otherburg, K.L., and Garwood, D.L. 2007. New cosmogenic ^{10}Be exposure age chronology for Payette moraines, Central Idaho, USA. Geological Society of America Abstracts with Programs 39, 514.

Phillips, W.M., Rittenour, T.M., and Hoffman, G. 2009. OSL chronology of late Pleistocene glacial outwash and loess deposits near Idaho Falls, Idaho. Geological Society of America Abstracts with Programs 41, 12.

Pierce, K.L. 1985. Quaternary history of movement on the Arco segment of the Lost River fault, central Idaho, *in* Stein, R.S., and Bucknam, R.C., eds., Workshop on the Borah Peak, Idaho, earthquake, 28th, Proceedings. U.S. Geological Survey Open-File Report, p. 195-206.

Pierce, K.L., and Colman, S.M. 1986. Effect of height and orientation (microclimate) on geomorphic degradation rates and processes, late glacial terrace scarps in central Idaho. Geological Society of America Bulletin 97, 869-885.

Pierce, J. L., Meyer, G. A. & Timothy Jull, A. J. 2004. Fire-induced erosion and millennial-scale climate change in northern ponderosa pine forests. Nature 432, 87-90, doi: http://www.nature.com/nature/journal/v432/n7013/suppinfo/nature03058_S1.html.

Pierce, K.L., and Morgan, L.A. 1990. The track of the Yellowstone hotspot: Volcanism, faulting, and uplift. U.S. Geological Survey Open File Report 90-415, 1-48.

Pierce, K.L., Muhs, D.R., Fosberg, M.A., Mahan, S.A., Rosenbaum, J.G., Licciardi, J.M., and Pavich, M.J. 2011. A loess-paleosol record of climate and glacial history over the past two glacial-interglacial cycles (~ 150 ka), southern Jackson Hole, Wyoming. Quaternary Research 76, 119-141.

Pierce, K.L., and Scott, W.E. 1982. Pleistocene episodes of alluvial-gravel deposition, southeastern Idaho, *in* Bonnichsen, B., and Breckenridge, R.M., eds., Cenozoic geology of Idaho. Idaho Bureau of Mines and Geology Bulletin 26, 685-702.

Porter, S. C., K. L. Pierce & T. D. Hamilton. 1983. Late Wisconsin mountain glaciation in the Western United States. *In* S. C. Porter, ed., Late Quaternary environments of the United States. Minneapolis: University of Minnesota Press. 71-111.

Poulos, M.J., Pierce, J.L., and Pierce, K.L. 2008. Drainage basin influences on alluvial fan processes in the Lost River Range, Idaho. Geological Society of America Abstracts with Programs 40, 195.

Prescott, J. R. and Hutton, J. T.. 1994. Cosmic ray contributions to dose rates for luminescence and ESR dating: Large depths and long-term time variations. Radiation Measurements 23, 497-500.

Rathburn, S.L.. 1993. Pleistocene cataclysmic flooding along the Big Lost River, east central Idaho. Geomorphology 8, 305-319.

Refsnider, K. A., B. J. C. Laabs, M. A. Plummer, D. M. Mickelson, B. S. Singer, and M. W. Caffee. 2008. Last glacial maximum climate inferences from cosmogenic dating and glacier modeling of the western Uinta ice field, Uinta Mountains, Utah. Quaternary Research 69, 130-144.

Reheis, M. 1999. Highest pluvial lake shorelines and Pleistocene climate of the western Great Basin. Quaternary Research 52, pp. 196-205.

Reiners, P.W., Ehlers, T.A., Mitchell, S.G., and Montgomery, D.R. 2003. Coupled spatial variations in precipitation and long-term erosion rates across the Washington Cascades. Nature 426, 645-647.

Reyes, A.V., Wiles, G.C., Smith, D.J., Barclay, D.J., Allen, S., Jackson, S., Larocque, S., Laxton, S., Lewis, D., Calkin, P.E., and Clague, J.J. 2006. Expansion of alpine glaciers in Pacific North America in the first millennium A.D. Geology 34, 57-60.

Rittenour, T.M. 2008. Luminescence dating of fluvial deposits: applications to geomorphic, palaeoseismic and archaeological research. Boreas 37, 613-635.

Rittenour, T. M., and J. L. Pederson. 2010. Enhanced sediment hillslope supply to the Colorado River and its tributaries during MIS 5-3. Geological Society of America Abstracts with Programs 42, 75.

Ritter, J.B., Miller, J.R., Enzel, Y., and Wells, S.G. 1995. Reconciling the roles of tectonism and climate in Quaternary alluvial fan evolution. Geology 23, 245-248.

Rizza, M., Mahan, S., Ritz, J.F., Nazari, H., Hollingsworth, J., and Salamati, R. 2011. Using luminescence dating of coarse matrix material to estimate the slip rate of the Astaneh fault, Iran. Quaternary Geochronology 6, 390-406.

Roberts, R.G., Yoshida, H., Galbraith, R.F., Laslett, G.M., Jones, R., and Smith, M. 1998. Single-aliquot and single-grain optical dating confirm thermoluminescence age estimates at Malakunanja II rock shelter in northern Australia. Ancient TL 16, 19-24.

Rodnight, H., Duller, G.A.T., Wintle, A.G., and Tooth, S. 2006. Assessing the reproducibility and accuracy of optical dating of fluvial deposits. Quaternary Geochronology 1, 109-120.

Scott, W.E., Pierce, K.L., and Hait, M.H., J.R. 1985. Quaternary tectonic setting of the 1983 Borah Peak earthquake, central Idaho. Bulletin of the Seismological Society of America 75, 1053-1066.

Sharp, W.D., Ludwig, K.R., Chadwick, O.A., Amundson, R., and Glaser, L.L. 2003. Dating fluvial terraces by 230Th/U on pedogenic carbonate, Wind River Basin, Wyoming. Quaternary Research 59, 139-150.

Shuman, B., Henderson, A.K., Colman, S.M., Stone, J.R., Fritz, S.C., Stevens, L.R., Power, M.J., and Whitlock, C. 2009. Holocene lake-level trends in the Rocky Mountains, U.S.A. Quaternary Science Reviews 28, 1861-1879.

Simpson, D.T., Kolbe, T.E., Ostenaa, D.A., Levish, D.R., and Klinger, R.E.. 1999. Lower Big Lost River chronosequence - Implications for glacial outburst flooding. Geological Society of America Abstracts with Programs 31, A-56.

Skipp, B., and Hait, M.H., J.R. 1977. Allochtons along the northeast margin of the Snake River Plain, Idaho. Wyoming Geological Association Guidebook, 499-515.

Snyder, N.P., Whipple, K.X., Tucker, G.E., and Merritts, D.J. 2000. Landscape response to tectonic forcing: Digital elevation model analysis of stream profiles in the Mendocino triple junction region, northern California. Geological Society of America Bulletin 112, 1250-1263.

Sohn, M.F., Mahan, S.A., Knott, J.R., and Bowman, D.D. 2007. Luminescence ages for alluvial-fan deposits in Southern Death Valley: Implications for climate-driven sedimentation along a tectonically active mountain front. Quaternary International 166, 49-60.

Spencer, J.Q.G., and Robinson, R.A.J. 2008. Dating intramontane alluvial deposits from NW Argentina using luminescence techniques: Problems and potential. Geomorphology 93, 144-155.

Stevens, L.R., Stone, J.R., Campbell, J., and Fritz, S.C. 2006. A 2200-yr record of hydrologic variability from Foy Lake, Montana, USA, inferred from diatom and geochemical data. Quaternary Research 65, 264-274.

Stock, J.D., Schmidt, K.M., and Miller, D.M. 2008. Controls on alluvial fan long-profiles. Geological Society of America Bulletin 120, 619-640.

Svenson, L., Pierce, J.L., Wilkins, D., and Whitman, J. 2009. Fire and Climate in a Lodgepole-pine Forest in Central Idaho: Annual, Interannual, Centennial, and Millennial Perspectives, Association of American Geographers Abstracts: Las Vegas, USA.

Thackray, G.D. 2008. Varied climatic and topographic influences on Late Pleistocene mountain glaciation in the western United States. Journal of Quaternary Science 23, 671-681.

Thackray, G.D., Lundeen, K.A., and Borgert, J.A. 2004. Latest Pleistocene alpine glacier advances in the Sawtooth Mountains, Idaho, USA: Reflections of midlatitude moisture transport at the close of the last glaciation. Geology 32, 225-228.

Truelsen, J.L., and Wallinga, J. 2003. Zeroing of the OSL signal as a function of grain size: Investigating bleaching and thermal transfer for a young fluvial sample. Geochronometria 22, 1-8.

Vandenberghe, D., Hossain, S.M., De Corte, F., and Van den haute, P. 2003. Investigations on the origin of the equivalent dose distribution in a Dutch coversand. Radiation Measurements 37, 433-439.

Vincent, K.R., W.B.Bull, and Chadwick, O.A. 1994. Construction of a soil chronosequence using the thickness of pedogenic carbonate coatings. Journal of Geological Education 42, 316-324.

Wallinga, J. 2002. Optically stimulated luminescence dating of fluvial deposits: a review. Boreas 31, 303-322.

Western Regional Climate Center, Historical Climate Information, accessed May 2009, http://www.wrcc.dri.edu/

Whipple, K.X., Kirby, E., and Brocklehurst, S.H. 1999. Geomorphic limits to climate-induced increases in topographic relief. Nature 401, 39-43.

Whipple, K.X., Parker, G., Paola, C., and Mohrig, D. 1998. Channel dynamics, sediment transport, and the slope of alluvial fans: Experimental study. The Journal of Geology 106, 677-693.

Whitlock, C., C. E. Briles, M. C. Fernandez, and Gage, J. 2011. Holocene vegetation, fire and climate history of the Sawtooth Range, central Idaho, USA. Quaternary Research 75, 114-124.

Winograd, I.J., Landwehr, J.M., Coplen, T.B., Sharp, W.D., Riggs, A.C., Ludwig, K.R., and Kolesar, P.T. 2006. Devils Hole, Nevada, δ18O record extended to the mid-Holocene. Quaternary Research 66, 202-212.

Winograd, I. J., J. M. Landwehr, K. R. Ludwig, T. B. Coplen, and A. C. Riggs. 1997. Duration and structure of the past four interglaciations. Quaternary Research 48, 141-157.

Wobus, C.W., Hodges, K.V., and Whipple, K.X.. 2003. Has focused denudation sustained active thrusting at the Himalayan topographic front? Geology 31, 861-864.

Zdanowicz, C.M., Zielinski, G.A., and Germani, M.S. 1999. Mount Mazama eruption: Calendrical age verified and atmospheric impact assessed. Geology 27, 621-624.

APPENDIX A

Soil Descriptions

Soils were described at most locations where OSL samples were collected using the guidelines outlined in Birkeland et al. (1991).

Table A.1 Criteria used to determine stage of CaCO3 developent in LRR soils. From Table A-6 in Birkeland et al. (1991).

Stage	Gravelly parent material	Nongravelly parent material
I	Thin discontinuous clast coatings; some filements; matrix can be calcereous next to stones; about 4% $CaCO_3$.	Few filaments or coatings on sand grains; <10% $CaCO_3$.
I+	Many or all clast coatings are thin and continuous.	Filaments are common.
II	Continuous clast coatings; local cementation of few to several clasts; matrix is loose and calcareous enough to give somewhat whitened appearance.	Few to common nodules; matrix between nodules is slightly whitened by carbonate (15-50% by area), and the latter occurs in veinlets and as filaments; some matrix can be noncalcareous; about 10-15% $CaCO_3$.
II+	Same as stage II, except carbonate in matrix is more pervasive.	Common nodules; 50-90% of matrix is whitened; about 15% $CaCO_3$.
Continuity of fabric high in carbonate		
III	Horizon has 50-90% of grains coated with carbonate, forming an essentially continuous medium; color mostly white; carbonate-rich layers more common in upper part; about 20-25% $CaCO_3$.	Many nodules, and carbonate coats so many grains that over 90% of horizon is white; carbonate-rich layers more common in upper part; about 20% $CaCO_3$.
III+	Most clasts have thick carbonate coats; matrix particles continuously coated with carbonate or pores plugged by carbonate; cementation more or less continuous; >40% $CaCO_3$.	Most grains coated with carbonate; most pores plugged; >40% $CaCO_3$.
Partly or entirely cemented (irrespective of parent material)		
IV	Upper part to K horizon is nearly pure cemented carbonate (75-90% $CaCO_3$) and has a weak platy structure due to the weakly expressed laminar depositional layers of carbonate; the rest of the horizon is plugged with carbonate (50-75% $CaCO_3$).	
V	Laminar layer and platy structure are strongly expressed; incipient brecciation and pisolith (thin, multiple layers of carbonate surrounding particles) formation.	
VI	Brecciation and recementation (multiple generations), as well as pisoliths, are common.	

Table A.2 Soil description for site 1 at Willow Creek Alluvial Fan.

Depth (cm)	Horizon or Deposit	Moist Color	Structure (grade/ped type)	Gravel (%)	Consistence (Dry)	Texture	Lower Boundary	Parent Material	$CaCO_3$ Stage	Notes
0-2	O/A	10 YR 4/3	2/sbk	15	so	SiL	abrupt and straight	loess	NA	Mild reaction with acid. Evidence of bioturbation and inflation.
2-15	Bw	10YR 5/3	2/sbk	<10	sh	SiCL	clear and wavy	loess, minor gravels	NA	Moderate reaction with acid. Evidence of bioturbation and inflation. Minor carbonate on clasts within horizon.
15-32	Bw_2	10YR 4/3	2/sbk	40	so	SiL	clear and wavy	loess and alluvial fan gravles	NA	Moderate reaction with acid. Evidence of bioturbation and inflation. Minor carbonate on clasts within horizon.
32-46	Bk_1	10YR 3/2	2/sbk	60	lo	SiL	abrupt and straight	alluvial fan gravels and minor loess	II	Strong reaction with acid.
46-59	$2Bk_1$	10YR 4/2	1/sbk	70	h	SiL	clear and wavy	alluvial fan gravels	II+	Strong reaction with acid.
59-95	$2Bk_2$	10YR 2/1	1/sbk	75	lo	LS	clear and wavy	alluvial fan gravels	I+	
95-121	$2Bk_3$	10YR 2/1	1/sbk	80	so	LS	clear and wavy	alluvial fan gravels	I	Strong reaction with acid.
121-205	C	10YR 4/2	m	75	lo	L	bottom of trench	alluvial fan gravels	NA	Unaltered alluvial fan gravels and sheetflood couplets

Table A.3 Soil description for site 2 at Willow Creek Alluvial Fan.

Depth (cm)	Horizon or Deposit	Moist Color	Structure (grade/ped type)	Gravel (%)	Consistence (Dry)	Texture	Lower Boundary	Parent Material	$CaCO_3$ Stage	Notes
0-14	A	10YR 4/2	2/sbk	30	so	SiL	clear and wavy	loess	NA	Bioturbation and inflation.
14-26.5	Bw	10YR 4/3	2/sbk	25	so	SiL	abrupt and straight	loess	NA	Bioturbation and inflation.
26.5-42	Bk_1	10YR 4/2	2/sbk	25	so	SiCL	clear and straight	loess	I+	Peds better formed than above. End of obvious loess. Strong reaction with acid.
42-63	Bk_2	10YR 4/2	2/sbk	35	sh	SiL	clear and straight	alluvial fan gravels	I+	Minor loess infiltration. Bioturbation present. Strong reaction with acid. Appears darker than above horizon in profile.
63-88	$2Bk_1$	10YR 3/2	m	60	lo	SL	clear and straight	alluvial fan gravels	II+	Strong reaction with acid.
88-101	$2Bk_2$	10YR 3/1	2/sbk	75	sh	LS	abrupt and straight	alluvial fan gravels	II+	Strong reaction with acid.
101-235	C	10YR 3/1	2/sbk			LS	bottom of trench	alluvial fan gravels	NA	Unaltered parent material-- sheetflood couplets apparent.

Table A.4 Soil description for site 3 at Birch Springs Alluvial Fan.

Depth (cm)	Horizon or Deposit	Moist Color	Structure (grade/ped type)	Gravel (%)	Consistence (wet)	Texture	Lower Boundary	Parent Material	$CaCO_3$ Stage	Notes
0-9	A	10 YR 4/3		20	so/po	SL	c/s			evidence of inflation. Strong effervec.
9-51	Bw	10 YR 4/2		25	so/po	SL	g/w			bioturbation and frost inflation. Strong eff (slightly stronger than above)
51-76	Bk	10 YR 4/3		60	so/po	SL	c/s			slightly increased sand from above. Stage II calc carb. Slightly stronger effervec than above. Evidence of bioturbation. Fining up gravel
76-91.5	2Bw	10 YR 5/3		<10	so/po	SL	w			change in PM to all alluvial, no loess component. Strong effervec.
91.5-183	C	10 YR 4/1 and 10YR 5/2					bottom of trench			parent material. Alternating gravel and sand lenses. Still come caco3 coats stage I+ (?). Mottled color. Strong effervec.

Table A.5 Soil description for site 4 at Birch Springs Alluvial Fan.

Depth (cm)	Horizon or Deposit	Moist Color	Structure (grade/ped type)	Gravel (%)	Consistence (wet)	Texture	Lower Boundary	Parent Material	$CaCO_3$ Stage	Notes
0-4	O/A	10YR 4/2	2/sbk	15	so	SiL	a/s	loess	NA	Moderate reaction with acid.
4-20	Bw	10YR 4/3	2/sbk	15	sh	SiL	c/s	loess and alluvial fan gravels	NA	Moderate reaction with acid. Peds show more structure than above. Mixing by bioturbation and inflation.
20-39	Bk_1	10YR 5/3	1/sbk	45	sh	SL	c/w	alluvial fan gravels with minor loess	II+	Strong reaction with acid. Some bioturbation visible. Sheetflood copulets poorly defined.
39-59	2Bkw	10YR 4/3	1/gr	70	lo	LS	c/s	Alluvial fan gravels	I	Moderate to strong reaction with acid. Horizon shows reddened color.
59-82	$2Bk_2$	10YR 5/2	1/gr	80	sh	LS	c/s	Alluvial fan gravels	I	Weak-moderate reaction with acid. Some local carbonate cementation.
82-94	$2Bk_3$	10YR 5/2	2/abk	65	sh	LS	g/w	Alluvial fan gravels	I	Color appears lighter than above in profile and whitened in places. Weak-moderate reaction with acid.
94-230	C	10YR 5/2	1/sbk	70	sh	LS	bottom of trench	Alluvial fan gravels	NA	

Table A.6 Soil description for site 5 at Birch Springs Alluvial Fan.

Depth (cm)	Horizon or Deposit	Moist Color	Structure (grade/ped type)	Gravel (%)	Consistence (dry)	Texture	Lower Boundary	Parent Material	$CaCO_3$ Stage	Notes
0-7	A	10 YR 3/2	weak/sbk	<15	so	SiL	c/w			Silt loam, slightly gritty. Mild rxn with acid. PM is loess and fluvial gravels.
7-26	1Bk1	10 YR 4/2	weak/sbk	40	so	L	c/w			Stron rxn with acid. Pm is loess and gravels. Stage II+ carbonate which increases with depth
26-50	2Bk1	10 YR 3/3		60		S	c/w			Mild to moderate rxn with acid. Stage I+-II carbonate. Decreased carbonate from above. Also iron oxide (?) on clasts. Reddish appearance seems related to rooth depth ??
50-75	2Bk2	10 YR 3/4		60		S	g/w			Carbonate stage III. Moderate to strong rxn with acid. Coats on rocks are poorly developed but matrix is cemented and platy. Still some reddened color. Lower boundary is defined by decrease in carbonate.
75-230	C			60						PM is fluvial sands and gravels. Sheetflood couplets are poorly defined but some sections of well-sorted and some open framework. Weak carbonate development. Grain sizes --> fine couplets avg 0.5-1.0 cm. Coarser couplets average 4-5 cm. largest clasts up to ~25 cm. Large cobbles common throughout. Better sorted zones at ~50-80 cm depth and 1.6 m to base

General notes: gravelly surface with little loess accumulation.

Table A.7 Soil description for site 6 at Birch Springs Alluvial Fan.

Depth (cm)	Horizon or Deposit	Moist Color	Structure (grade/ped type)	Gravel (%)	Consistence (dry)	Texture	Lower Boundary	Parent Material	$CaCO_3$ Stage	Notes
0-4	A	10 YR 4/3	abk	<15	sh	SiL	c/s			moderate rxn with acid. Pm is loess, some gravels
4-18	1Bkw	10 YR 4/3	weak/sbk	15	so	SiL	c/s			SiL, but increased sand content from above. Moderate rxn with acid. Stage I+ carbonate. PM is loess, some sand and gravels.
18-40	2Bk	10YR 5/3		50		SL	a/s			Very strong rxn with acid. Stage III carbonate. PM is fluvial gravels with some loess infill
40-79	3Bkw	7.5 YR 4/4		60		LS	c/s			Moderate to strong rxn with acid. PM is fluvial sands and gravels. Horizon appears reddish in profile
79-240	C			50-60			bottom of trench			Fluvial sands and gravels. Poorly defined couplets. Some very small sand lenses (one sampled for OSL). Finer portions predominately coarse sand size. Coarser portions ~2-5 cm b-axis. Largest clasts ~18 cm b-axis. Overall smaller grain sizes than lower trench. Moderate sorting. Some channel fills visible?? Overall whitish appearance but maybe only stage I to I+ carbonate. Clast supported deposit. Tops of clasts stained red.

General notes: little to no loess cap. Surface is mainly gravels. Some distinct couplets. Seems to have smaller D50 than lower trench. Clasts up to 10-15 cm b-axis. Subdued bar and swale topography.

Table A.8 Soil description >35 ka moraine on the surface of site 6, Birch Springs Alluvial Fan.

Depth (cm)	Horizon or Deposit	Moist Color	Structure (grade/ped type)	Gravel (%)	Consistence (dry)	Texture	Lower Boundary	Parent Material	$CaCO_3$ Stage	Notes
2-0	O									very sparse O horizon
0-15	1Bw	10 YR 4/4	sbk	<10	sh	SiL	w			Vesicular loess cap. Mild rxn with acid. Bottom boundary marked by increase in CaCO3.
15-40	2Bk	10 YR 5/3		30-40		SL	c/w			PM is moraine/outwash, 0-30 cm boulders. Zone of max carbonate accumulation, stage III+ to IV: laminar in places. Bottom boundary defined by decrease in carbonate.
40-55	2Bwk	10 YR 3/4 mottled		30-41		LS	w			PM is glacial till/outwash. Very vesicular, large vesicles with increased roots. Some reddened appearance again -- maybe redox feature ralated to change in water table belwo carbonate? Bottom boundary defined by decrease in carbonate
55-200	C	10 YR 4/2				SL				PM is till and outwash. Texture is sany loam, but stickier/more fines than other trenches at this depth

Table A.9 Soil description for site 12 at Upper Cedar Creek Alluvial Fan.

Depth (cm)	Horizon or Deposit	Moist Color	Structure (grade/ped type)	Gravel (%)	Consistence (dry)	Texture	Lower Boundary	Parent Material	$CaCO_3$ Stage	Notes
0-50	1Bw		abk to sbk	<5 %	friable	SiL	c/s	loess		boundary defined by increased carbonate and gravel
50-95	2Bk						c/s	sheetflood gravels with loess	II+	boundary defined by decreased CaCO3 and loess infill and increased gravel. All clasts have carb coat on bottom, some local cementation, white appearance of horizon
82-170										loess infill stops at ~82 cm. sheetflood/channel gravels. couplets defined and ~10-15 cm thick. B-axis small couplet ~0.5-1 cm. B-axis coarse ~3-4 cm and up to ~10 cm.

Table A.10 Soil description for site 13 at Upper Cedar Creek Alluvial Fan.

Depth (cm)	Horizon or Deposit	Moist Color	Structure (grade/ped type)	Gravel (%)	Consistence (dry)	Texture	Lower Boundary	Parent Material	$CaCO_3$ Stage	Notes
0-5	AO	10YR 4/3	Grade: sg Ped type: gr	10	sh	SiL	abrupt and straight	loess	NA	Slight reaction with acid. Thin O of roots and twigs.
5-24	Bkw	10YR 5/3	Grade: 1 Ped type: pl and sbk	15	sh	SiL	clear and wavy	loess	?	Peds slightly harder than above. Texture more velvety than above. Color B, no significant clay accumulation. Stronger reaction with acid than above.
24-33	Bkw_2	10YR 6/3	Grade: 1 Ped type: sbk	25	sh	SiL	clear and wavy	loess with some alluvial gravels	I+	Vesicular. Inflation. Base of obvious loess infiltration.
33-41	Bk_1	10YR 6/2	Grade: 2 Ped type: sbk	35	h	SiL	abrupt and straight	alluvial gravels with some loess	III+ to IV	Well cemented top of K and slightly laminar. Strong reaction with acid SiL with more sand.
41-55	Bk_2	10YR 4/2	Grade: 1 Ped type: sbk	40	sh	SiL	clear and straight	alluvial gravels with some loess	II+	Well cemented. Strong reaction with acid. Less gritty than above.
55-71	2Bkw	10YR 3/1	Grade: m	50	lo	SL	gradual and straight	alluvial gravels	I	Moderate reaction with acid.
71-209	2C	10YR 3/1	Grade: m	75	lo	SL	bottom of trench	alluvial gravels	NA	Moderate reaction with acid. Sheetflooded couplets. Sandier than unit above.

Table A.11 Soil description for site 18 at Ramshorn Alluvial Fan.

Depth (cm)	Horizon or Deposit	Moist Color	Structure (grade/ped type)	Gravel (%)	Consistence (dry)	Texture	Lower Boundary	Parent Material	$CaCO_3$ Stage	Notes
0-2	A-O	10YR 3/4		40		SiL		loess		
2-37	Bw	10YR 3/3		30		SiL		loess and gravels		loess mixed with gravels by bioturbation and inflation, thin or absent carbonate coats, moderate effervescence
37-64	Bk	10YR 4/4		65		SL				called it a gravelly sandy loam, mixed loess and gravel, bioturbation and frost inflation, stage I carbonate development, some filaments between clasts, violent effervescence RH-NS-0524-01
64-105	2Bk1	10YR 3/4		75		SL				gravelly sandy loam, gray limestone subangular clasts, overall deposit is gray gravel with white clasts, sheetflood gravel PM (PM change here), approx 20 cm couplets with coarse gravel approx 5 cm, fine approx 2 cm with coarse and fine sand in coarse couplet, stage II+ carbonate development, approx 1mm coats. color is of matrix RH-NS-0524-01
105-187	2C?	10YR 4/2		75		SL				gravelly sandy loam, PM is sheetflood deposits of limestone clasts, no carbonate development, thin to absent coats on bottom of clasts, bottom of trench **OSL sample RH-MK-0524-01**

Table A.12 Soil description for site 19 at Ramshorn Alluvial Fan.

Depth (cm)	Horizon or Deposit	Moist Color	Structure (grade/ped type)	Gravel (%)	Consistence (dry)	Texture	Lower Boundary	Parent Material	$CaCO_3$ Stage	Notes
0-4	A-O	10YR 3/2		20		SiL		loess		Loess parent material, pebbles on surface, bioturbation, strong effervescence,
4-40	Bw	10YR 3/3		30		SiL		loess and fluvial gravels		Gravelly silt loam, mixed loess and gravel, bioturbation frost mixed zone, weak to absent carbonate coats on clasts, moderate to weak effervescence
40-82	2Bk1	10YR 4/3		65		LS		fluvial gravels		Gravelly loamy sand, sheetflood gravels PM, stage II+ carbonate development, ~.9mm coats, carbonate weakly binds soil matrix, absent dense coats, violent eff., RH-NS-0524-02
82-126	2Bk2	10YR 4/2		80		LS		fluvial gravels		Gravelly loamy sand, limestone sheetflood PM, stage I+ carbonate development with ~0.2mm coats, violent eff,, weaker cementation than above, RH-NS-0524-02
126-175	2Bk3	10YR 4/3		80		LS		fluvial gravels		gravelly loamy sand, sheetflood deposits, stage I carbonate with ~ 0.1mm coats, but thicker on edges due to open framework deposits, violent eff., RH-NS-0524-02
175-200	2C	10 YR 5/3		80		LS		fluvial gravels		gravelly loamy sand again, sheetflood deposits, thin carbonate coats but little development, violent eff.

Table A.13 Soil description for site 20 at Ramshorn Alluvial Fan.

Depth (cm)	Horizon or Deposit	Moist Color	Structure (grade/ped type)	Gravel (%)	Consistence (dry)	Texture	Lower Boundary	Parent Material	$CaCO_3$ Stage	Notes
0-6	A-O	10 YR 3/3		<10		SiL	d	loess		loess PM
6-29	Bw	10YR 4/3		<10		SiL	c/w	loess		loess PM, mixing by bioturb and inflation, platy structure, base is end of rooting, diffuse upper contact
29-51	Bt1	10YR 5/3	2/sbk	<10		SiL	d	loess		loess PM, bioturbation and insect burrowing evident, blocky peds, moderate and subangular, more clay than above, contact with above is clear but undulating
51-69	Bt2	10YR 5/3		10		SiL	w	loess		loess PM, frost action and bioturbation, slightly increased clay but weaker structure, contact with above diffuse
69-78	Bwb	10YR 5/3		<10		SiL		loess		less clay than above, weak soil in loess is PM, has pores with halo, contact with above wavy, weak to no structure, mod eff
78-92	2Btb	10YR 4/3		25		L	c/w	loess and alluvial gravels	I	buried Bt soil, increased sand from above and increased clay, mixture of loess and alluvial clasts as PM, stage I carbonate, coats on all sides of clasts, mod eff., has clay lined pores
92-114	3Bk1	10YR 6/2		60		SiL		alluvial gravels with loess	II	buried soil, overprinting in current soil, alluvial gravels, PM is alluvial gravels with loess, stage II carbonate, powdery carbonate in matrix, violent eff., RH-NS-0524-03
114-158	4Bk	10YR 6/2		75		SL		alluvial gravels with little loess	II	increased sand, fine texture and color of matrix probably due to carbonate content, alluvial gravel and alluvial transported loess, probably sheetflood deposits with loess component, stage II carbonate, more clast supported than above, contact @158 cm is
158-180	4Ck							alluvial gravels		sheetflood deposits, increased sand, coats on clasts but less carbonate in matrix, coats sampled **OSL RH-MK-0524-03**

Table A.14 Soil description for site 21 at Ramshorn Alluvial Fan.

Depth (cm)	Horizon or Deposit	Moist Color	Structure (grade/ped type)	Gravel (%)	Consistence (moist)	Texture	Lower Boundary	Parent Material	$CaCO_3$ Stage	Notes
0-30	1Bkw	10 YR 3/4	massive to sbk	20-30	vfr	SiL				no A horizon, ~1cm O over B. Loess PM. Gravel ~14 cm b-axis. Very weak reaction to acid.lower boundary is contact with gravels. Increased sand with depth. Perhaps reddening of soil? CaCO3 ppt at bdy with cobbles
30-95	2Bk	10 YR 5/3		60		SL				light CaCO3, loess filling in pore space. sheetflod PM from 30-170 cm. slight reddening to ~95 cm. strong reaction with acid. Whitening apparent. Coats on underside of clasts. Stage II CaC03. lower boundary defined by CaCO3. CaC)3 coats from 35-45 cm up to ~1.6 mm.
95-170	C									less loess below ~130 cm in interspaces. Sheetflood couplets ~20-30 cm thick. Fine couplets avg size 2-3 cm, coarse 5-10 cm

Table A.15 Soil description for site 22 at Ramshorn Alluvial Fan.

Depth (cm)	Horizon or Deposit	Moist Color	Structure (grade/ped type)	Gravel (%)	Consistence (dry)	Texture	Lower Boundary	Parent Material	$CaCO_3$ Stage	Notes
0-6	O/A	7.5 YR 4/2	sbk to platy	<10	slightly hard	SiL	g/w	loess and alluvial gravels		gradually darker color, dec. eff. W HCl above 5 cm, slightly wavy.
6-50	1Bkw	10 YR 3/4	sbk	50		SiL	c	alluvial gravel	I-II	lower boundary clear, defined by increased CaC03. gravel content increases with depth. loess matrix in 2-5 cm subrounded clasts. Stage I-II CaCO3
50-100	2Bk	10 YR 4/2		70		LS	c	alluvial gravel	II	defined by decreased CaCO3. Increased sand . PM fan gravels with ~2-5 cm B-axis. From 50-70 cm stage II+ CaCO3, distinct white layer, ~1 mm coats. From 70-100 cm stage II CaCO3, decreased carbonate with depth
100-180								alluvial gravel		sheetflood deposti but couplets not well defined. Some infilling with loess in some units. Clasts horizontally oriented. Signs of carbonate dissolution at 120 cm. ~2-10 cm clasts, some as large as 20 cm
180-240	2Bkb	10 YR 5/4 (distinct tan)		65		SCL	bottom of pit			buried soil (?). Hard and platy structure at top with clay. PM sheetfloods with secondary clay in matrix, sandy matrix. Old B horizon with upper A and B stripped off? Sample from bottom of pit still very sticky (clay does not decrease). More small pebbles in PM ~1 cm in size.

Table A.16 Soil description for site 24 at King Canyon Alluvial Fan.

Depth (cm)	Horizon or Deposit	Moist Color	Structure (grade/ped type)	Gravel (%)	Consistence (dry)	Texture	Lower Boundary	Parent Material	$CaCO_3$ Stage	Notes
0-3	AO	10 YR 3/2	2/abk	<10	sh	SiL	a/s	loess	NA	loess Pm. Very mild eff. Fits SiL, but slightly grittier other SiL's
3-10	Bw1	10 YR 3/2	2/sbk	<10	sh	SiL	a/s	loess	NA	loes PM, smaller peds than above, more consolidated than above. Mild to moderate eff.
10-34	Bw2	10YR 4/2	1/sbk	<10	so	SiCL	c/s	loess	NA	more consolidated than above but peds less well formed. Moderate to strong eff. Loess PM
34-55	Bk1	10YR 4/2	2/sbk	10	h	SiCL	c/w	loess	II	but lighter than above in profile. hard to get off exposure. Very consolidated. Stron eff. Stage II caco3. Loess PM
55-66	Bk2	10YR 4/2	2/abk	20	h	SiCL	c/w	loess with little aluvial gravel	II	less consolidated than above, slightly grittier than above. Strong eff. Peds slightly stronger than above. Stage II CaCO3
66-80	Bk3	10 YR 4/2	1/sbk	25	sh	SiL	c/w	loess, some alluvial gravels	II	less consolidated. Mainly less loess PM with inflaction of gravels. Strong eff. Stage II CaCO3
80-97	2Bk1	10YR 4/3	1/sbk	50	so	SiL	a/w	alluvial gravels	I+	PM sheetflood with loess infill. Much less consolidated. Few peds. Stage I+ CaCO3. Moderate to strong eff.
97-250	C	10YR 4/3	m	75	lo			alluvial gravels	NA	with darker coarse sand. bottom of exposure. PM sheetflood gravels. Moderate to strong eff.

General notes: Loess obvious until 100 cm, with bioturbation and inflation. Unaltered sheetfloods below.

Table A.17 Soil description for site 25 at King Canyon Alluvial Fan.

Depth (cm)	Horizon or Deposit	Moist Color	Structure (grade/ped type)	Gravel (%)	Consistence (moist)	Texture	Lower Boundary	Parent Material	$CaCO_3$ Stage	Notes
0-4	O/A		Sbk	<5	fr	SiL	c/w	loess		lower boundary defined by harder consistence below. really not much of an A horizon. Weakly developed, mostly more friable than below. Loess PM
4-88	1Bkw		Abk to Sbk	<5	vfr to fr	SiL	c/w	loess		lower boundary defined by increase in gravel, decrease in loess. Increase in CaCO3 with depth. Stage I+ to II in non-gravel PM. Lots of bioturbation with burrows and rodent bones. As a result structure and CaCO3 stage vary some. Some areas more cemented, more white in color.
88-108	2Bk			60	vfr to fr	SiL	c/w	alluvial gravels, some loess	II	more friable than above. Lower boundary defined by decrease in carbonate. Less white color below. PM is sheetflood deposits with some loess infiltration. Stage II carbonate
108-237				70			c/w	alluvial gravels		sheetflood deposits. Couplets poorly defined. Increase in fines below ~190 cm. Couplets ~20 cm thick. Fine couplet b-axis ~1-4 cm. Coarse couplets b-axis ~5-6 cm, up to ~14 cm.
237-250	3Bwb		some sbk	50-60		L				no structure visible. marked increase in fine matrix material. Also maybe less clast supported in sections? No color change to indicate a buried soil, but texture is more like loess with possible peds and structure to matrix. PM possibly sheetflood /channel deposits/ overbank/loess?? Horizon does not appear continuous across bottom.

Table A.18 Soil description for site 26 at King Canyon Alluvial Fan.

Depth (cm)	Horizon or Deposit	Moist Color	Structure (grade/ped type)	Gravel (%)	Consistence (dry)	Texture	Lower Boundary	Parent Material	$CaCO_3$ Stage	Notes
0-35	1Bkw		weak/sbk	15	sh	SiL	c/s	loess with alluvial gravels	I+	boundary defined by increase in carbonate, increase in white color, decrease in loess content. Stage I+ carbonate: underside of clasts well coated, little carbonate in matrix. PM is loess and sheetflood gravels. Frost inflation and bioturbation. Really no A horizon and very thin O in places
35-115	2Bk			70		L	c/w	alluvial gravels with some loess	III	Sheetflood PM with some loess to 80 cm. boundary defined by decreased carbonate. Stage III carbonate, quite cemented for probably young age and thin coates. Carb content decreases with depth.
115-200	sheetflood gravels			>75			bottom of trench	alluvial gravels		Poorly defined couplets. Fine couplets b-axis ~0.5-1 cm. Coarse b-axis ~3 cm, up to ~10 cm, a few up to 15-20 cm

General notes: ~40 cm loess cap. Sheetflood couplets poorly defined. Grain sizes appear smaller than higher trench on same fan and other

APPENDIX B

Measured Thicknesses of Pedogenic Carbonate Coats and Description of Calcium Carbonate Stages

The following tables contain data for the measured thicknesses of pedogenic carbonate coats developed on the underside of clasts within soil profiles on fan surfaces. For most sites coats were collected only from the best developed carbonate horizon. For some sites, coats were collected and measured from all carbonate horizons. However, only the coats from the best developed carbonate horizon were used to generate Fig. 2.17b.

Table B.1 Pedogenic carbonate coat thicknesses for site 1.

Alluvial fan	Willow Creek	**Site no**	1	
Depth (cm)	**26-42**	**43-63**	**63-88**	**88-101**
	1	0.5	0.6	0.3
	1.4	1	0.4	0.1
	1	1	0.4	0.2
	1.1	0.4	1.1	0.2
	0.8	0.8	0.5	0.2
	0.9	1.1	1	0.4
	1.1	0.9	1.1	0
	1.5	0.5	0.9	0
	1.9	1.1	0.4	0.1
	1.2	1.2	0.7	0.2
	0.5	1.4	0.9	0
	1.7	0.9	1.3	0.6
	1.4	0.6	0.9	0
	0.7	0.6	0.7	0.1
	1.3	0.9	0.3	
	0.6	0.1	1.2	
	1.5	0.6	0.6	
	0.5	0.6	0.8	
	1	0.7	0.4	
	1.6	0.8	1.1	
	0.7		1.1	
	1.4		0.9	
	1			
Average (mm)	1.12	0.79	0.79	0.17
Standard deviation (mm)	0.39	0.31	0.30	0.17

Table B.2 Pedogenic carbonate coat thicknesses for site 5.

Alluvial fan	Birch Springs	**site no**	5		
1.3	3	0.8	0.5	0.8	
0.8	1	1.1	0.7	3	
1	3	2	0.6	1.5	
0.6	2.8	0.6	1.2	1.5	
1	1	1.1	0.8	1.2	
1.1	1.4	1.7	1.5	1.2	
Average (mm)	1.33	**Standard deviation (mm)**	0.73		

Table B.3 Pedogenic carbonate coat thicknesses for site 6.

Alluvial fan	Birch Springs	**site no**	6		
4	2.6	4	3	2.6	
2.9	1.3	3.3	1.4	2	
3.4	1	2	2.2	4	
1.2	4	4	3.5	2	
2.7	2.9	1.5	2.2	3	
2.6	3.5	2.6	6.5	2.3	
Average (mm)	2.81	**Standard deviation (mm)**	1.13		

Table B.4 Pedogenic carbonate coat thicknesses for site 9.

Alluvial fan	Upper Cedar Creek	**site no**	9		
0.4	0.9	0.7	1.5	1	
0.5	0.6	1	0.4	0.9	
0.5	1	0.6	1	0.8	
0.7	1.6	0.9	1	0.6	
0.9	1.5	0.3	1.1	1.1	
1	0.5	0.8	1.2	0.8	
Average (mm)	0.86	**Standard deviation (mm)**	0.33		

Table B.5 Pedogenic carbonate coat thicknesses for site 11.

Alluvial fan	Upper Cedar Creek	**site no**	11		
0.9	0.8	1.5			
2	2.6	1.4			
1.1	1.9	1.2			
2.1	1.4	0.6			
0.8	0.6	1.2			
1.6	0.8				
Average (mm)	1.32	**Standard deviation (mm)**	0.57		

Table B.6 Pedogenic carbonate coat thicknesses for site 12.

Alluvial fan	Upper Cedar Creek	**site no**	12		
0.3	1.5	0.6	0.9	0.7	
1.1	1.4	2	1	0.3	
1	0.5	1	0.5	1	
1.1	0.4	0.5	0.7	0.7	
1	0.8	0.5	0.1	0.5	
1	0.7	1.2	1.2		
Average (mm)	0.83	**Standard deviation (mm)**	0.41		

Table B.7 Pedogenic carbonate coat thicknesses for site 13.

Alluvial fan	Upper Cedar Creek	**site no**	13		
2.3	4	1.4	2.4	2.8	3.3
1.3	2.8	2	1.6	2.4	
2.1	3	1.2	3.2	1.8	
2.2	1.8	2.4	2.3	4.6	
1.9	3	1.1	2	1.6	
1.8	2.1	2.5	1.8	1.8	
Average (mm)	2.27	**Standard deviation (mm)**	0.79		

Table B.8 Pedogenic carbonate coat thicknesses for site 15.

Alluvial fan	Upper Cedar Creek	**site no**	15		
4	2	3	3.2	1.4	1.5
4	3	2.8	5	3	
3	3.8	2	3	3.3	
2.3	3	2.3	2.7	4	
1.9	2.3	2.6	2.4	2.5	
2	3.3	2.5	1	4	
Average (mm)	2.80	**Standard deviation (mm)**	0.88		

Table B.9 Pedogenic carbonate coat thicknesses for site 16.

Alluvial fan	Upper Cedar Creek	**site no**	16		
4.3	1.7	1.8	3.5	3.2	
1.8	1.1	2.6	6.5	2.6	
3.5	1.6	2	2.8	4.5	
2.4	2.1	1.8	2.4	1.1	
1.5	2.7	5.8	3.6	1.1	
2.3	3	2.4	2.2	2.6	
Average (mm)	2.68	**Standard deviation (mm)**	1.28		

Table B.10 Pedogenic carbonate coat thicknesses for site 18.

Alluvial fan	Ramshorn	**Site no**	18	
	37-64 cm	**64-105**		
	1	2.6		
	0.8	1.1		
	0.8	0.8		
	0.4	1		
	0.4	1.2		
	0.8	1.1		
	1.5	1.6		
	0.6	1.3		
	1.2	0.6		
	0.7	1.5		
	1.1	0.8		
	0.9	0.8		
	0.8	1.3		
	0.5	2.1		
	0.9	1.3		
	1.1			
	1.4			
	0.8			
	1.1			
	1.7			
	1.6			
	0.9			
	1			
	1.20			
	0.60			
	0.90			
	1.80			
	1.20			
	3.20			
	2.20			
Average (mm)	1.10	1.27		
Standard deviation (mm)	0.57	0.53		

Table B.11 Pedogenic carbonate coat thicknesses for site 19.

Alluvial fan	Ramshorn	**Site no**	19		
	4-38 cm	**38-80**	**80-126**	**126-175**	**126-175**
	1.9	1.2	0.8	0	0.8
	1.1	0.7	1.6	0.1	0.7
	1.6	0.8	1.2	0	1.1
	1.9	1.1	1.3	0	0.6
	2	0.7	1.1	0.1	0.5
	1.4	1.3	1	0	0.7
	1.2	0.8	1.1	0	0.6
	1	0.9	0.5	0.3	0.6
	1	1.4	0.8	0	0.6
	1.2	0.6	0.4	0	1.1
	1.6	0.5	0.1	1	0.6
	0.9	0.8	0.2	0	0.7
	0.7	0.8	0	0.4	1.1
	0.8	0.5	0.1	0	0.5
	1	0.6	0	0.5	0.7
	1.1	0.4	0	0	0
	0.6	0.3	0.1	0	0.5
	1.3	0.3	0.7	0	1
	0.5	0.6	0	0	1.5
	1.1	0.5		0.1	0.6
	0.8				0.6
	0.6				1.5
	1				0.4
	1.7				0.5
	0.8				0.5
	0.5				1
	0.9				0.7
	3.1				0.3
					1.4
					0.5
					0.5
					0.6
					1.1
					0.4
					0.4
					0
					0.1
					0.4
					0.2
					0.3
					0.8
					0.5
Average (mm)	1.19	0.74	0.58	0.13	0.65
Standard deviation (mm)	0.57	0.31	0.53	0.25	0.35

Table B.12 Pedogenic carbonate coat thicknesses for site 21.

Alluvial fan	Ramshorn	**site no**	21		
1.5	1.8	1.1	1.1		
1.1	1.5	0.9	1.2		
1.7	1.6	2	1.1		
1.5	2.5	1.4			
1.8	1.4	0.4			
1.8	2	2.2			
Average (mm)	1.50	**Standard deviation (mm)**	0.48		

Table B.13 Pedogenic carbonate coat thicknesses for site 22.

Alluvial fan	Ramshorn	**site no**	22		
1.7	0.9	1.5	1.4	0.7	
1.4	0.8	1.4	0.6		
1.2	0.4	2.2	0.7		
0.9	1	2.9	0.9		
1.7	0.7	1.8	1.6		
1.8	1.3	1.7	1.2		
Average (mm)	1.30	**Standard deviation (mm)**	0.57		

Table B.14 Pedogenic carbonate coat thicknesses for site 25.

Alluvial fan	King Canyon	**site no**	25		
0.5	0.6	0.8	1.1	0.1	1.2
0.8	0.8	1.5	2	0.8	1
0.5	0.9	0.8	1.3	1	1
0.6	2	1	0.9	0.5	
1.1	0.5	0.9	0.6	1.5	
0.9	1	0.1	1.1	0.6	
Average (mm)	0.91	**Standard deviation (mm)**	0.43		

Table B.15 Pedogenic carbonate coat thicknesses for site 26.

Alluvial fan	King Canyon	**site no**	26		
0.5	0.7	0.4	0.6	0.5	
0.1	1	0.2	0.4	0.6	
0.8	0.5	0.3	0.2	0.5	
0.6	0.3	1	0.1	0.5	
0.6	0.5	0.1	1.1	0.1	
0.4	0.2	0.3	0.2	0.5	
Average (mm)	0.46	**Standard deviation (mm)**	0.27		

APPENDIX C

Grain Size Data

Grain size data for Lost River Range Alluvial Fans. Site numbers, where given, refer to those in Figs. 1.2 and 2.5-2.9.

Table C.1 Grain size data for site 1 on Willow Creek Alluvial Fan.

FAN	Willow Creek
SITE NO.	1
LOCATION	back-hoe trench closer to fan toe
EASTING	268457
NORTHING	4892365
grain size fraction (μm)	**mass (g)**
63.00	60.12
63-125	50.45
125-250	127.53
250-500	128.83
500-1000	218.31
1000-2000	338.17
2000-4000	644.88
4000-19000	2632.3
19000-25000	587.79
25000-50000	463.43

Table C.2 Grain size data for site 2 on Willow Creek Alluvial Fan.

FAN	Willow Creek
SITE NO.	2
LOCATION	back-hoe trench closer to fan apex
EASTING	269179
NORTHING	4893144
grain size fraction (μm)	**mass (g)**
63	29.87
63-125	30.55
125-250	70.44
250-500	64.76
500-1000	108.4
1000-2000	168.25
2000-4000	287.56
4000-19000	1457.85
19000-37500	589.99
37500-50000	258.83
50000-128000	306.99

Table C.3 Grain size data for site 4 on Birch Springs Alluvial Fan.

FAN	Birch Springs
SITE NO.	4
LOCATION	back-hoe trench on northern fan surface
EASTING	270262
NORTHING	4889519
grain size fraction (μm)	**mass (g)**
63.00	152
63-125	199.6
125-250	248.7
250-500	374.1
500-1000	431.8
1000-2000	431.7
2000-4000	571.3
4000-9620	1025.6
9620-25000	2148.3
25000-50000	2759.9
50000-128000	5302.1

Table C.4 Grain size data for 1 of 2 samples from inferred late Pleistocene surface near apex cross-section on Birch Springs Alluvial Fan.

FAN	Birch Springs
SITE NO.	NA
LOCATION	roadcut near apex cross-section
EASTING	272430
NORTHING	4890189
grain size fraction (μm)	mass (g)
63	81.97
63-125	48.1
125-250	87.9
250-500	139.75
500-1000	209.75
1000-2000	260.65
2000-4000	327.07
4000-19000	1009.1
19000-37500	437.44
37500-50000	0
50000-128000	2400.95

Table C.5 Grain size data for 2 of 2 samples from inferred late Pleistocene surface near apex cross-section on Birch Springs Alluvial Fan.

FAN	Birch Springs
SITE NO.	NA
LOCATION	second sample from different part of exposure in roadcut near apex cross-section
EASTING	272430
NORTHING	4890189
grain size fraction (µm)	mass (g)
63	92.73
63-125	98.43
125-250	110.19
250-500	215.8
500-1000	250.22
1000-2000	286.36
2000-4000	377.35
4000-19000	1074.82
19000-37500	342.84
37500-50000	175.6
50000-128000	1882.7

Table C.6 Grain size data for 1 of 2 samples from active channel near apex cross-section on Birch Springs Alluvial Fan.

FAN	Birch Springs
SITE NO.	NA
LOCATION	one of two samples from active channel at apex cross-section
EASTING	272430
NORTHING	4890189
grain size fraction (µm)	**mass (g)**
63	16.08
63-125	11.69
125-250	22.13
250-500	47.62
500-1000	106.7
1000-2000	168.68
2000-4000	295.33
4000-19000	1339.95
19000-37500	823.21
37500-50000	408.56
50000-128000	785.82

Table C.7 Grain size data for 2 of 2 samples from active channel near apex cross-section on Birch Springs Alluvial Fan.

FAN	Birch Springs
SITE NO.	NA
LOCATION	two of two samples from active channel at apex cross-section
EASTING	272430
NORTHING	4890189
grain size fraction (µm)	**mass (g)**
63	0.46
63-125	0.54
125-250	0.78
250-500	2.07
500-1000	9.43
1000-2000	34.12
2000-4000	114.56
4000-19000	721.42
19000-37500	478.38
37500-50000	451.57
50000-128000	4037.52

Table C.8 Grain size data for inferred Holocene surfacel near apex cross-section on Birch Springs Alluvial Fan.

FAN	Birch Springs
SITE NO.	NA
LOCATION	sample from inferred Holocene deposit near apex cross-section, from low terrace just above active channel
EASTING	272251
NORTHING	4890211
grain size fraction (µm)	**mass (g)**
63	229.24
63-125	115.2
125-250	96.96
250-500	78.27
500-1000	133.4
1000-2000	148.71
2000-4000	167.62
4000-19000	650.97
19000-37500	697.52
37500-50000	323.11
50000-128000	1487.35

Table C.9 Grain size data from inferred Holocene surface near apex cross-section on Birch Springs Alluvial Fan.

FAN	Birch Springs
SITE NO.	NA
LOCATION	from older of inferred Holocene deposits near apex cross-section.
EASTING	272251
NORTHING	4890211
grain size fraction (µm)	**mass (g)**
63	117.13
63-125	82.14
125-250	99.06
250-500	103.27
500-1000	182.57
1000-2000	254.47
2000-4000	306.92
4000-19000	1255.62
19000-37500	958.73
37500-50000	418.72
50000-128000	1054.86

Table C.10 Grain size data from sample 1 of 2 from active channel at mid-fan cross-section on Birch Springs Alluvial Fan.

FAN	Birch Springs
SITE NO.	NA
LOCATION	sample 1 of 2 from active channel at mid-fan cross-section site
EASTING	271164
NORTHING	4889508
grain size fraction (µm)	**mass (g)**
63	153.77
63-125	1.89
125-250	93.79
250-500	132.7
500-1000	159.24
1000-2000	159.2
2000-4000	175.74
4000-19000	1019.09
19000-37500	877.85
37500-50000	96.95
50000-128000	748.88
128000-256000	1466.86

Table C.11 Grain size data from inferred LGM surface at mid-fan cross-section on Birch Springs Alluvial Fan.

FAN	Birch Springs
SITE NO.	NA
LOCATION	sample from inferred LGM surface at mid-fan cross-section
EASTING	272251
NORTHING	4890211
grain size fraction (µm)	**mass (g)**
63	155
63-125	17.76
125-250	109.31
250-500	175.96
500-1000	219.72
1000-2000	269.53
2000-4000	384.93
4000-19000	1209.5
19000-37500	1646.14
37500-50000	681.2
50000-128000	807.94

Table C.12 Grain size data from ~21-26 ka surface of Upper Cedar Creek Alluvial Fan.

FAN	Upper Cedar Creek
SITE NO.	NA
LOCATION	exposure of ~21-26 ka surface created by escaped irrigation ditch, north side active channel, near site 10. Coordinates for site 10.
EASTING	286390
NORTHING	4875329
grain size fraction (µm)	**mass (g)**
63	14.2
63-125	67.1
125-250	147.5
250-500	204.8
500-1000	160.9
1000-2000	190.1
2000-4000	258
4000-9620	451
9620-25000	888
25000-50000	1415
50000-128000	0

Table C.13 Grain size data from Holocene aged surface of Upper Cedar Creek Alluvial Fan.

FAN	Upper Cedar Creek
SITE NO.	NA
LOCATION	Sample from holocene surface at upper fan cross-section. Sample included sand lens.
EASTING	286709
NORTHING	4876204
grain size fraction (µm)	**mass (g)**
63	130.3
63-125	294.93
125-250	337.82
250-500	489.65
500-1000	240.68
1000-2000	156.88
2000-4000	127.13
4000-19000	238.49
19000-37500	226.26
37500-50000	0
50000-128000	690.97

Table C.14 Grain size data from Holocene aged surface of Upper Cedar Creek Alluvial Fan.

FAN	Upper Cedar Creek
SITE NO.	NA
LOCATION	Sample from holocene surface at upper fan cross-section.
EASTING	286709
NORTHING	4876204
grain size fraction (µm)	**mass (g)**
63	78.7
63-125	54.77
125-250	78.85
250-500	105.77
500-1000	134.35
1000-2000	171.74
2000-4000	246.07
4000-19000	759.38
19000-37500	883.48
37500-50000	375.27
50000-128000	1869.1

Table C.15 Grain size data from mid-way up ~30 m exposure on Upper Cedar Creek Alluvial Fan.

FAN	Upper Cedar Creek
SITE NO.	NA
LOCATION	sample from mid-way up ~30 m exposure near site 13. Coordinates are for site 13
EASTING	286089
NORTHING	4874890
grain size fraction (µm)	**mass (g)**
63	79.3
63-125	71.69
125-250	154
250-500	221.74
500-1000	219.36
1000-2000	238.43
2000-4000	430.22
4000-19000	2263.72
19000-37500	596.2
37500-50000	87.94
50000-128000	78.07

Table C.16 Grain size data from active channel on Upper Cedar Creek Alluvial Fan.

FAN	Upper Cedar Creek
SITE NO.	NA
LOCATION	one of two samples from active channel at site of upper fan cross-section
EASTING	286709
NORTHING	4876204
grain size fraction (µm)	**mass (g)**
63	115.28
63-125	115.35
125-250	202.17
250-500	249.47
500-1000	165.68
1000-2000	100.02
2000-4000	105.72
4000-19000	551.71
19000-37500	673.2
37500-50000	427.35
50000-128000	2294.44

Table C.17 Grain size data from active channel on Upper Cedar Creek Alluvial Fan.

FAN	Upper Cedar Creek
SITE NO.	NA
LOCATION	two of two samples from active channel at site of upper fan cross-section
EASTING	286709
NORTHING	4876204
grain size fraction (µm)	**mass (g)**
63	27.8
63-125	31.91
125-250	64.12
250-500	78.99
500-1000	127.66
1000-2000	196.36
2000-4000	213.82
4000-19000	972.66
19000-37500	695.07
37500-50000	479.67
50000-128000	2426.44

Table C.18 Grain size data from active channel on Upper Cedar Creek Alluvial Fan.

FAN	Upper Cedar Creek
SITE NO.	NA
LOCATION	one of two samples from active channel at site of fan toe cross-section
EASTING	285800
NORTHING	4870790
grain size fraction (µm)	**mass (g)**
63	105.6
63-125	164.06
125-250	216.86
250-500	185.42
500-1000	109.72
1000-2000	74.62
2000-4000	106.43
4000-19000	1351.85
19000-37500	892.5
37500-50000	600.77
50000-128000	233.32

Table C.19 Grain size data from active channel on Upper Cedar Creek Alluvial Fan.

FAN	Upper Cedar Creek
SITE NO.	NA
LOCATION	two of two samples from active channel at site of fan toe cross-section
EASTING	285800
NORTHING	4870790
grain size fraction (µm)	**mass (g)**
63	65.11
63-125	95.97
125-250	109.36
250-500	57.87
500-1000	24.51
1000-2000	24.91
2000-4000	42.38
4000-19000	556.37
19000-37500	1510.87
37500-50000	416.6
50000-128000	2616.76

Table C.20 Grain size data from inferred Holocene surface of Upper Cedar Creek Alluvial Fan.

FAN	Upper Cedar Creek
SITE NO.	NA
LOCATION	sample from inferred Holocene surface at fan toe cross-section
EASTING	285800
NORTHING	4870790
grain size fraction (µm)	**mass (g)**
63	238.87
63-125	33.67
125-250	216.31
250-500	184.7
500-1000	127.15
1000-2000	128.58
2000-4000	194.54
4000-19000	1227.16
19000-37500	622.2
37500-50000	605.18
50000-128000	1214.27

Table C.21 Grain size data from late Pleistocene surface of Upper Cedar Creek Alluvial Fan.

FAN	Upper Cedar Creek
SITE NO.	11
LOCATION	sample from abandoned gravel mine at fan toe near Mackay Reservoir Dam
EASTING	285560
NORTHING	4870684
grain size fraction (µm)	**mass (g)**
63	97.82
63-125	13.87
125-250	136.32
250-500	252.36
500-1000	224.44
1000-2000	253.17
2000-4000	351.29
4000-19000	1343.87
19000-37500	736.83
37500-50000	565.35
50000-128000	429.48

Table C.22 Grain size data from late Pleistocene surface of Upper Cedar Creek Alluvial Fan.

FAN	Upper Cedar Creek
SITE NO.	11
LOCATION	sample from abandoned gravel mine at fan toe near Mackay Reservoir Dam
EASTING	285560
NORTHING	4870684
grain size fraction (µm)	**mass (g)**
63	54.7
63-125	59.3
125-250	139.38
250-500	177.11
500-1000	159.14
1000-2000	184.17
2000-4000	258.92
4000-19000	972.02
19000-37500	690.6
37500-50000	339.86
50000-128000	1554.7

Table C.23 Grain size data from mid-fan Holocene surface of Upper Cedar Creek Alluvial Fan.

FAN	Upper Cedar Creek
SITE NO.	NA
LOCATION	sample from holocene surface across active channel from site 13
EASTING	286089
NORTHING	4874890
grain size fraction (µm)	**mass (g)**
63	52.88
63-125	16.94
125-250	78.72
250-500	158.59
500-1000	222.77
1000-2000	227.89
2000-4000	225.66
4000-19000	1209.67
19000-37500	1142.09
37500-50000	409.41
50000-128000	1508.67

Table C.24 Grain size data from late Pleistocene surface of Upper Cedar Creek Alluvial Fan.

FAN	Upper Cedar Creek
SITE NO.	15
LOCATION	sample from back-hoe trench of site 15 on northern portion of fan
EASTING	283917
NORTHING	4872908
grain size fraction (µm)	**mass (g)**
63	87.27
63-125	84.81
125-250	128.82
250-500	204.23
500-1000	156.21
1000-2000	194.95
2000-4000	298.12
4000-19000	1405.31
19000-37500	991.31
37500-50000	315.51
50000-128000	958.72

Table C.25 Grain size data from late Pleistocene surface of Ramshorn Alluvial Fan.

FAN	Ramshorn
SITE NO.	18
LOCATION	sample from back-hoe trench at site 18
EASTING	312157
NORTHING	4852251
grain size fraction (µm)	**mass (g)**
63	104.2
63-125	143.1
125-250	147
250-500	162.5
500-1000	191.3
1000-2000	277.3
2000-4000	436.9
4000-19000	820.3
19000-37500	1614
37500-50000	2185.2
50000-128000	1437

Table C.26 Grain size data from late Pleistocene surface of Ramshorn Alluvial Fan.

FAN	Ramshorn
SITE NO.	19
LOCATION	sample from back-hoe trench at site 19
EASTING	312150
NORTHING	4852032
grain size fraction (µm)	**mass (g)**
63	98
63-125	172.2
125-250	129
250-500	157.6
500-1000	222
1000-2000	245.3
2000-4000	418.9
4000-19000	975.7
19000-37500	2017.4
37500-50000	2486.1
50000-128000	1437

Table C.27 Grain size data from late Pleistocene surface of Ramshorn Alluvial Fan.

FAN	Ramshorn
SITE NO.	20
LOCATION	sample from back-hoe trench at site 20
EASTING	312930
NORTHING	4852740
grain size fraction (µm)	**mass (g)**
63	187.5
63-125	236.9
125-250	271.7
250-500	215.4
500-1000	109.6
1000-2000	107.8
2000-4000	187.5
4000-19000	496.4
19000-37500	1194.6
37500-50000	2025.9
50000-128000	671.2

Table C.28 Grain size data from late Pleistocene surface of King Canyon Alluvial Fan.

FAN	King Canyon
SITE NO.	24
LOCATION	sample from back-hoe trench at site 24
EASTING	313178
NORTHING	4847002
grain size fraction (µm)	**mass (g)**
63	326.62
63-125	252.52
125-250	274.5
250-500	262.72
500-1000	256.18
1000-2000	305.48
2000-4000	386.02
4000-19000	2390.47
19000-37500	2391.84
37500-50000	791.76
50000-128000	1088.79

APPENDIX D

Preparation of Tephra Sample for ICP-MS Analysis

Ash deposits from large eruptions like that of Mt. Mazama in Oregon (now the site of Crater Lake) can spread ash for hundreds to thousands of kilometers, often forming distinct deposits that can be identified in the field. The extent of ash fall for many large eruptions has been well documented, the elemental composition of the ash from the eruption well characterized, and the age of the eruption well established through other dating methods. As such, ash deposits can be very useful in geochronological work as the deposit, if identifiable, marks a point in time. (See list of resources at end of document for more information on tephrochronology.)

The goal in preparing an ash sample for analysis by ICP-MS is to isolate only the identifiable glass shards from the sample. The glass will then be totally digested in preparation for introduction to the ICP-MS.

1. Pour entire sample in large container and fill with tap water to make a slurry. Fill container with water and rinse sample several times with tap water, letting sample settle for about a minute before decanting off fine material still in suspension.
2. Sonicate sample in dark room with probe. Place sample in container large enough that it's not a thick layer at bottom, or sonicate smaller portions of sample separately. Fill container with tap water and set up probe so that the tip is about 2 cm from bottom and water height on probe is correct. The amount of time a sample is sonicated will depend on how effectively it's working to break apart any clumps of material. The progress can be checked periodically under a microscope. Also looks for signs that glass shards are getting broken up too much into unusable sizes. Once sonication is complete, let the sample settle for a minute or so, and decant to remove the fines that are still in suspension.

3. Soak sample in 10% formic acid, with enough acid to cover sample. Let sit for approximately one hour. Decant the acid, rinse with tap water one time, decant, then repeat with another 1 hour soak in 10% formic acid. Decant acid, and rinse/decant sample at least five more times to continue removing fine grain sizes.
4. Transfer sample to oven safe container and dry at about 80 °C.
5. Once samples are totally dry, find a suitable set of sieves with sizes of approximately 63 µm, 100 µm, 250 µm, 500 µm, and 1000 µm. Larger sieves can be used as well if a sample contains a lot of coarser grain sizes. You may need to break up clumps if there are any still visible. Label containers with sample name and the size fraction (for example < 63 µm, 100-250 µm etc).
6. Examine a small portion of the 100-250 µm and 250-500 µm size fractions. Continue to work with the largest size fraction that still has a high percentage of glass. Larger pieces of glass improve results.
7. Run selected size fraction through Frantz magnetic separator first at 0.5 amps with the ramp at 20°. Retain both the magnetic and non-magnetic portions. Run the non-magnetic portion through again at 1.0 amps and 20°. Retain both magnetic and non-magnetic portions, but continue to work the magnetic portion from this run through the Frantz. Examine magnetic portion under microscope. If there is still a high percentage of grains that are not glass, run the sample through the Frantz again. The amps can be adjusted as well as the degree of tilt of the ramp until the desired separation is achieved.
8. Pick out any contaminating fragments under the microscope. Place a small portion of sample (approximately 100 mg or less) into a small plastic dish and fill

half way with ethanol. There are a variety of ways to get isolate the glass. Gently swirling the dish may separate glass and non-glass, and either portion can be removed with a pipette. Further picking of non-glass can be done with dental picks, tweezers, and a pipette. Continue until full sample or desired amount is "clean." (Approximately 100 mg is needed for digestion, and replicates will likely be needed.) When a sample is clean, transfer it to a container that can tolerate acetone and can be placed under a heat lamp (weighing paper folded diagonally both directions and secured in a small box works well). Pipette off excess ethanol and rinse with acetone, removing excess acetone as well. Dry well under heat lamp. Sample is now ready for total digestion.

Additional Resources

Pearce, N.J.G., Westgate, J.A., Perkind, W.T., and Preece, S.J., 2004. The application of ICP-MS methods to tephrochronological problems. Applied Geochemsitry 19, 289-322.

Walker, M., 2005. Quaternary Dating Methods. John Wiley and Sons, Ltd: West Sussex, England. 277pp